MAGNETOSPHERIC CHEMICAL RELEASE STUDY

Billy M. McCormac, et al

Lockheed Missiles and Space Company, Incorporated

Prepared for:

Office of Naval Research

1 November 1973

UNCLASSIFIED

Security Classification

AD769 929

DOCUMENT CONTROL DATA - R & D

(Security classification of title, body of abstract and indexing annotation must be entered when the overall report is classified)

1. ORIGINATING ACTIVITY *(Corporate author)*
Lockheed Palo Alto Research Laboratory
3251 Hanover Street
Palo Alto, CA 94304

2a. REPORT SECURITY CLASSIFICATION
UNCLASSIFIED

2b. GROUP --

3. REPORT TITLE
Magnetospheric Chemical Release Study

4. DESCRIPTIVE NOTES *(Type of report and inclusive dates)*
Final Technical Report

5. AUTHOR(S) *(First name, middle initial, last name)*
Billy M. McCormac, John E. Evans, Stephen B. Mende,
G. T. Davidson, C. R. Chappell

6. REPORT DATE	7a. TOTAL NO. OF PAGES	7b. NO. OF REFS
November 1, 1973	107	53

8a. CONTRACT OR GRANT NO.	9a. ORIGINATOR'S REPORT NUMBER(S)
N00014-73-C-0130	
b. PROJECT NO. Program Code No. 913500	
c. ARPA Order No. 2260	9b. OTHER REPORT NO(S) *(Any other numbers that may be assigned this report)*
d.	

10. DISTRIBUTION STATEMENT
Unlimited Distribution

11. SUPPLEMENTARY NOTES	12. SPONSORING MILITARY ACTIVITY
Monitored by: Office of Naval Research Arlington, Virginia	Defense Advanced Research Projects Agency Arlington, Virginia

13. ABSTRACT

Wave particle interactions in the magnetosphere can produce ULF and VLF amplification, affect the diffusion of energy from the magnetosphere to the ionosphere, and may affect the trapping of energetic electrons and protons. Chemical releases of barium or lithium may modify the wave particle interactions in the magnetosphere such that the phenomena can be better investigated and may lead to techniques for producing desired wave particle interactions.

Under this study results of a barium release in the outer magnetosphere and OGO-5 satellite results have been reviewed to obtain guidance in planning future satellite experiments. The possibility of using cold plasma chemical releases to reduce trapped betas from nuclear detonations has been studied. Data on previous observations of electrons and protons in the magnetosphere have been collected. General requirements for satellite experiments are given.

107

DD FORM 1 NOV 68 1473

UNCLASSIFIED

Security Classification

14. KEY WORDS	LINK A		LINK B		LINK C	
	ROLE	WT	ROLE	WT	ROLE	WT
Alpha particles						
Angular distribution						
Barium release						
Cold plasma injection						
Electric Fields						
Electrons						
Energy flux						
Energy spectra						
Equatorial pitch angles						
Geosynchronous satellites						
Lithium release						
Magnetic Fields						
Magnetosphere						
McIlwain L parameter						
OGO-5						
Particle environments						
Planetary activity index, K_p						
Protons						
Spacecraft charging						
Spacecraft sensors						
Thermal ions						
Thermal plasmas						
Trapped electrons						
ULF wave amplification						
VLF wave amplification						
Wave particle interactions						

LMSC D354601

MAGNETOSPHERIC CHEMICAL RELEASE STUDY

FINAL TECHNICAL REPORT

ARPA Order Number: 2260

Program Code Number: 3F10

Contractor:
Lockheed Missiles & Space Company, Inc.

Effective Date of Contract:
September 18, 1972

Contract Expiration Date:
September 18, 1973

Amount of Contract: $74,088

Contract Number: N00014-73-C-0130

Principal Investigator: B. M. McCormac
Telephone: (415) 493-4411, Ext. 45314

Scientific Officer: Dr. John Dardis

Short Title of Work:
Magnetospheric Chemical Release Study

Sponsored By
Advanced Research Projects Agency
ARPA Order Number 2260

November 1, 1973

ib

Radiation Physics Laboratory
Lockheed Palo Alto Research Laboratory
3251 Hanover Street
Palo Alto, California 94304

ABSTRACT

Wave particle interactions in the magnetosphere can produce ULF and VLF amplification, affect the diffusion of energy from the magnetosphere to the ionosphere, and may affect the trapping of energetic electrons and protons. Chemical releases of barium or lithium may modify the wave particle interactions in the magnetosphere such that the phenomena can be better investigated and may lead to techniques for producing desired wave particle interactions.

Under this study results of a barium release in the outer magnetosphere and OGO-5 satellite results have been reviewed to obtain guidance in planning future satellite experiments. The possibility of using cold plasma chemical releases to reduce trapped betas from nuclear detonations has been studied. Data on previous observations of electrons and protons in the magnetosphere have been collected. General requirements for satellite experiments are given.

TABLE OF CONTENTS

Chapter		Page
	Abstract	ii
1	REPORT SUMMARY	1
	1.1 Technical Problem	1
	1.2 Results	2
	1.3 DOD Implications	5
	1.4 Further Research Requirements	6
	1.5 References	7
2	CHEMICAL RELEASES FOR THE PRODUCTION OF ARTIFICIAL EFFECTS IN THE MAGNETOSPHERE	9
	2.1 Introduction	9
	2.2 The BIC Project of September 21, 1971	11
	2.3 Discussion of Instabilities	12
	2.4 State of the Magnetosphere During the NASA/MPI (BIC) Barium Release	16
	2.5 Conclusion	19
	2.6 References	20
3	OGO-5 OBSERVATIONS AND INTERPRETATION	35
4	SPACECRAFT FLIGHT REQUIREMENTS	37
5	THEORETICAL ASPECTS OF TRAPPED RADIATION BELT MODIFICATION	39
	5.1 Introduction	39
	5.2 The Pitch Angle Diffusion of Trapped Electrons	40
	5.3 The Growth of Whistler Waves in a Plasma	46
	5.4 Discussion and Conclusions	49
	5.5 References	63
6	CHARGED PARTICLE ENVIRONMENT IN THE EQUATORIAL REGION FROM 4 TO 9 R_e	65
	6.1 Introduction	65
	6.2 Energetic Electron Environment	67
	6.3 Energetic Proton Environment	70
	6.4 Thermal Plasmas	73
	6.5 Energetic Alpha Particle Environment	74
	6.6 References	75

Chapter 1
REPORT SUMMARY

B. McCormac

1.1 TECHNICAL PROBLEM

An important objective for investigating ionospheric and magnetospheric phenomena and their interrelationship is for the design and optimization of ground based and satellite communications, navigation, detection, and surveillance systems employing ULF and VLF. Research on natural phenomena has clearly shown that wave-particle interactions (WPI) are responsible for ULF and VLF signal amplification, modification of the distribution function of energetic particles, and energy diffusion within the earth's magnetosphere.

Under certain poorly understood circumstances, WPI's result in large amplification of ULF and VLF waves. Better understanding of these amplification processes may lead to controlled amplification for communications or for jamming.

WPI's play a very important role in the coupling between the magnetosphere and the ionosphere. Much of the energy deposited into the ionosphere above about 45° Inv. Lat., comes from the solar wind into the magnetosphere and then into the ionosphere. This energy flow into the ionosphere is very significant in modeling the ionosphere, but is currently ignored as a result of a lack of data and understanding.

WPI's may affect the trapping limit of betas from nuclear detonations, resulting in a much lower environment than that computed on the basis of equating the energy in trapped betas to that of the ambient earth's magnetic field.

WPI's may be used to produce ionospheric absorption due to the precipitation of charged particles from cold plasma injection.

Chemical releases of barium or lithium may modify the WPI in the magnetosphere such that the phenomena can be better investigated and may lead to techniques for producing desired WPI's. Barium releases may affect VLF and lithium ULF waves.

A study effort investigated the 5 tasks listed below:

1.1. Investigate the significance of the artificial barium plasma injection experiment of September 21, 1971.

1.1.2 Investigate the applicability of OGO-5 Satellite data.

1.1.3 Prescribe general experimental requirements for a satellite flight in SESP.

1.1.4 Calculate the effects of WPI on trapped betas from nuclear detonation.

1.1.5 Provide characteristic flux, spectra, and pitch angle distributions for the ambient energetic particle environment outside of the plasmasphere.

The Second Magnetospheric Wave-Particle Interaction Workshop was conducted at Lockheed Palo Alto Research Laboratory during the period February 6 - 8, 1973. Twenty-nine persons participated. A 65 page summary was published by us (McCormac and Evans, 1973). The results of this Workshop are also reflected in this Final Technical Report.

1.2 RESULTS

1.2.1 Related Experiments

The magnetospheric barium release experiment of the Max-Planck-Institut and the OGO-5 data provide some assistance in planning magnetospheric chemical releases. These data have significant limitations for the applications of

interest, but they have been adequately investigated to support the following statements.

Barium Release. On September 21, 1971, a barium cloud was released at 32,000 km altitude at L = 7.2 which is near to synchronous altitude.

The details of this analysis are provided in Chapter 2. The conclusions are:

- A barium release can provide a cold plasma cloud injection in the magnetosphere.
- The rapid striation formation in the cloud implies that cold plasma clouds are unstable in the magnetosphere.
- No VLF amplification was observed and the implications of a structured cloud on a WPI experiment are not resolved.

OGO-5. Analysis of OGO-5 data is of limited value because of lack of adequate particle and wave data. Electrons with energies < 50 keV were not measured; therefore, the most important part of the electron spectrum is missing. No ULF search coil magnetometers were carried on OGO-5 and the fluxgate data lack sensitivity for this application. Since it was a single satellite temporal and spatial effects cannot be separated.

The analysis is limited to ELF which shows that the higher energy electron data is consistant with the ELF waves observed. More detail is provided in Chapter 3.

1.2.2 WPI Satellite Experiment

Chemical releases in the magnetosphere near synchronous orbit should be useful for investigating WPI's: lithium for ULF and barium for VLF. In summary (see Chapter 4 for more detail):

- Two satellites are needed, one with a chemical release payload.

1.2.4 Ambient Energetic Particle Environment

Energetic electron and proton phase space data are essential for performing WPI analyses. Particuarly for energies < 50 keV the data is insufficient. However, it is necessary to collect the available experimental data for theoretical work.

Charged particle fluxes, energy spectra, angular distributions (and in some cases, densities) have been collected from the recent literature and presented as functions of L, local time, and K_p where that information is available. The environment is presented in terms of 4 groups of charged particles; energetic electrons, energetic protons, thermal plasmas and energetic alpha particles. In many cases where there are a limited number of measurements or are for a limited set of conditions, the data are presented as examples. These examples should be used in calculations and to make predictions only when there is a full realization of the low statistical significance of these data and especially of the data changes due to changing conditions. However, this collection of environmental data should give a good picture of the range of particle environments which can be anticipated for planning experiments in the L = 4 to 9 region with an indication of the probability of a particular particle environment occurring. The data are given in Chapter 6.

1.3 DOD IMPLICATIONS

1.3.1 WPI's are of great importance in the diffusion of energy within the magnetosphere. Little is known about them and the theoretical status is very poor. The Soviets and French have significant research programs.

1.3.2 No exciting brief for any potential military applications can be given at this time. On the other hand, it cannot be said that WPI's will never be important. The data base is too poor.

- WPI's affect the magnetosphere-ionosphere coupling at high latitudes and will be essential for development of a high-latitude ionosphere. The military importance of this is yet to be defined.

- WPI's through cold plasma releases do not look promising for reducing the amount of high energy trapped betas or for producing communication blackout.
- The use of chemical releases for deliberate stimulation of ULF and VLF amplifications to transmit information and for jamming holds no promise.
- Previous barium releases show that a cold plasma injection to investigate VLF amplification can be made. No past data will help resolve how interesting it will be and there is no use in additional study of the old data.
- All previous satellite experiments are lacking in key data to help determine the conditions for useful ULF and VLF experiments. There is agreement that natural WPI events do occur at VLF and probably at ULF. Additional study of the old data such as OGO-5 will not assist in resolving any of the key problem areas.
- The sensors for a potential satellite experiment for WPI interactions from lithium and barium releases can be planned. It will cost far more than the naive cost estimates floating around. However, one does not know the conditions, geometry, etc., to properly define a satellite experiment.
- In principle a satellite experiment is last in the sequence of experimental events. One should go through a series of rocket and ground experiments to prove the desirability and to define the details for a satellite experiment. Planning experiments for WPI has suffered from a continued effort to initially jump to the ultimate satellite experiment or to orbit a potpourri of ill-related spare equipment sitting on shelves.

1.4 FURTHER RESEARCH REQUIREMENTS

1.4.1 Ionospheric Models

An analysis of how WPI's affect the characteristics of the high latitude ionosphere needs to be made to determine its significance and to establish whether there is a justification to perform chemical releases for this application.

1.4.2 Nonlinear Theoretical Studies

Nonlinear theoretical calculations are needed for ULF and more is needed for VLF.

1.4.3 ULF Amplification

The first experimental step for a chemical release of lithium to investigate ULF amplification needs to be defined. This should be a minimal experiment to advance one stage in our knowledge and not to try to specify the ultimate experiment. Consideration should be given to the GEOS Satellite to be launched in July 1976.

1.4.4 VLF Amplification

The needed experimental step for a chemical release of barium to study VLF amplification needs to be defined. Attention should be given to the other on going VLF experiments, such as GEOS, ARAKS, Siple, etc.

1.5 REFERENCES

McCormac, B. M., and J. E. Evans, "Summary of the Second Magnetospheric Wave-Particle Interaction Workshop," February 1973, Lockheed Palo Alto Research Laboratory, LMSC D313118, 1973.

Chapter 2

CHEMICAL RELEASES FOR THE PRODUCTION OF ARTIFICIAL EFFECTS IN THE MAGNETOSPHERE

S. Mende

2.1 INTRODUCTION

The controlling of the magnetospheric environment would permit the utilization of some magnetospheric effects for defense purposes. The magnetospheric energetic particles environment is strongly dependent on conditions arising after high altitude bursts. If methods could be found in which the magnetospheric radiation belts could be artificially depleted, new types of defense and offensive capabilities could be developed. The dumping of magnetospheric particles into the atmosphere is governed by wave particle interaction. The magnetospheric waves control the entry of particles into the loss cone and the removal of the trapped radiation in the atmosphere. The frequency range of waves which have interactions with electrons is in the VLF range, whereas the proton wave interaction takes place in the ULF range. Because of the interest in using VLF and ULF for communication, the magnetospheric ULF/VLF amplification is of some considerable interest.

For the investigation of the possibility of controlling the magnetosphere artificially, several attempts have been made. Some of these use wave injection. For example, the Siple VLF transmitter has been used to demonstrate the artificial triggering of magnetospheric waves (Helliwell, private communications, 1973). Whether or not detectable changes take place in the particle environment due to such VLF injection has yet to be verified. Another method is the injection of particles in the form of hot or cold plasma.

Amongst the cold plasma experiments, two show the most promise for magnetospheric experiments. In one of them (AEC code named OOSIK), the barium shaped charge has been released from low altitude rocket. This

experiment was performed during a reasonably disturbed period and its effects could not be distinguished from natural occurrences. In this experiment, the shape charge technique was used. The technique uses an explosive driven chemical shaped charge usually of barium. The generated barium jet can have velocities up to 12-15 km per second and thus it can reach several thousand kilometers in a reasonably short time. Low altitude rockets can be used to release the barium shaped charge and the barium jet will climb to high altitudes where it can produce effects on a large portion of a field line. In these experiments, barium is chosen because it ionizes reasonably rapidly when illuminated by solar UV. Barium metal is suitable for another reason because its thermodynamic properties make it ideal for use in a shaped charge. Cornwall (1972) has discussed the necessity of using lighter metals than barium to create maximum magnetospheric wave particle effects. Lithium was suggested as a suitable candidate for such releases. Unfortunately, lithium is unsuitable for shaped charges (Michel, private communication, 1973).

The alternative to the shaped charge release and vaporization is the in situ release from a cannister containing the metal and chemicals for a suitable thermite reaction. This technique has been used for numerous low altitude Ba releases and for some high altitude releases. In March 1969, a cannister was deployed from the HEOS satellite at some 12 earth radii distance, and a weak Ba cloud was formed. Because of the weakness of the distant cloud, very little diagnostic information could be gathered from this experiment. Much more extensive preparations preceded the 1971 September 21 Scout experiment, and therefore the body of data available from this experiment provides a useful base to evaluate in situ magnetospheric releases.

2.2 THE BIC (BARIUM ION CLOUD) PROJECT OF SEPTEMBER 21, 1971

The September 21, 1971 barium was carried to altitude by a 4-stage Scout rocket and the barium was released at some 32,000 km altitude close to a field line of L = 7.2. The cloud was monitored from several stations in the continental U.S., in Chile, South America, and from islands off the African coast. Many photographs were taken of the barium cloud. These observational results are summarized by the articles by Adamson et al. (1973) and Mende (1973).

The most startling feature of these observations is that the cloud was seen to fracture into small striations. At first the ionized plasma expanded along the magnetic field line with the velocity which was somewhat greater than the neutral expansion velocity. There was some evidence of acceleration of the cloud along the field line. Perpendicular to the magnetic field, the expansion of the cloud was limited by the forces exerted by the earth's magnetic field. The cloud took up a field aligned filamentary structure. These filaments, otherwise known as striations, were created as early as 30 secs after release. These striations are more diffuse than the central core of the cloud and they move with a velocity different to that of the main cloud. This differential velocity moves the striations away from the main core. During the first 8 mins after release, the high density main core part eroded to a very narrow strip of 12 km in width. This is less than the diameter of the gyro-orbit of the initial velocity barium ions in the ambient magnetic field. A few minutes after release when the cloud becomes optically thin, it is also non-diamagnetic. The rapid fragmentation of the cloud to such narrow forms has interesting implications on the stability of dense magnetospheric plasma clouds, even of natural origin. It should also be noted that any artificial cold plasma injection experiments has to reckon with the possibility of the cold plasma cloud breaking up into small filamentary structures of the order of 1 gyro-diameter width.

2.3 DISCUSSION OF INSTABILITIES

Because of the overwhelming importance of the stability of cold magnetospheric clouds, the discussion of possible instabilities is in order. This discussion is given in spite of the fact that there is no clear picture yet of which instability is the most important in explaining the barium cloud observations.

A summary of the cloud behavior has been given by a previous report, McCormac and Evans (1973). During the early phases of the cloud lifetime, the plasma of the cloud was strongly diamagnetic, i.e. the magnetic pressure due to the barium was much above the ambient field pressure. Any striations which are formed during this time could be caused by a type of flute instability (Pilipp,1971) which occurs due to the deceleration of the barium plasma as its expansion is braked by the ambient magnetic field. During this time, the plasma undergoes its initial expansion to form the cloud. Such an instability is analogous to the gravitational instability described by Rosenbluth and Longmire (1957). In the growth rate expression, however, one would have to replace the gravitational acceleration with the deceleration of the expansion against the magnetic field.

Highly diamagnetic plasmas are unstable and even when there are no decelerating forces. One might follow Longmire (1963) in considering the stability of a very highly diamagnetic plasma configuration. In this case, the instability is associated with the fact that the curvature of the magnetic field becomes larger at the crest of any perturbation. Hence, a weakness is developed in the field and if the plasma pressure and field pressure were previously in equilibrium, then the weak field will have to give and thus the plasma will expand. Since the crests are able to expand from the dense plasma and the troughs will contract, a process which is an instability is produced. As we have discussed, the BIC cloud had a very small radius and thus only a single flute is used in the Longmire (1963) expression for the growth rate. Using the proper substitution, the growth times are about 60 secs.

Mende (1973) has shown that the cloud became diamagnetically weak minutes after its creation. Thus, none of the above highly diamagnetic instabilities apply to striations which are developed at later times. The evidence that even the weak barium cloud generated striations is very important, especially if we consider natural weak plasma clouds in the magnetosphere. There are such plasma clouds mainly caused by the detachment from the plasmasphere (Chappell, 1972). Recently (Chappell, private communication , 1973) evidence is developing that these detached regions are indeed striated. If cold plasma is as important in causing precipitation through wave particle interaction as it is suppose to be, then one might speculate that auroral precipitation is caused by cold plasma interaction. Furthermore, one might suppose that auroral structure is caused by the highly structured cold plasma controlling the wave particle interaction and its ensuing precipitation.

Suggestions have been made that the striations in the high altitude cloud, such as BIC, are similar to the striations caused in atmospheric barium releases. So far no good theoretical model has been postulated to show that the low altitude mechanism could be effective. If one were to take the high altitude barium cloud and disregarded its interaction with the ionosphere, then there would be no suitable deceleration or drag forces to account for striation formation. The reader should be reminded that all the theories involving striation production in low altitude plasma clouds use the E/B drift instability (Simon, 1963; Linson and Workman, 1970; Simon, 1970; Völk and Haerendel, 1971). The basis of all these theories is the fact that collisions with the neutrals at low altitudes generate currents which are perpendicular to the field line. These currents determine the electrostatic field distribution in and around the cloud. Denser parts of the cloud have higher electric conductivity and thus they tend to short out the electric fields. Because of this, differential motion between the higher and low density parts is observed. Thus, in drifting clouds, the denser portions attach themselves to the neutrals more then the weaker portions and the hind parts of the moving cloud become unstable.

In the high altitude ion cloud there are no currents perpendicular to the magnetic field which could be used to discharge the electrostatic polarization fields, thus this type of instability cannot work at all.

If we include the whole of the magnetic field line containing the cloud and its regions within the ionosphere where cross conduction is possible, a somewhat different picture arises. This is illustrated on Fig. 2.1. The cloud is moving in a direction perpendicular out of the paper. The polarization charges are represented on the cloud which are created by the electric field associated with the motion of the cloud. Estimates such as Mende (1973) show that the cloud mass is approximately 100 times as much as the total ion content of the field tube. The ion cloud will therefore move the entire plasma content of the field line with it approximately at its own velocity. The time taken to establish this situation is of the order of the time for an Alfven wave to pass from the equatorial point to the end of the field line. Using a simple field model, this time is about 24 secs. Scholer (1970) discusses the possibility of reflections at the ionosphere and a gradual deceleration of the plasma cloud. However, a few reflections of the Alfven waves at the ends of the field lines should make sure that all transient effects disappear. After that the entire field tube should move with a quasi-constant velocity with the barium cloud. The time taken for the plasma cloud and its field line to decelerate is the time taken for the current loop (going down to the field line across the ionosphere and up to the cloud again) to discharge the polarization charges associated with the plasma cloud. The energy of the plasma cloud will be then dissipated through the Pedersen current in the ionosphere completing the current flow.

From this simple model, one can easily calculate a deceleration time. The density of the cloud was 1.3×10^4 per cc at about 4 mins after release. Its length was about 200 km and the width was about 15 km. The RC time constant of the discharge of the capacitors created by the plasma cloud can be calculated. If the height integrated Pedersen conductivity

of the ionosphere is taken as 1 mho centimeter, then this time constant comes out to be about 5,000 secs. This result is in good order of magnitude agreement with the observations.

Returning to the consideration of instabilities, it is difficult to see how the ExB instability has anything to do with the striation formation. If we perturb the ion cloud at the high altitude and examine how the perturbation develops, we should find no effect. This is because the discharge current and the corresponding drift instability should develop in the ionosphere but this ionosphere is presumably uniform and there is no reason why the non-uniformity at the cloud should impress itself on the ionosphere. Thus, provided the ionosphere is uniform, the instability will not develop.

One serious possibility suggests itself if one abandons the restriction of the uniform ionosphere. In qualitative terms, the presence of the cloud would generate an electric field and a consequent drift motion in the ionosphere. The ionosphere would then striate according to the ExB instability as discussed by numerous authors. The differential drifts which are caused in the ionosphere due to the differential ion densities are then impressed upon the original cloud and we can see striations there. It is impossible to estimate the growth rate of such striations without knowing the initial density gradient in the ionosphere.

2.4 STATE OF THE MAGNETOSPHERE DURING THE NASA/MPI (BIC) BARIUM RELEASE

Very little weight was given in setting the launch criteria to the geomagnetic environment at the time of release. Much of the geophysical data accompanying this release is discussed by Davis et al. (1973) and by Mozer and Carpenter (1973). The geophysical environment can be well described from using the standard magnetometer observatories and satellites which are at relevant places at the time of release. Specialized measurements were carried out at the time of the release near the foot of the field line which was close to Great Whale River. These experiments at Great Whale River included auroral all-sky cameras, magnetometers, HF auroral radar, ionosonde, and 13 MHz, 21 MHz and 30 MHz riometers.

At the time of the barium release, a magnetosphere was very quiet and has already recovered from an early storm which began during September 17, 1971 (see Fig 2.2). From the magnetograms collected, one can see that there have been magnetospheric substorms on September 20, 1971 near 1200 hrs, 1600 hrs, 1930 and 2315 hrs. A small substorm appeared near 0130 on September 21, which preceded the release by 1.5 hrs. (Fig. 2.3). However, this was a very small storm and the activity was very low during the time of the barium release. The activity continued to decrease and after release it was very low until about 0630 when a small substorm occurred. This substorm is also evident from the ATS-5 data.

The ATS-5 was in synchronous orbit approximately at the release altitude about 1 hr local time westwards from the release. The UCSD plasma experiment was measuring the plasma continuously during these periods and the results for September 20 and 21 are presented on Fig. 2.4a, b, c and d. (courtesy of C.E. McIlwain). Note that the satellite is at midnight at about 0600 UT and thus its most sensitive in detecting substorms around that period. Prior to 6 o'clock, it is most sensitive in detecting the proton injections which are drifting westwards and after 6 o'clock, it is most sensitive to electron injection because of the eastward drift of electrons. Bearing this in mind, the ATS-5 is an excellent indicator of

substorms, especially substorms occurring near the field line of the barium cloud. Substorms can be extrapolated (McIlwain, 1972) on the September 21st from both the perpendicular and parallel proton spectrums. If the proton cloud traces are extrapolated towards the maximum energy, it can be seen that they intersect at around 1:30 representing the substorm previously mentioned. At the time of release at 3:05, these protons appear to be present on the ATS field line. The rising slope of the proton cloud traces are due to the fact that the more energetic protons drift faster and arrive to the observer quicker while the slower ones arrive later. Thus, each trace is the remain of a substorm injection which occurred at the extrapolated point. The ATS-5 data also draws our attention to a substorm occurred around 6:30 on the 21st which is mainly evident in the electrons.

In Fig. 2.4a and b the parallel and perpendicular spectra is shown for the previous day, the 20th of September 1971. This preceding day is somewhat more active then the day of the release, Fig. 2.4e and d. At the time of the release marked with R, the ambient energetic particle population consists mainly of protons. There are a few high energy electrons but hardly enough to provide any significant effect even if they were totally dumped. Because of the narrowness of the cloud, there appears to be no reasons why the protons should be effected.

The Great Whale River magnetogram shows a small positive bay extending from 1800 on the 20th of September to 0250 on the 21st of September. This positive bay occurs during a small substorm evident also on the rapid run magnetograms and delta H is near zero or slightly positive just prior to release and up to 0400. If the baselines which are used are assumed correct, then one can represent this by ionospheric line current, an eastward current just south of Great Whale River at the time of release. A minor variation at 0252 was correlated with the VLF burst recorded at burst station (Mozer and Carpenter, 1973). This event was finished before the release at 0305.

There are no magnetic signatures attributed to the barium cloud. The sky was cloudy at Great Whale at the time of release, but from photometry measurement, some weak auroral activity was determined. None of these, nor the auroral radar returns, could be attributed to the barium release. The riometers also showed absorption of .7 - .9 db throughout the release period. This absorption was not seen in 20 MHz and 38 MHz riometer records. This could be an indication of the ionization density or that these temporary riometers were not set up properly. The minor event at 0252 was recorded by the riometers. The ionosondes indicated weak activity after 0045 on September 21, 1971. This weak activity and all the other data seems to suggest that there was indeed some precipitation at Great Whale River at the time of release and thus the magnetospheric trough region which is observed before 0045 UT must have moved southward.

During the time of the BIC high altitude release, electric field measurements were carried out at the foot of the field line containing the cloud. The electric field measurements are discussed by Mozer and Carpenter (1973). The balloon electric field measurements disagreed with the field measurements obtained in the magnetosphere by motion of the Ba cloud and motion of the VLF whistlers. These discrepancies could be due to the different spatial locations of the measurement or some field aligned electric fields. The electron density was found to be 38 ± 16 el/cc at $L = 4.5$. Extrapolating this to the BIC cloud altitude, the electron density was estimated to be 16 ± 7 el/cc. This estimate could be an order of magnitude wrong because of the structure of the plasmasphere (Chappell, 1972).

The only measure of direct precipitation near the foot of the magnetic field was by balloon x-ray detectors. The curve obtained by the balloon x-ray detector is shown on Fig. 2.5. Note that the altitude of the balloon reached 28 km only at 0330, 25 mins after release. (28 km is the altitude at which the attenuation factor is about 10.) Prior to this the x-ray detectors were insensitive to x-rays.

2.5 CONCLUSION

In order to investigate ULF-VLF waves and their interaction with energetic magnetospheric particles, cold plasma injection seems to be a promising method.

The best diagnosed in situ experiment was the NASA/MPI September 21, 1971 barium release near synchronous altitude.

The rapid striation formation in this cloud implies that cold plasma clouds are essentially unstable in the magnetosphere. In the early diamagnetic phase several mechanisms could be responsible for the striation generation. Later, however, there is evidence that the cloud is too weak to be diamagnetic. During this later phase (few minutes after release) the striation formation is not clearly understood. It could be caused by an ExB instability operating in a non-uniform ionosphere or it could be caused by some instability associated with the coupling mechanism between the ionosphere and magnetosphere.

The magnetosphere was a few days after a magnetic storm at the time of the release. There were several weaker substorms preceding the release. Looking at the ATS-5 synchronous altitude satellite, fairly close to the release point the energetic particle environment can be well established. The ATS-5 shows complete absence of electrons in the energy range of 200-15,000 eV. Since the barium cloud was only a few kilometers in diameter, much less than the proton gyro-diameter, one would have only expected electron VLF interaction. Although there were some protons present (remains of the 0130) injection theoretically one does not expect any precipitation or significant interaction with the narrow ion cloud.

There were no significant measurements at the foot of the field line since photometry was hindered by clouds and the x-ray balloon was not at altitude at the significant time.

2.6 REFERENCES

Adamson, D., C.L. Fricke, S.A.T. Long, W.F. Landon, and D.L. Ridge; "Preliminary Analysis of NASA Optical Data Obtained in Barium Ion Cloud Experiment of September 21, 1971," J. Geophys. Res. 78, 1973.

Chappell, C.R.; "Recent Satellite Measurements of the Morphology and Dynamics of the Plasmasphere," Rev. Geophys. Space Phys., 10, 951, 1972.

Chappell, C.R.; Private communication, 1973.

Cornwall, J.M.; "Precipitation of Auroral and Ring Current Particles by Artificial Plasma Injection," Rev.Geophys.Space Phys., 10, 993, 1972.

Davis, T.N., G.M. Stanley and J.S. Boyd; "The Geophysical Disturbance Environment During the NASA/MPI Barium Release at 5 Re on September 21, 1971," J. Geophys. Res., 78, 5732, 1973.

Helliwell, R.C.; Private communications, 1973.

Linson, L.M. and J.B. Workman; "Formation of Striations in Ionospheric Plasma Clouds," J. Geophys. Res. 75, 3211, 1970.

Longmire, C.L.; Elementary Plasma Physics. Interscience Monographs and Texts in Physics and Astronomy, Vol. IX, Ed. R.E. Marshak; Interscience Publishers, New York, pp. 241-249, 1963.

McCormac, B.M. and J.E. Evans, "Summary of the Second Magnetospheric Wave-Particle Interaction Workshop," February 1973, Lockheed Palo Alto Research Laboratory, LMSC D315118, 1973.

McIlwain, C.E.; "Plasma Convection in the Vicinity of the Geosynchronous Orbit," Earth's Magnetospheric Processes, Ed. B.M. McCormac, D. Reidel Publ. Co., Dordrecht-Holland, pp. 268-279, 1972.

Mende, S.B.; "The Morphology of the Magnetospheric Barium Release," J.Geophys. Res., 78, 5751, 1973.

Michel, F.W.; Private communication, 1973.

Mozer, F.S. and D.L. Carpenter; "Balloon and VLF Whistler Measurements of Electric Fields, Equatorial Electron Density, and Precipitating Particles During a Barium Cloud Release in the Magnetosphere," J. Geophys. Res., 78, 5736, 1973.

Pilipp, W.G.; "Expansion of an Ion Cloud in the Earth's Magnetic Field," Planet. Space Sci. 19, 1095, 1971.

Rosenbluth, M.N. and C.L. Longmire; "Stability of Plasma Confined by Magnetic Fields," Ann. Phys. N.Y. 1, 120, 1957

Scholer, M.; "On the Motion of Artificial Ion Clouds in the Magnetosphere," Planet. Space Sci. 18, 977, 1970.

Simon, A.; "Growth and Stability of Artificial Ion Clouds in the Ionosphere," J. Geophys. Res. 75, 6287, 1970.

Simon, A.; "Instability of a Partially Ionized Plasma in Crossed Electric and Magnetic Fields," Phys. of Fluids 6, 382-388, 1963.

Völk, H.J. and G. Haerendel; "Striations in Ionospheric Ion Clouds," J. Geophys. Res. 76, 4541, 1971.

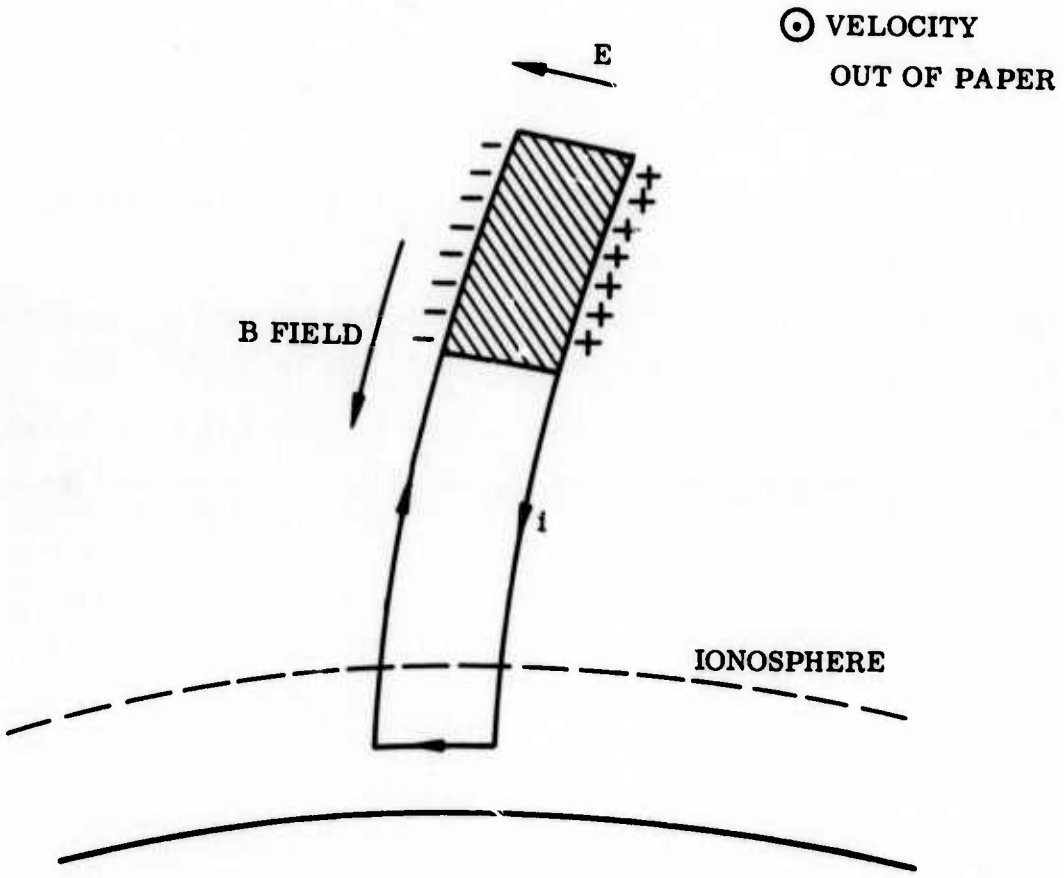

Figure 2.1 The high altitude barium cloud and the ionosphere, a schematic view.

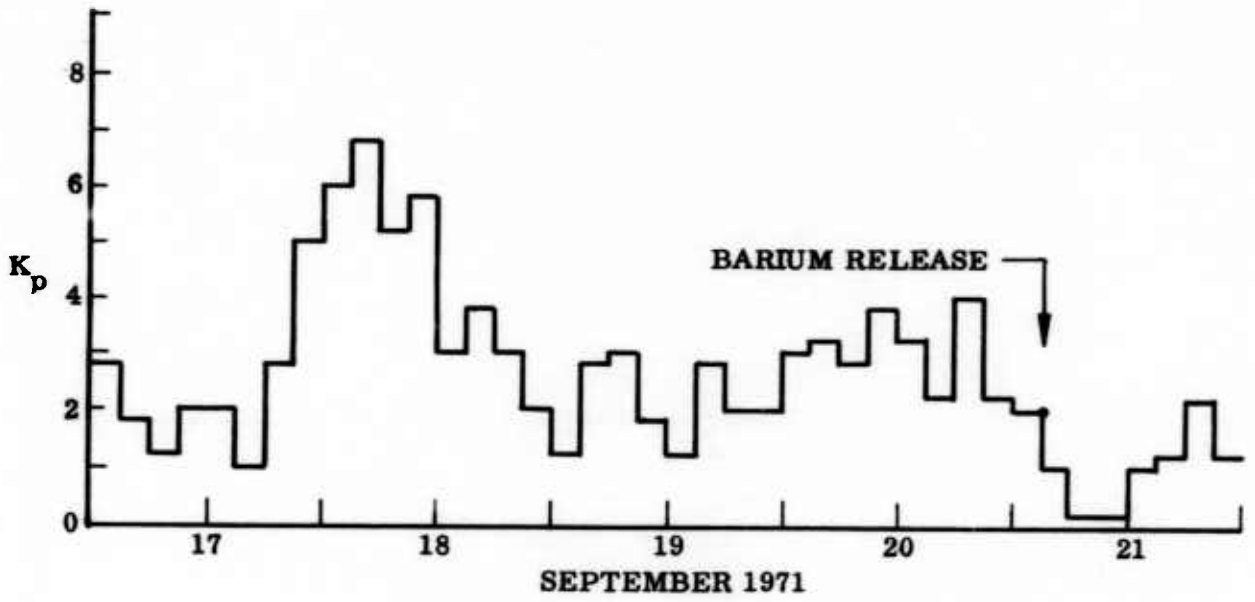

Figure 2.2 Planetary Kp indices for the period 17 through 21 Sept. 1971.

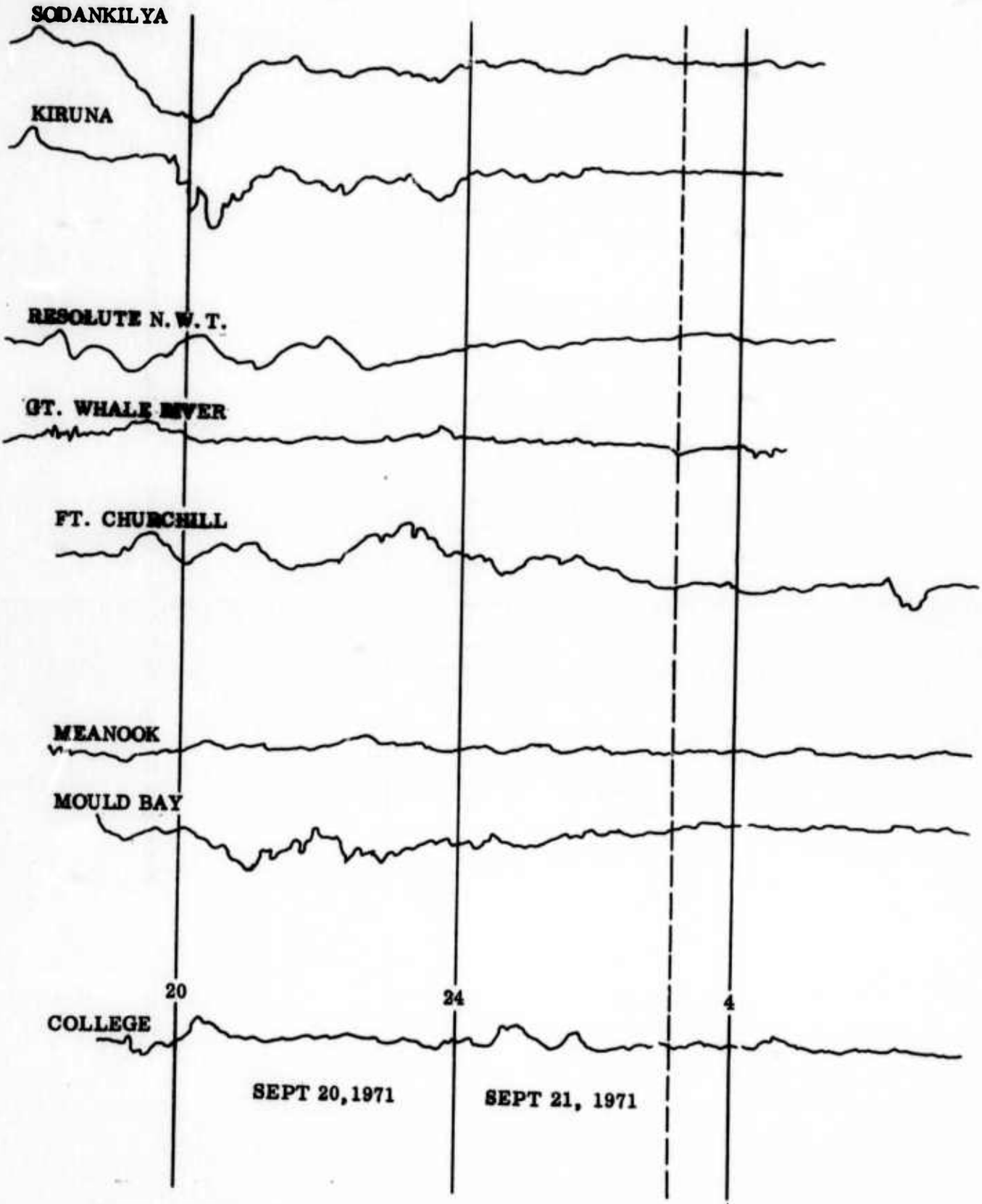

Figure 2.3 Auroral zone magnetograms at times near the release experiment. The time of release is indicated by the vertical dashed line.

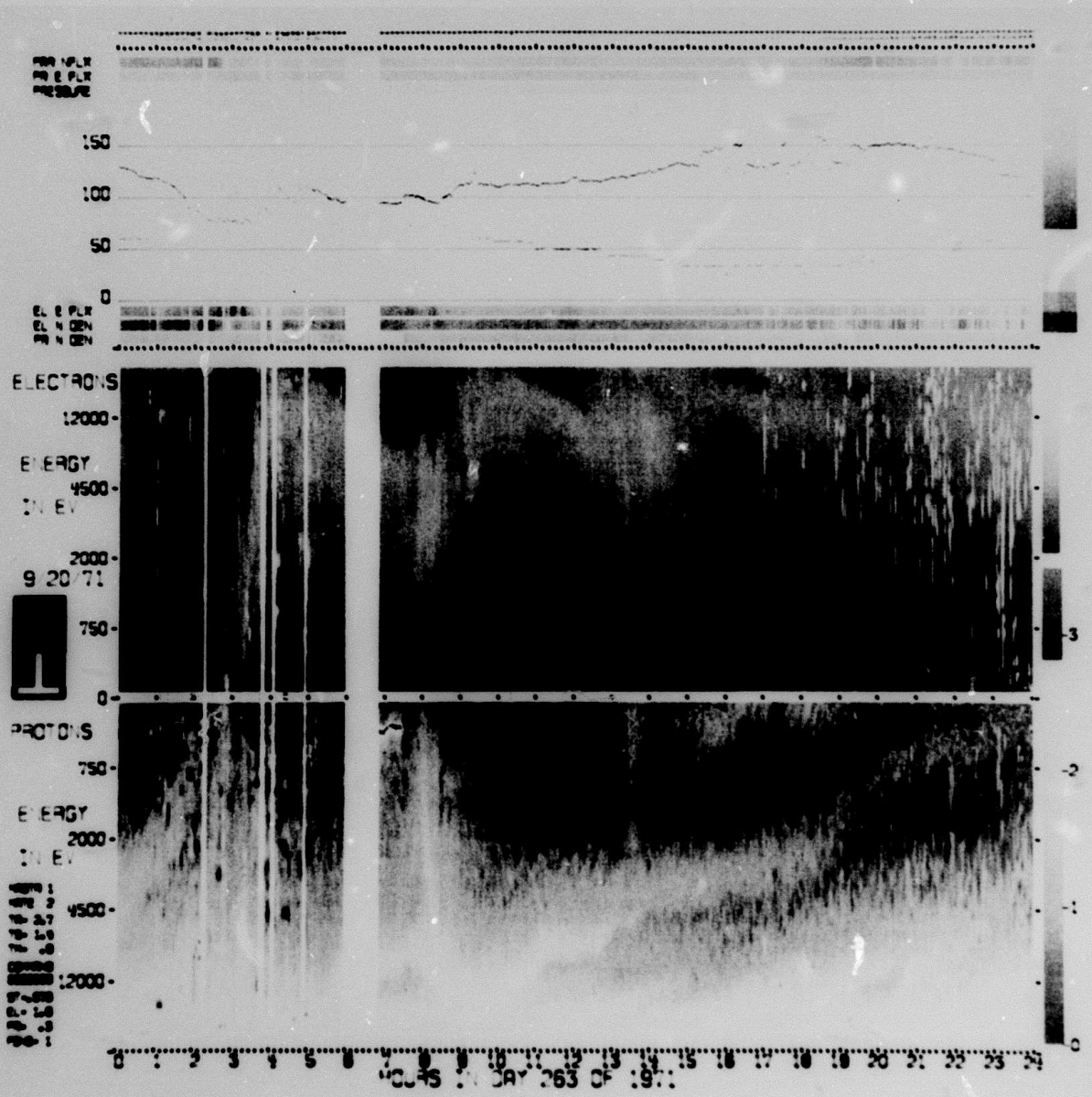

Figure 2.4a

ATS-5 particle spectrogram for 20th September 1971. Electrons and protons measured perpendicular to spacecraft axis.

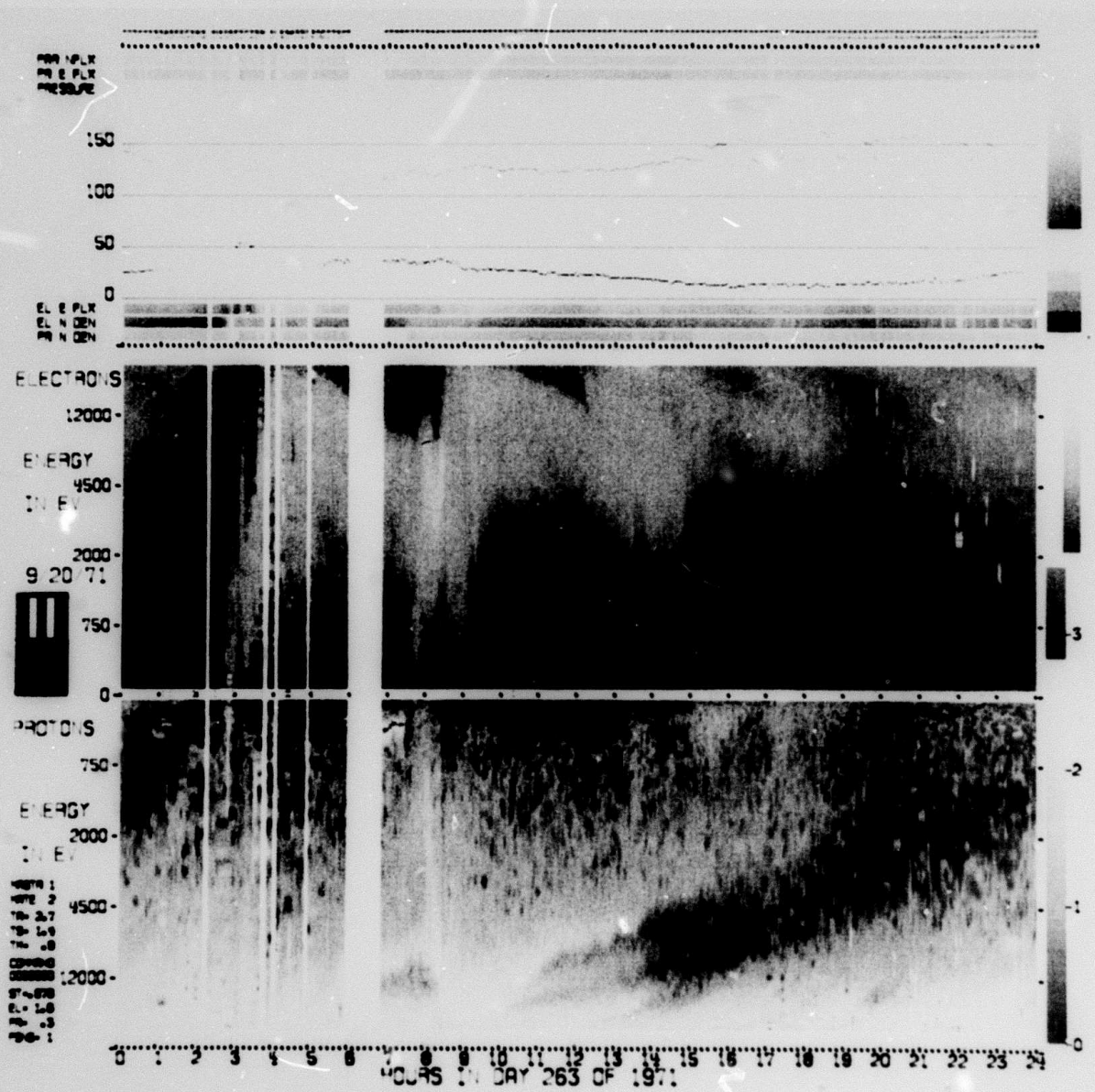

Figure 2.4b

ATS-5 particle spectrogram for 20th September 1971. Electrons and protons measured parallel to spacecraft axis.

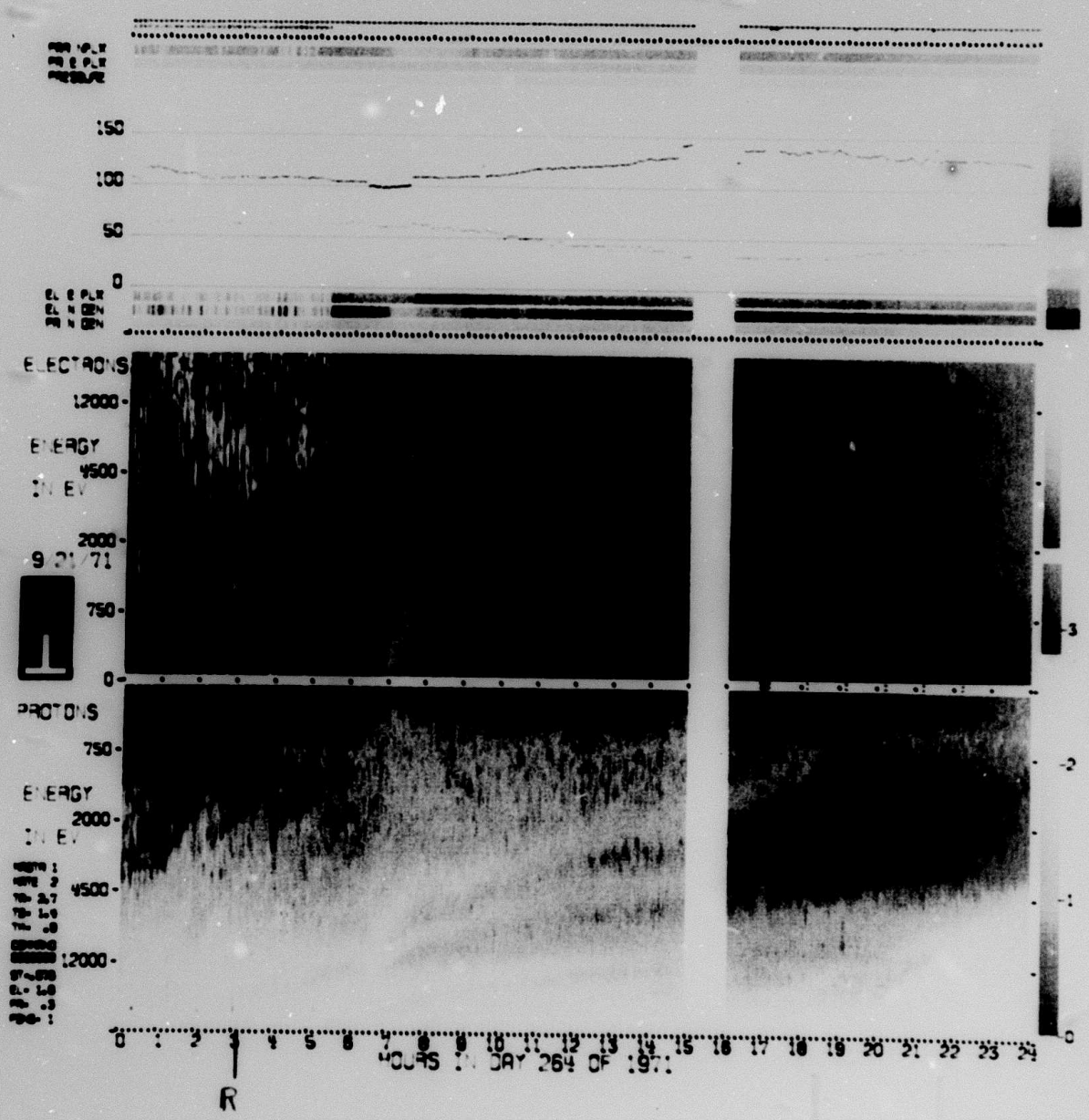

Figure 2.4c

ATS-5 particle spectrogram for 21st September 1971. Electrons and protons perpendicular to spacecraft axis. BIC release is denoted with R.

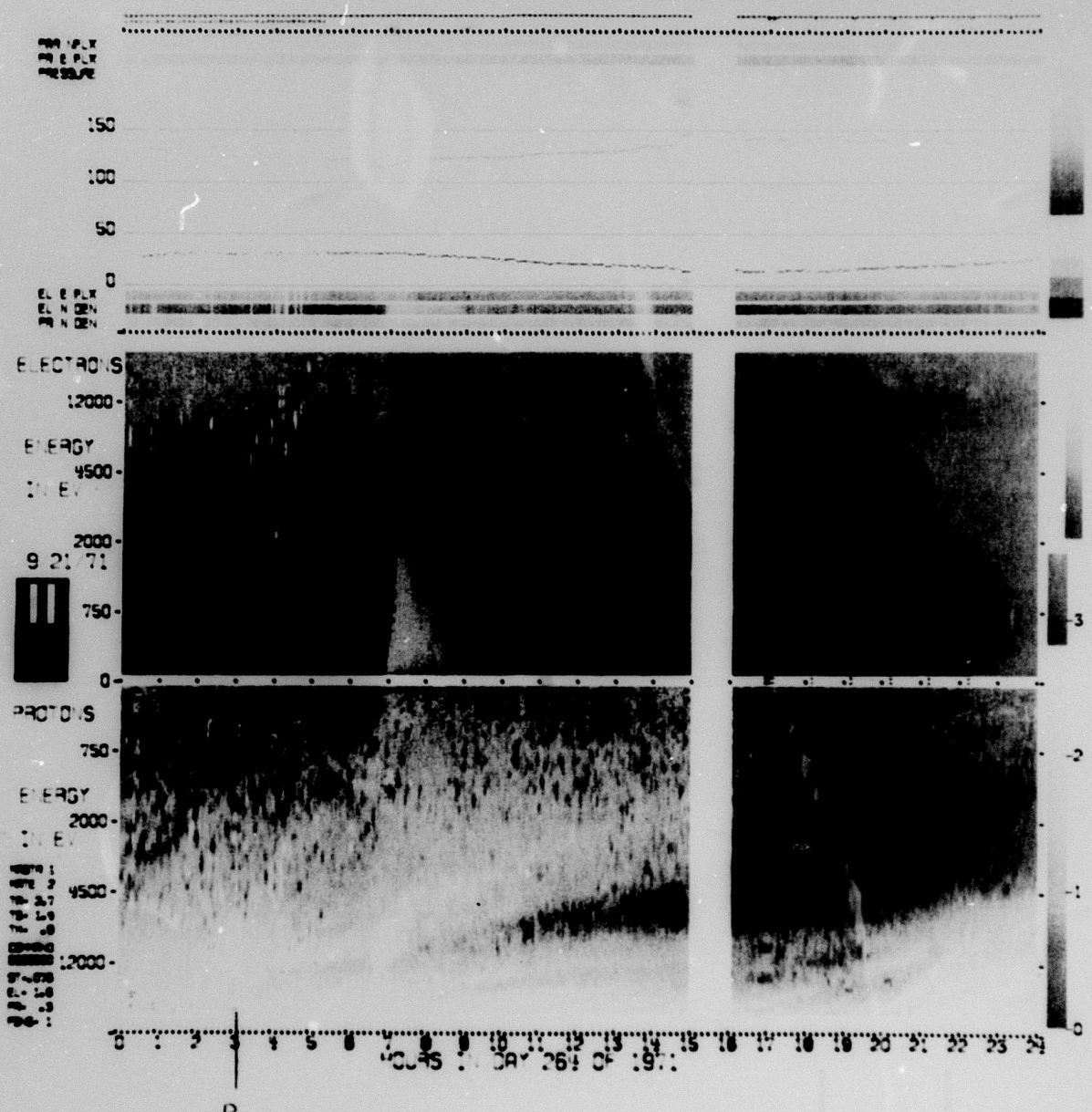

Figure 2.4d

ATS-5 particle spectrogram for 21st September 1971 Electrons and protons parallel to spacecraft axis. BIC release is denoted with R.

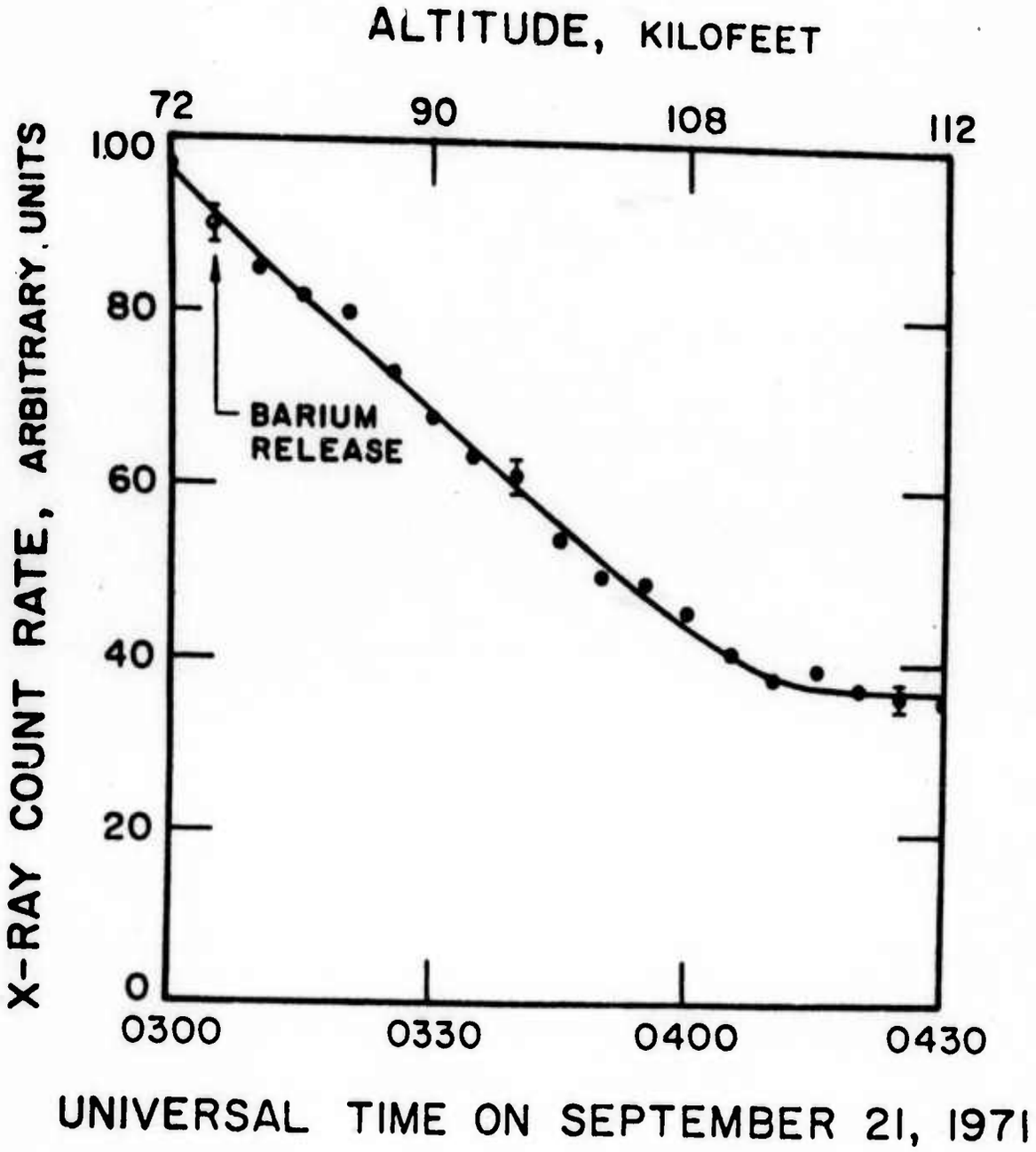

Figure 2.5 Balloon x-ray detector counting rates.

Chapter 3

OGO-5 OBSERVATIONS AND INTERPRETATION

C. R. Chappell

The study of a few cases from OGO-5 has shown that there is wave generation directly correlated with the detached plasma regions and this wave generation is found only inside the regions where the cold plasma density exceeds several particles cm^{-3}. These preliminary results give some indication that the injection of sufficient densities of cold plasma (protons and electrons) into a region of energetic electrons whose fluxes are near the stable trapping limit will result in the generation of ELF (40 to 120 Hz) waves.

In particular, the correlated studies of the Lockheed light ion mass spectrometer, the UCLA search-coil magnetometer (not at ULF), the UCLA energetic particle detector, and the UCLA fluxgate magnetometer data in the enhanced density regions have given the following information:

1) When the satellite entered regions of enhanced cold plasma density, ELF waves of frequencies 40 - 120 Hz are found.

2) When the observed waves are at frequencies which are resonant with the > 50 keV electrons (as measured by the UCLA experiment), these observed electrons are found to have fluxes which exceed the stable trapping limit as predicted by theory. In cases where the > 50 keV electrons are resonant, and their fluxes do not exceed the stable trapping limit no ELF waves are observed.

3) The frequencies of the ELF waves are the expected frequencies which result from the Doppler-shifted electron cyclotron resonance interactions.

4) The ELF waves were right-hand polarized and were normally propagating within 30° of the magnetic field direction indicating that they may well be trapped (or ducted) in the enhanced plasma regions.

5) The peak power in the ELF waves is approximately 10^{-4} γ^2 Hz^{-1}.

6) There were no noticeable effects on the distribution of the energetic (> 50 keV) electrons in the detached plasma regions. This is to be expected since the drift time of the electrons through the cold plasma regions is of the order of a few minutes and the effective pitch angle diffusion time is of the order of an hour. We should point out that because of incomplete particle measurements we cannot exclude the possibility of enhanced particle precipitation among the lower energy protons and electrons which would certainly affect E and F region ionospheric modeling studies.

7) ULF waves of period 20 seconds were occasionally present. Their generation may be caused by the more energetic (> 100 keV) protons present in the trough region.

Of the cases studied there have been no observations of ULF waves of a few second period that are expected to be generated by the ring current protons. However, none of the cases studied have been equatorial measurements and the few second period waves which are expected to be generated at the equator may not propagate to the higher latitudes of the satellite.

Chapter 4

SPACECRAFT FLIGHT REQUIREMENTS

B. McCormac

Chemical releases should be useful for investigating WPI in the magnetosphere. A wide range of experiments and platforms may be employed. Proof that chemical releases seem useful might be obtained from a rocket release of a chemical supported by ground observations. The experimental technique can finally become so sophisticated that a large array of satellite observations are required before and after a satellite borne chemical release.

The spacecraft experiment is the most complicated and expensive and should be the last step in a series of increasingly complex experiments. It is difficult to finalize the design of a spacecraft experiment until the results of the preliminary experiments are in. For these WPI investigations, the requirements are changing faster than one can really design a spacecraft experiment. After additional effort is spent on theory and other studies and some preliminary experimental data are obtained, the experimental requirements for a spacecraft, ambient conditions, geometry, amount and distribution of chemicals, and the location and type of sensors will change drastically from those indicated by today's state-of-knowledge.

A spacecraft experiment will be expensive and it is important to assure that it will provide some positive answers. Even though the objectives of a spacecraft experiment are somewhat obscure the following constraints will apply:

1) The experiment must be performed beyond the plasmasphere, e.g. around synchronous orbit.

2) The only chemicals seriously considered for release are Li and Ba. The quantities and distribution volume needed requires more study. However, practical efficiencies and repeated releases should lead to a heavy payload. It is necessary to ensure that the chemical release does not contaminate the

satellite instrumentation. Each kg of chemical will require 2 to 3 kgs of containers, release and timing mechanisms, etc. Therefore it is hard to imagine a practical chemical payload less than 100 kg and it well may be much heavier.

3) At least 2 satellites are required to separate temporal and spatial effects. A single satellite cannot tell where particles, plasma, and waves are going after detection or where they come from. It is unrealistic to think that a satellite of opportunity already in orbit will provide the array of data needed to match the satellite launched under this program.

4) The following sensors are needed:

a. Energetic particles. Phase space distribution of electrons and protons from 0 to 100 keV.

b. Electric fields. DC and 10 to 10^5 Hz.

c. Magnetic fields. DC and 0.1 to 10 Hz plus higher frequencies if possible. The magnetic field sensitivity on the spacecraft should be 100 mγ at 0.1 Hz. Thus search coil magnetometers are required.

d. Thermal ions. Density, temperature and composition.

e. Spacecraft charging. At synchronous orbit spacecraft charging does occur and this will negate any thermal ion measurement as well as low energy energetic particles. The vehicle must be electrostatically clean and one must measure the charge on the vehicle.

Chapter 5

THEORETICAL ASPECTS OF TRAPPED RADIATION BELT MODIFICATION

G. Davidson

5.1 INTRODUCTION

A plasma can be unstable to the growth of waves if there are sufficient numbers of relatively energetic particles in resonance with the wave that can transfer their energy to the wave (Stix, 1962). In the case of whistler-mode waves travelling along the direction of an impressed magnetic field, the criterion which determines whether the waves can grow usually involves the anisotropy of the particles' velocity distribution. Electrons trapped in the geomagnetic field, concentrated at large pitch angles, are generally unstable to the generation of electron-whistlers — right-handed circularly polarized waves (Kennel and Petschek, 1966).

The wave growth instability criteria are modified by the presence of large numbers of relatively low energy charged particles; it is these particles which determine how waves propagate, and what the conditions are for resonance between the waves and energetic particles. It has been suggested by Brice (1970; 1971) that the generation of whistler waves could be enhanced by the injection of moderate amounts of plasma at nearly zero temperature. One application that suggests itself is the utilization of artifically generated whistlers for interhemispheric communications (Mc Cormac and Evans, 1973). Another application, with which we are mainly concerned here, is the modification and control of trapped radiation belts. Presumably the growth of waves takes up energy from charged particles and causes them to scatter out the ends of the "magnetic bottle" thereby affording a means of controlling the trapped particle population. If this concept were feasible, it might provide a means of depleting not just the natural trapped radiation belts, but the intense artificial radiation belts which can result from the high-altitude detonation of nuclear weapons.

Several independent studies (Cornwall, 1972; Cornwall and Schulz, 1973; Liemohn, 1972) have indicated that extremely large unstable wave

growth rates might be achieved through injection of cold plasma in the magnetosphere. Unfortunately there has been little or no experimental evidence to confirm the results of those studies (McCormac and Evans, 1973). A full-scale test would entail the injection of large amounts of barium or lithium at the most suitable locations, and would be a rather expensive undertaking. The intent of the study reported here is to examine some of the questions that have not yet been satisfactorily answered by the previous theoretical studies.

Our approach has been to consider some of the basic aspects of the problem without undue dependence on any particular model of the trapped radiation belts and the cold plasma cloud. We have considered in a qualitative way how the trapped electron's distribution would be altered by the growth of whistlers, and whether large numbers of electrons could be removed from the trapping regions; this topic is discussed in the following section (5.2). In section 5.3 we describe the results of an extensive study of the sensitivity of whistler wave growth to the various physical parameters of the plasma. A more complete description of this and related work is to appear under a separate cover (Davidson, 1973).

The results to be discussed presently tend to confirm that large growth rates are indeed possible but they are so sensitive to the velocity distribution of the trapped electrons that practical applications would seem to be ruled out at the present. The operational difficulties are mentioned in the concluding section 5.4.

5.2 THE PITCH ANGLE DIFFUSION OF TRAPPED ELECTRONS

A particularly useful way of viewing the interactions of whistler waves with fast electrons is to consider the paths the electrons must follow in velocity space. During a resonant interaction with a whistler, an electron's velocity component parallel to the magnetic field, $V_{\|}$, must satisfy the resonance condition (Brice, 1964; Kennel and Petschek, 1966).

$$V_{\parallel} = V_{\varphi} \frac{\omega - \Omega_e}{\omega} \tag{5-1}$$

where ω is the wave frequency, Ω_e the electron gyrofrequency, and V_{φ} the wave phase velocity. There is another condition on the velocity components; that is: the momentum (or velocity) in a reference frame moving with the wave must be constant (Kennel and Petschek, 1966; Gendrin, 1968). This second condition may be written

$$V_w^2 = V_{\perp}^2 + (V_{\parallel} - V_{\varphi})^2 \tag{5-2}$$

(The treatment here does not include relativistic corrections). A third equation relates the phase velocity to the wave frequency:

$$V_{\varphi} = C \sqrt{\frac{(\Omega_j + \omega)(\Omega_e - \omega)}{(\Omega_i + \omega)(\Omega_e - \omega) + \Omega_p^2}} \sim \sqrt{\frac{\omega(\Omega_e - \omega)}{\Omega_p^2}} \tag{5.3}$$

The ion gyrofrequency is denoted by Ω_i, and the plasma frequency by Ω_p. Eq. (5-1) and (5-3) are valid for right-handed electron whistlers when ω is positive, and for left-handed ion whistlers when ω is negative. Elimination of ω and V_{φ} leaves an equation in $V_{\parallel}$ and $V_{\perp}$ - the equation of the <u>diffusion trajectory</u>. The diffusion trajectories of relatively energetic electrons are nearly circular in $V_{\perp}$, $V_{\parallel}$ coordinates (Kennel and Petschek, 1966)(see Fig. 5.3 for example). This means that an electron loses little energy to whistler waves, but suffers a severe degradation of its pitch angle. The velocity space diffusion of trapped electrons is primarily <u>pitch angle diffusion</u>.

The diffusion trajectories can be used to formulate a convenient instability criterion. If electrons can go from one density contour in velocity space to a lower density contour while losing energy the plasma is unstable to growth of whistler waves. Fig. 5.1 shows how the density contours of trapped electrons might overlay the diffusion trajectories so that nearly all the electrons are unstable.

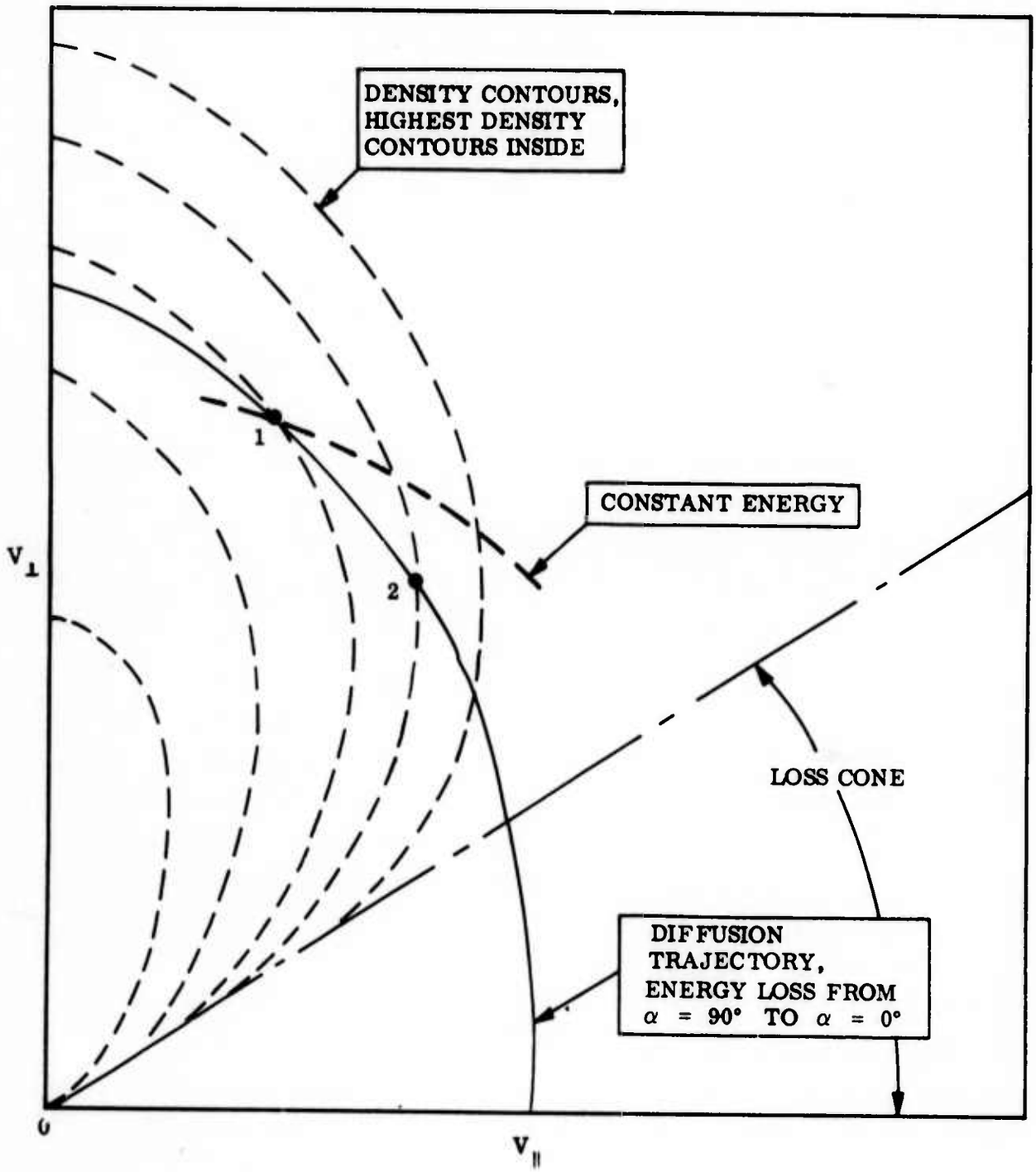

Figure 5.1 Density contours and diffusion trajectories in velocity space. A particle at point 1 could go down the density gradient to point 2 and suffer an energy loss. The plasma is therefore unstable to wave growth.

It turns out that an electron diffusing from a large pitch angle into the loss cone always suffers a loss of energy. The maximum energy loss from a 90° pitch to a 0° pitch angle is shown in Figure 5.2 as a function of a parameter which depends on the total electron density. It is convenient to let

$$Q = \frac{\Omega_p^2}{\Omega_e^2} = \frac{Nmc^2}{B_o^2/8\pi} \qquad (5\text{-}4)$$

where N is the electron density, and B_o the strength of the impressed magnetic field. The new parameter is obviously related to Brice's magnetic energy per particle, $B^2/8\pi N$ (1970, 1971). The abscissa, W, of Figure 5.2 is just $\sqrt{Q}$ times the velocity at 90°, divided by the speed of light. For small values of W the diffusion trajectories are highly elongated (along the $V_\perp$ axis) and not very favorable to instabilities. As W increases beyond 1 the diffusion trajectories rapidly approach a circular shape (which is unstable to growth of waves in a distribution of trapped electrons).

Now the effects of cold plasma injection can readily be imagined with reference to Figure 5.2. An increase in the total electron density shifts all the electrons to the right along the curve; in a trapped distribution this makes them less stable. It is just the electrons near W = 1 that are most sensitive to slight changes in the physical parameters of the plasma. These are the electrons which might be precipitated by cold plasma injection, but that might require one or even two orders of magnitude change in Q or N.

When temperature effects are included, the diffusion trajectories will drop sharply toward V = 0 at very large pitch angles. In Figure 5.3 are shown some representative diffusion trajectories for various values of the parameter

$$\beta \equiv QT/mc^2 \rightarrow \frac{N\langle E\rangle_a V}{B_o^2/8\pi} \qquad (5\text{-}5)$$

It is apparent from Figure 5.3 that the temperature effects become important

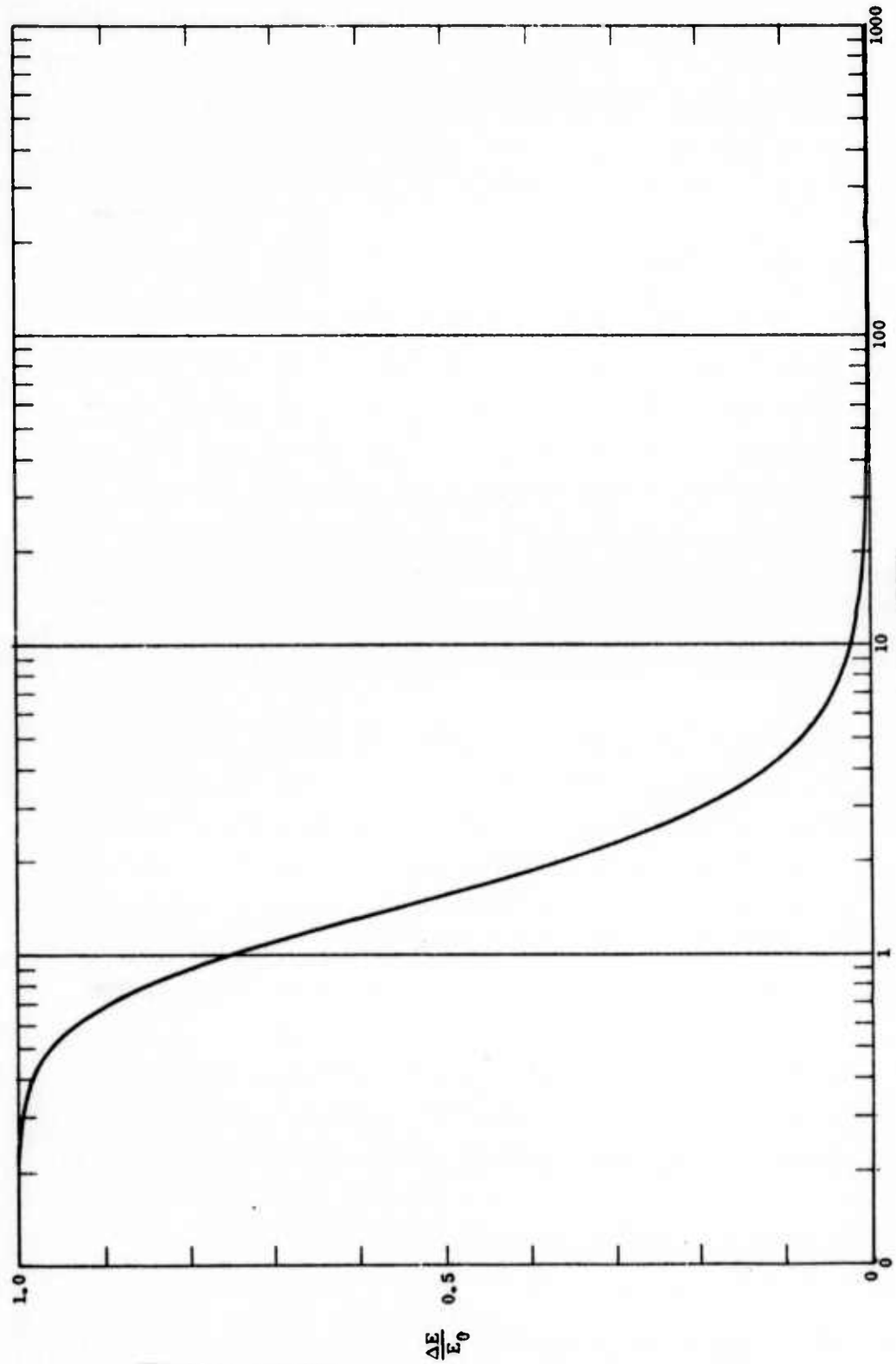

Figure 5.2 The energy loss of an electron diffusing under the influence of whistler waves from a pitch angle of 90° to a pitch angle of 0°. The abscissa is proportional to plasma density and to initial energy.

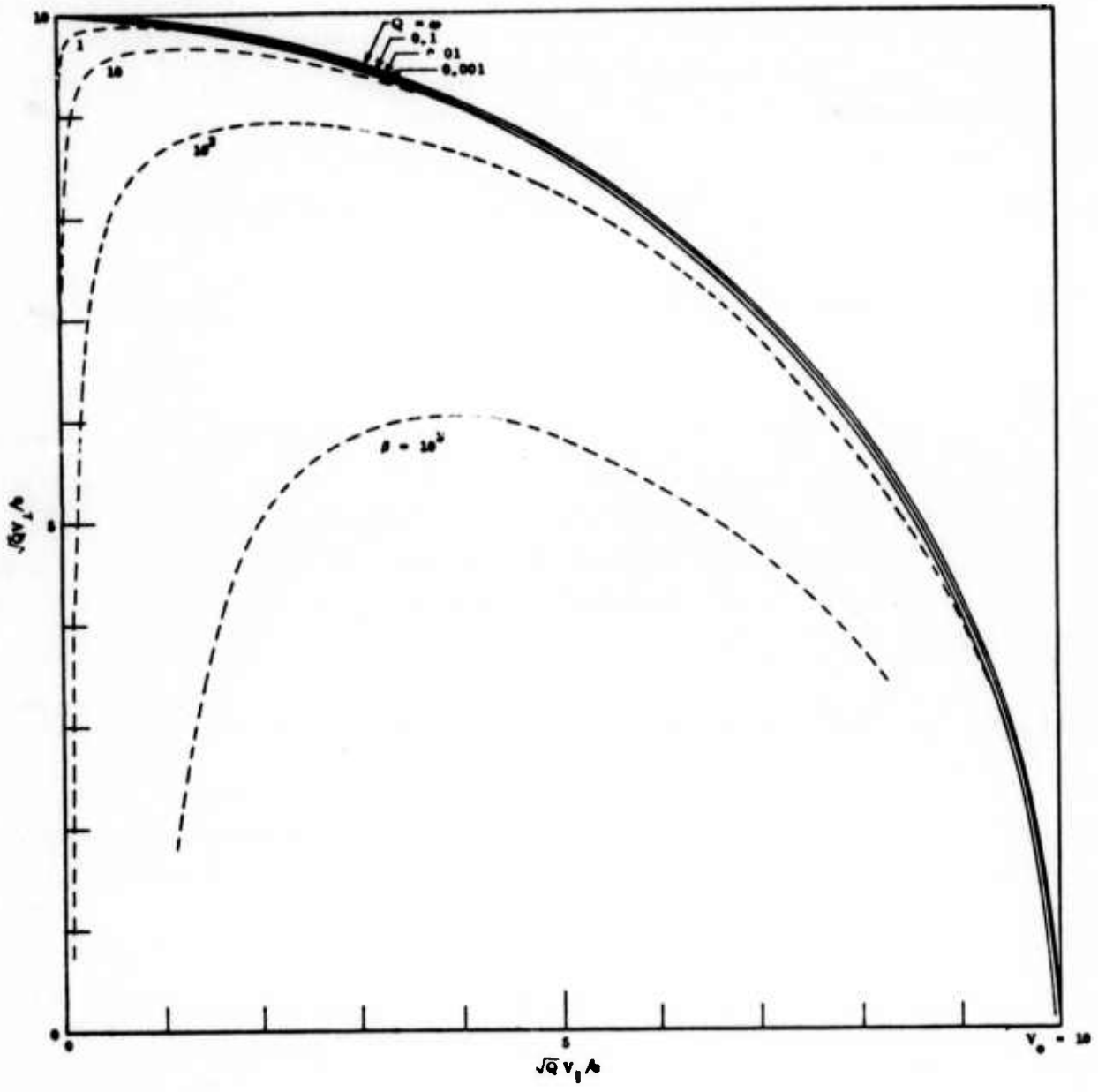

Figure 5.3 Some sample electron diffusion trajectories modified by high plasma temperatures; the labels on the curves refer to $\beta = QT/vnc^2$.

beyond some critical value of B. (Figure 5.3 is applicable to fairly high electron energies, in that case the critical β is unreasonably large.) As a rough estimate of the critical β we might say the temperature effects are important only when the diffusion trajectory bends over toward V = 0 at a pitch angle of 45°. When the diffusion trajectories are reduced to an elongated curve along the $V_{||}$ axis, all possibility of whistler-made instabilities disappears. The result is that there is no instability or diffusion of electrons with energies less than (Davidson, 1973)

$$E \leq 4\, mc^2 \frac{\sqrt{\beta}}{Q} \tag{5-6}$$

For the natural radiation belts, where the densities of "hot" electrons are far less than the densities of "cold" electrons, β is very small and the temperature effects are generally negligible. But it is possible for artificial radiation belts to have high enough values of β that the energy threshold of eq. (5-6) might be raised considerably above the upper limit implied by Figure 5.2.

5.3 THE GROWTH OF WHISTLER WAVES IN A PLASMA

The growth rate of whistler waves is the rate of increase of the wave amplitude. The appropriate formulae have been derived by other workers (Kennel and Petschek, 1966; Stix, 1962), and generally are proportional to an integral of the form (non-relativistic)

$$\int_0^\infty V_\perp dV_\perp \left[V_\perp \left[V_{||} \frac{\partial f}{\partial V_\perp} - V_\perp \frac{\partial f}{\partial V_{||}} \right] - \frac{2\,\omega V_{||}}{\Omega_e - \omega} f \right]_{V_{||} = V_\varphi \frac{\Omega_e - \omega}{\omega}} \tag{5-7}$$

The first term in the integrand - usually the dominant term - is proportional to a derivative of distribution function with respect to pitch angle; this is the term which is sensitive to the anisotropy. For the purpose of doing numerical computations we have found it convenient to change variables to

$$p = \sqrt{p_\parallel^2 + p_\perp^2}$$

$$\mu \equiv \cos\alpha = \frac{p_\parallel}{\sqrt{p_\parallel^2 + p_\perp^2}} \tag{5-8}$$

It is also convenient to reduce the frequency to a dimensionless parameters, $X \equiv \omega/\Omega_e$. The growth rate and amplification rate are equivalent; the amplification rate, δ, which we have computed is just the rate of change of wave amplitude with respect to distance. Finally, we have the amplification rate formula

$$Z \equiv \frac{\delta c}{\Omega_e} = -\frac{\pi^2\eta}{2} \frac{Q\sqrt{1-X}}{\sqrt{X[X(1-X)+Q]}} \int_{v_1}^{\infty} v\,dv \left\{v\left(1 - \frac{v_1^2}{v^2}\right)\right.$$

$$\left.\left[1 + \frac{X}{1-X}\frac{v_1^2}{v^2}\right]\frac{\partial \bar{f}}{\partial \mu} + 2\,v_1 \frac{X}{1-X}\left[1 + \frac{X}{1-X}\frac{v_1^2}{c^2}\right]\bar{f}\right\} \tag{5-9}$$

$$v_1 \cong c\sqrt{\frac{(1-X)^3}{X^2(1-X)+XQ}}$$

The electron density has been extracted from the distribution function; the distribution function for the <u>hot</u> particles is

$$f = N\eta\bar{f} = N_{hot}\bar{f} \tag{5-10}$$

where η is the "fraction" of hot particles.

Several types of velocity distributions have been considered, (for more details see Davidson, 1973) for all the results presented here the distribution function has been assumed separable:

$$\bar{f} = g(\mu)h(v) \tag{5-11}$$

One particular form of the velocity distribution is a maxwellian-like distribution

$$h(v) = \text{const}_1\, v^{\nu} \exp(-\text{const}_2 \times v^2) \tag{5-12}$$

If the temperature T is defined as $\frac{2}{3}$ the average energy, the distributions are, (for integer ν)

$$h(v) = \frac{\pi}{2} \frac{1}{1\cdot3\cdot5\cdots(\nu+1)} \left[\frac{(\nu+3)_{mc^2}}{3T}\right]^{3/2} \frac{1}{c^3} v^{\nu} \exp[-(\nu+3)mv^2/6T] \quad \nu \text{ even}$$

$$h(v) = \frac{1}{2\cdot4\cdot6\cdots(\nu+1)} \left[\frac{(\nu+3)_{mc^2}}{3T}\right]^{3/2} \frac{1}{c^3} v^{\nu} \exp[-(\nu+3)mv^2/6T] \quad \nu \text{ odd} \tag{5-13}$$

A distribution which resembles the maxwellian forms near v = 0, but diverges at very large velocities is

$$h(v) = \frac{\text{const}_1\, v^{\nu}}{[1+\text{const}_2\, v^2]^{\mu}} \tag{5-14}$$

$$h(v) = \frac{2^{\mu}(\mu-1)!}{\pi[1\cdot3\cdot5\cdots(\nu+1)][1\cdot3\cdot5\cdots(2\mu-\nu-5)]} \left[\frac{(\nu+3)_{mc^2}}{3(2\mu-\nu-5)T}\right]^{3/2+\nu/2} \frac{1}{c^3}$$

$$\times \frac{v^{\nu}}{[1+(\nu+3)mv^2/3(2\mu-\nu-5)T]^{\mu}} \quad \nu \text{ even}$$

$$h(v) = \frac{2^{\mu-1}(\mu-1)!}{\pi[2\cdot4\cdot6\cdots(\nu+1)][2\cdot4\cdot6\cdots(2\mu-\nu-5)]} \left[\frac{(\nu+3)_{mc^2}}{3(2\mu-\nu-5)T}\right]^{3/2+\nu/2} \frac{1}{c^3}$$

$$\times \frac{v^{\nu}}{[1+(\nu+3)mv^2/3(2\mu-\nu-5T]^{\mu}} \quad \nu \text{ odd}$$

For a $(\sin\alpha)^n$ type pitch angle distribution we have

$$g(\mu) = \frac{1}{\sqrt{\pi}} \frac{\Gamma(\frac{n+3}{2})}{\Gamma(\frac{n+2}{2})} (1-\mu^2)^{n/2} \tag{5-15}$$

where $\Gamma(x)$ denotes the gamma function

Amplification rates are shown in Figures 5.4 - 5.11 for several combinations of the above distributions. The abscissa is the value of Q, starting with only hot electrons and augmented by cold electrons, or

$$Q = Q_{hot} \frac{N_{hot}+N_{cold}}{N_{hot}} \quad . \tag{5-16}$$

The temperature is an independent parameter labelling each curve. The curves are similar for other values of Q_{hot} except for the point at which they are cut off on the left.

The most immediately striking aspect of Figures 5.4 - 5.11 is the extreme sensitivity to Q at low cold electron densities. But as the electron density increases the amplification rate approaches a limit (Liemohn, 1972) near which the sensitivity to Q is much reduced. The upper limits of the amplification rate are not very exact because the amplification rates approach the magnitude of the wave number K and the approximations in the theory break down. These computations can, however, be taken as a useful guide to the conditions that can result in high amplification rates - and consequently large disturbances in the particle distributions.

5.4 DISCUSSION AND CONCLUSIONS

If we are to relate the effects discussed above to the trapped radiation belts, we must have some knowledge of the ranges of the important parameters, especially Q. A semi-quantitative picture of the variation of Q with altitude is shown in Figures 5 12, 5-13. Inside the plasmapause we might accept a value of Q generally of the order of 100. Outside the plasmapause there is a rapid fall-off to as low a value as .01. It is the sudden changes in electron density in the vicinity of the plasmapause during geomagnetic storms that are believed to cause dumping of ring current protons, and other disturbances in the trapped particles (Chappel, 1972).

It was suggested in section 5.2 that a small change in Q could cause the loss of only those electrons for which $1 < W < 10$. Inside the plasmapause,

Figures 5.4 through 5.11

The maximum amplification rate, $Z = \frac{\delta c}{\Omega_e}$, for whistler waves as a function of $Q = \frac{(N_{hot} + N_{cold})mc^2}{B^2/8\pi}$. The left edge ($Q = 1$) corresponds to the distribution indicated at the top of hot electrons alone; only the number density of cold electrons, N_{cold}, is varied along the abscissa. The frequency, $X = \frac{\omega}{\Omega_e}$, at which the largest amplification rate occurs is plotted in dotted lines (the ordinate at the right is linear). The curves are labelled with the value of the effective temperature $T = 2/3\langle E\rangle_{av}$ of the hot electrons, in units of mc^2. (The labels are to the right of the starting point; in places where the label is not entirely clear the correct T can be inferred from the relative placement of the curves.)

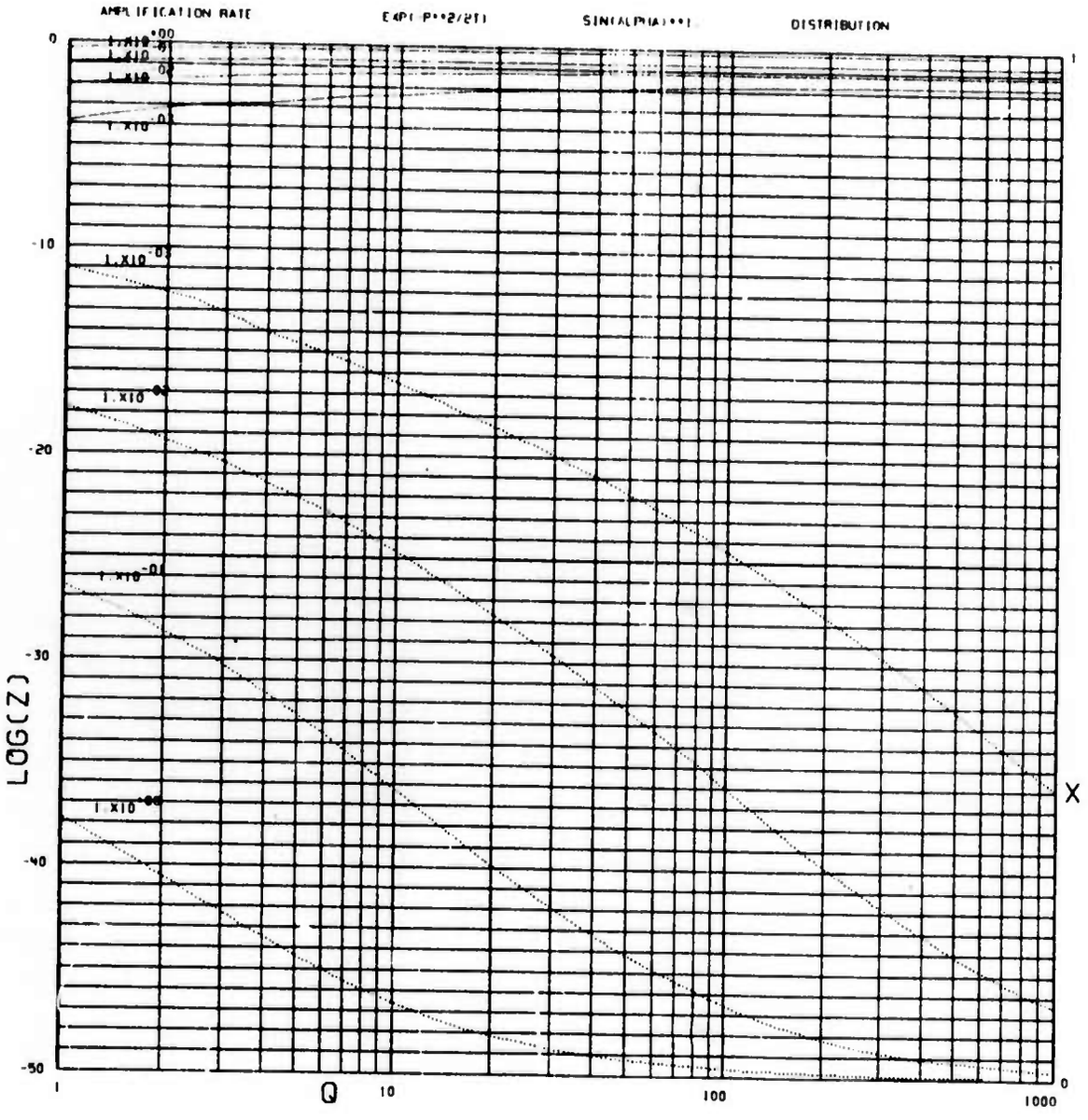
AMPLIFICATION RATE
EXP(P**2/2T)
SIN(ALPHA)**I
DISTRIBUTION
0
-10
-20
-30
-40
-50
LOG(Z)
1
0
X
1
10
100
1000
Q

Figure 5.4

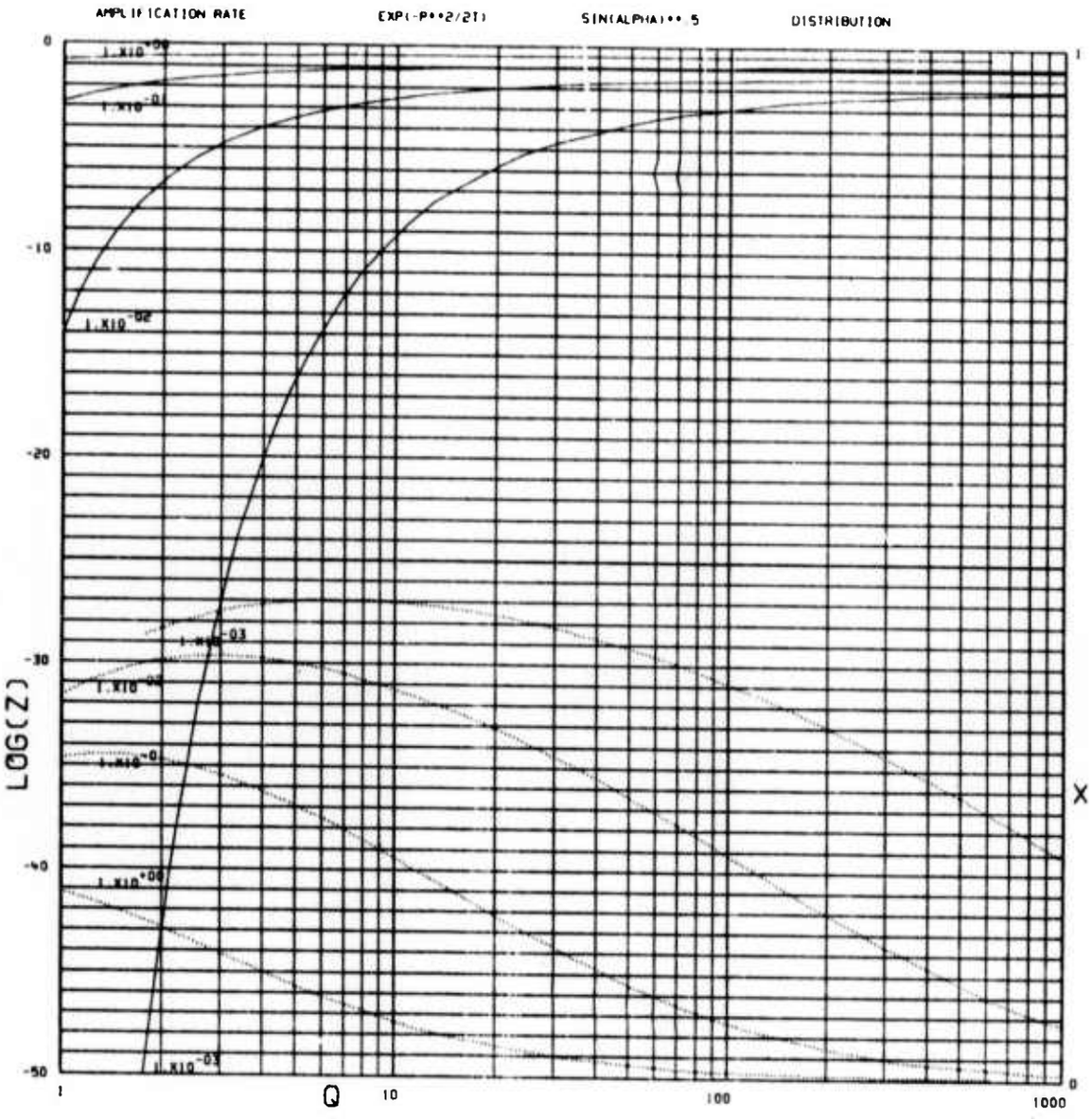
AMPLIFICATION RATE
EXP(-P**2/2T)
SIN(ALPHA)** 5
DISTRIBUTION
LOG(Z)
Q
X
0
-10
-20
-30
-40
-50
1
10
100
1000

Figure 5.5

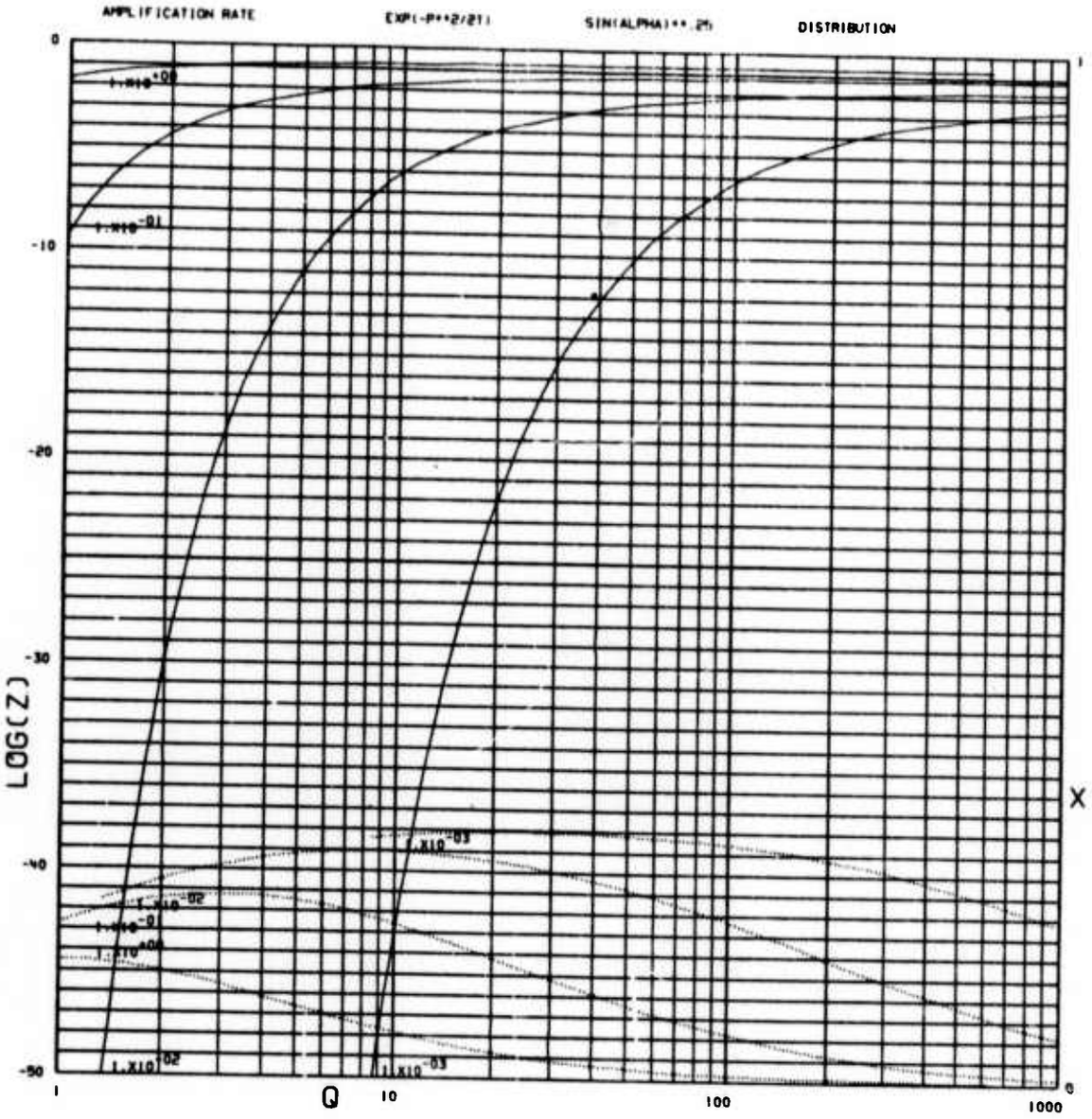
AMPLIFICATION RATE
EXP(-P**2/2)
SIN(ALPHA)**.25
DISTRIBUTION
0
-10
-20
-30
-40
-50
LOG(Z)
1
X
0
1
10
100
1000
Q
1.X10**-01
1.X10**-02
1.X10**-03
1.X10**02

Figure 5.6

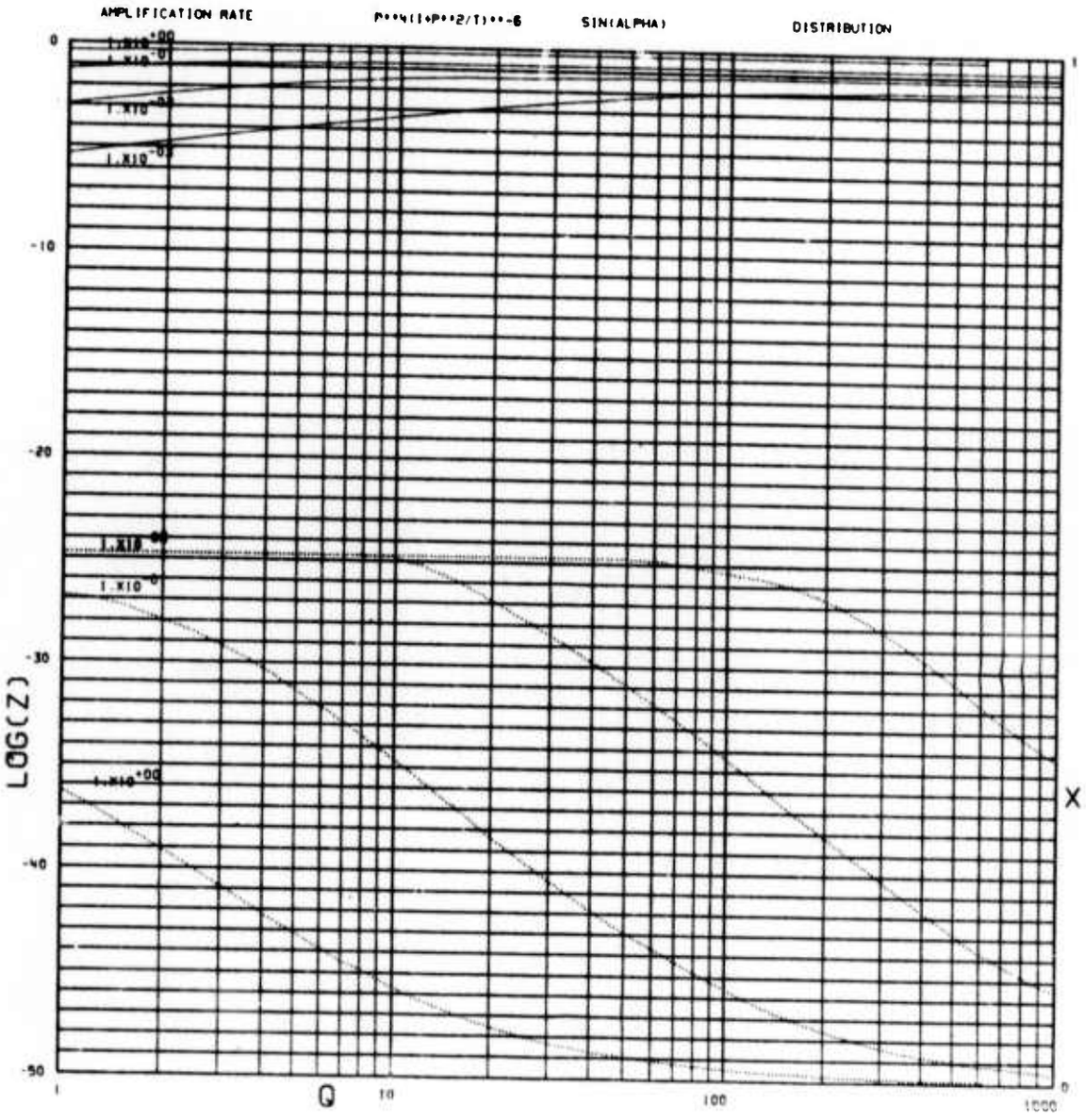
AMPLIFICATION RATE
SIN(ALPHA)
DISTRIBUTION
LOG(Z)
Q
X
0
-10
-20
-30
-40
-50
1
10
100
1000

Figure 5.7

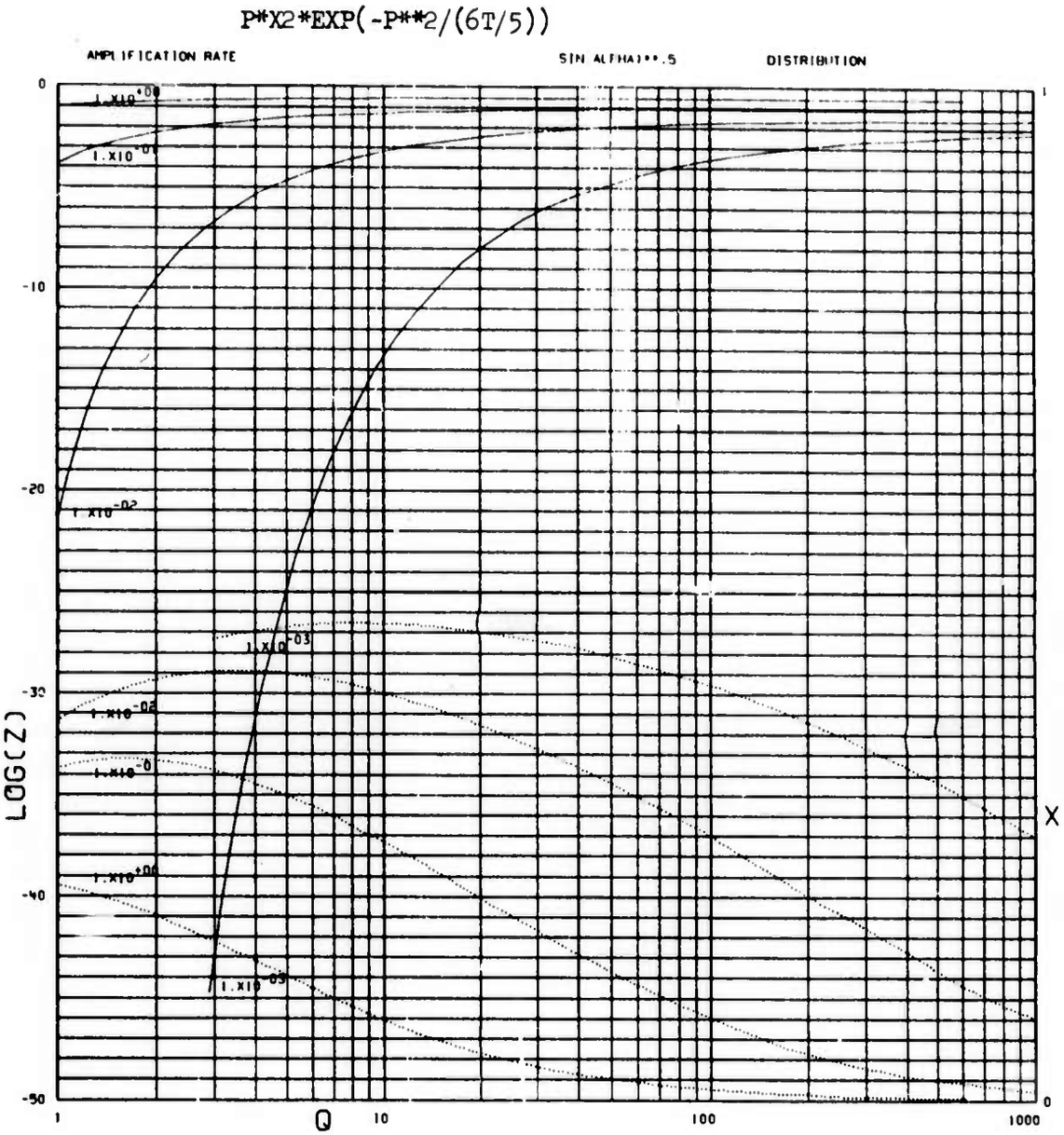
P*X2*EXP(-P**2/(6T/5))
AMPLIFICATION RATE
SIN ALPHA)**.5
DISTRIBUTION
LOG(Z)
Q
X
0
-10
-20
-30
-40
-50
1
10
100
1000
1.X10+00
1.X10-01
1.X10-02
1.X10-03
1.X10-04
1.X10-05
1.X10+06

Figure 5.8

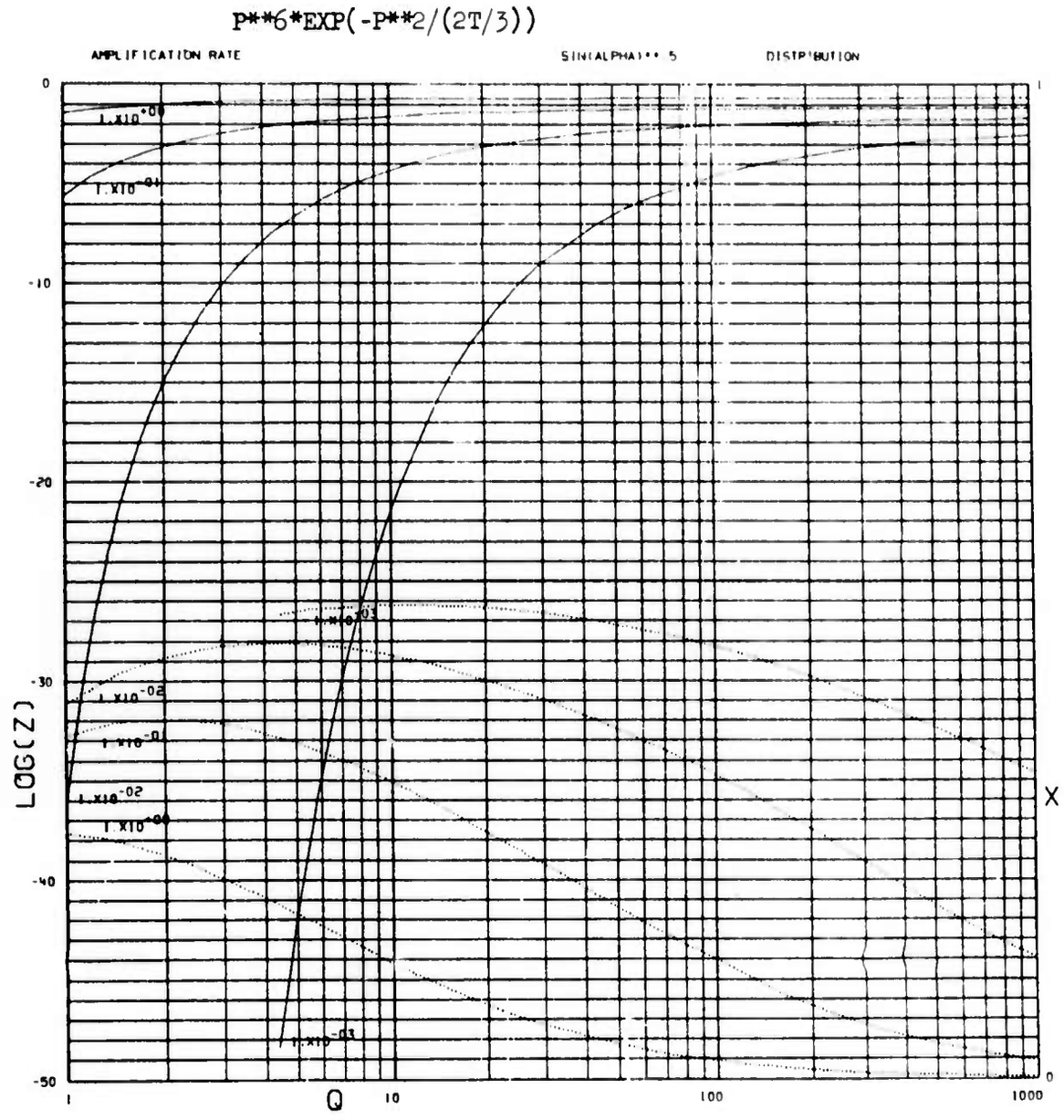
P**6*EXP(-P**2/(2T/3))
AMPLIFICATION RATE
SIN(ALPHA)** 5
DISTRIBUTION
0
-10
-20
-30
-40
-50
LOG(Z)
1.X10+00
1.X10-01
1.X10-02
1.X10-02
1.X10+00
1.X10-03
1
10
100
1000
Q
X

Figure 5.9

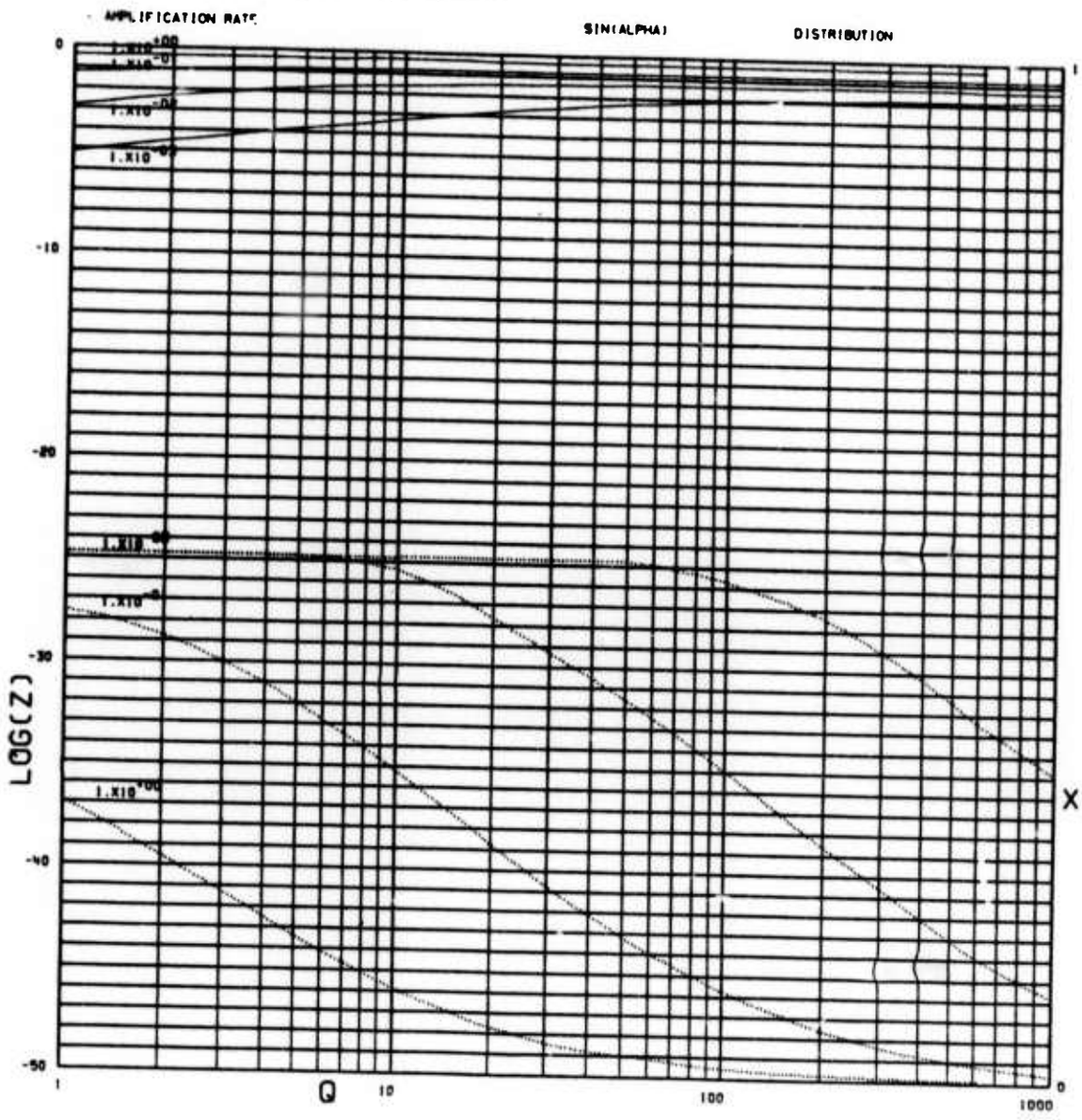
(1+P**2/3T)**-4
AMPLIFICATION RATE
SIN(ALPHA) DISTRIBUTION
LOG(Z)
Q
X
0
-10
-20
-30
-40
-50
1
10
100
1000
1.X10+00
1.X10-01
1.X10-02
1.X10-03
1.X10-04
1.X10-05
1.X10+00

Figure 5.10

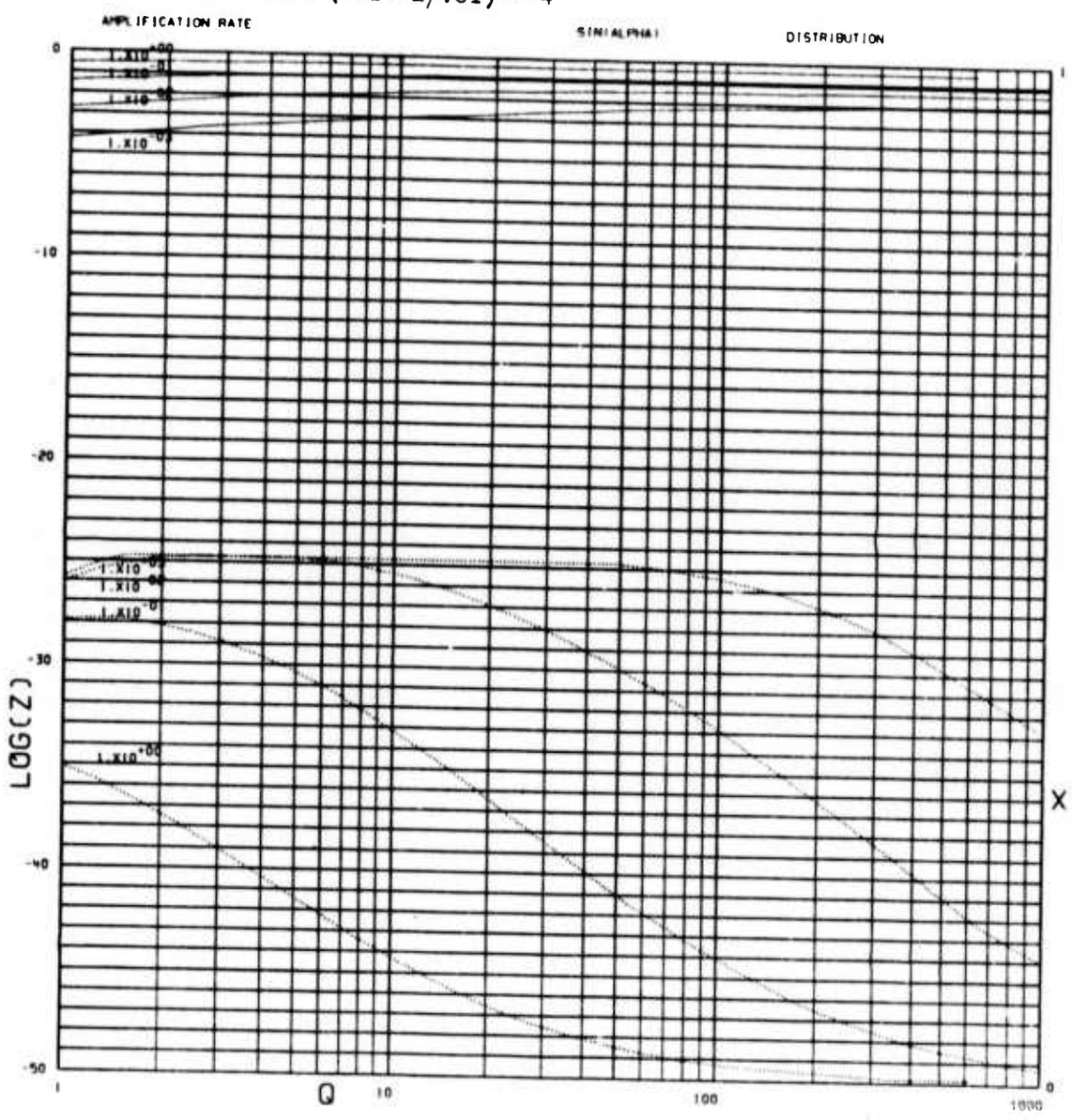
P**2(1+P**2/.6T)**-4
AMPLIFICATION RATE
SIN(ALPHA)
DISTRIBUTION
LOG(Z)
Q
X
0
-10
-20
-30
-40
-50
1
10
100
1000

Figure 5.11

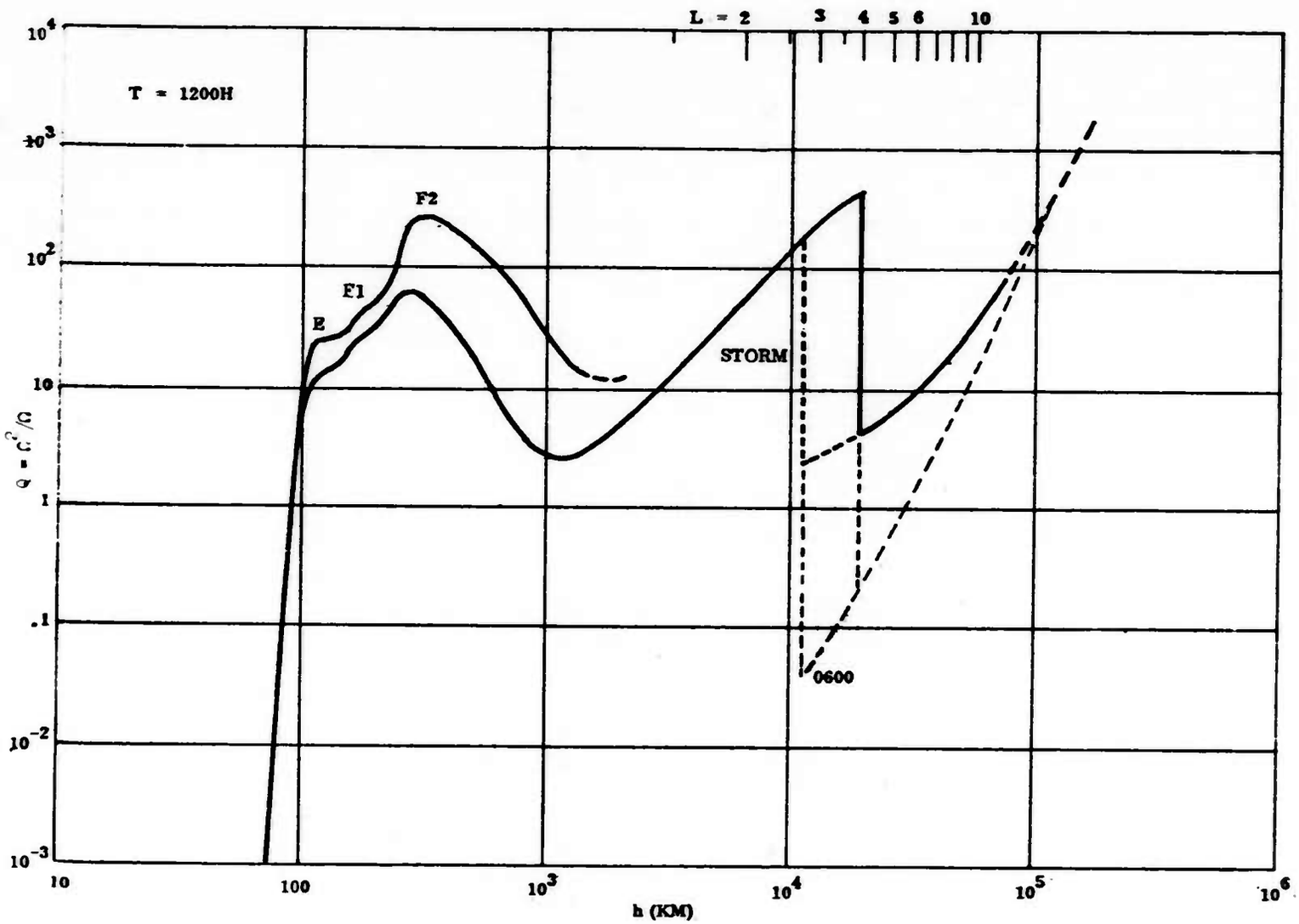

Figure 5.12 The daytime variation of $Q \equiv \Omega_p^2/\Omega_e^2$ with altitude in the equatorial plane (Hanson, 1965; Chappell, 1972). The inward motion of the plasmapause during a typical magnetospheric storm is indicated, the detailed changes in the electron density profile are not shown. The usual ranges of values are indicated; occasional excursions do occur beyond the limits indicated here.

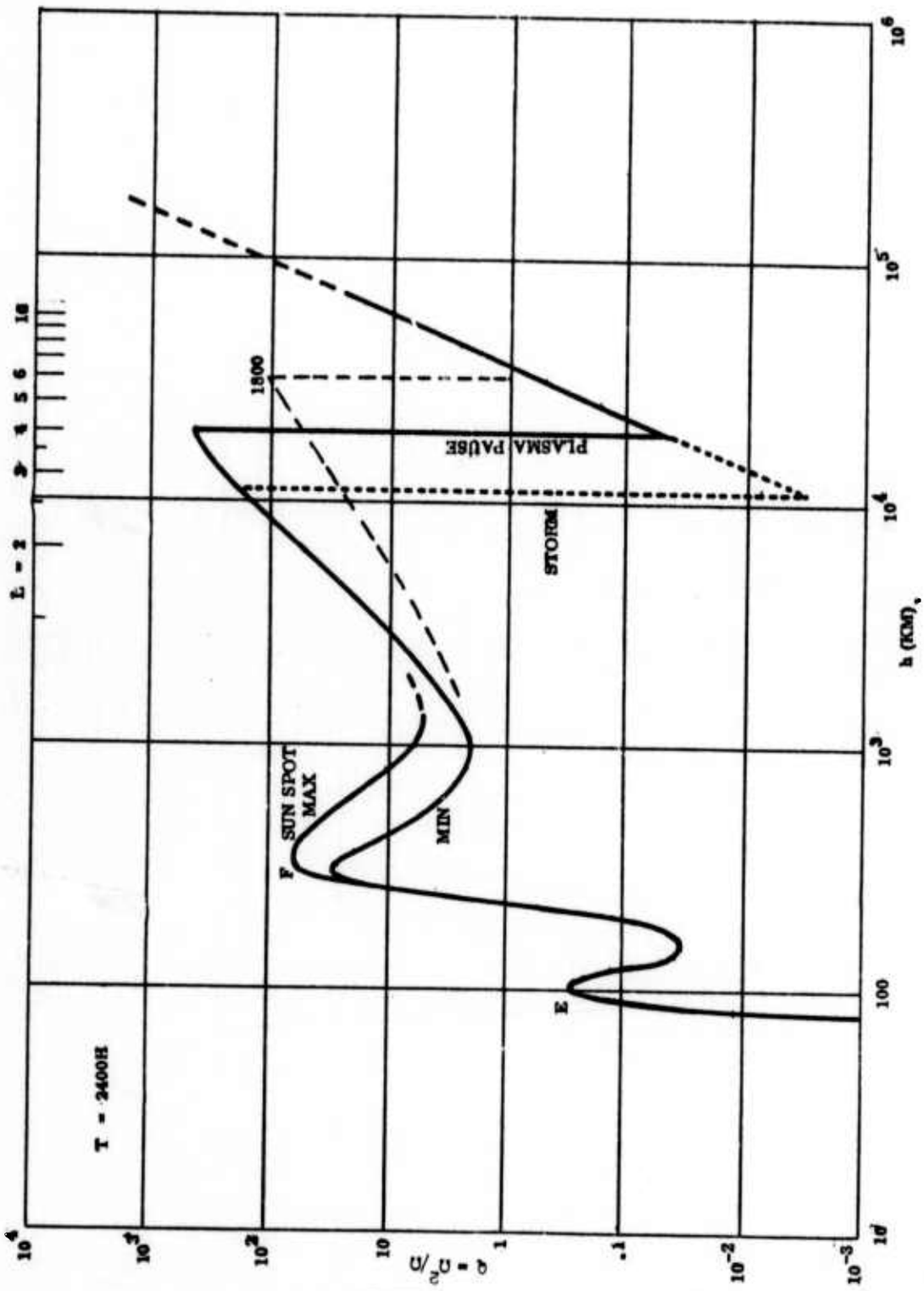

Figure 5.13 The nighttime variation of $Q = \Omega_p^2/\Omega_e^2$ with altitude in the equatorial plane. For a thorough discussion of the variability of the plasmapause region see Chappell (1972).

where $Q \approx 100$, the corresponding energy range is 2.5 keV < E < 250 keV. This energy range is raised considerably as Q is decreased. But it should be kept in mind that only electrons near the lower energy limit are drastically affected by the addition of small amounts of cold plasma. The higher energy trapped electrons are probably already unstable (Kennel and Petschek, 1966); and shifting the diffusion trajectories does not greatly affect the electrons near the loss cone, which are just the ones which drive the instability. In a highly anisotropic distribution (such as a "trapped" distribution) the only particles strongly affected by addition of cold electrons would be those electrons that are very near the borderline of instability (near $W \approx 1$). All of this leads us to believe that in an artificially trapped belt of predominantly relativistic electrons, only the relatively low energy component could be readily modified by cold plasma injection.

If sufficient amounts of artificially trapped electrons could be injected outside the plasmapause (ignoring the difficulties of attaining high β's due to ordinary hydromagnetic instabilities) the temperature correction could become significant. The temperature of fission electrons may be assumed to be about cm^2. The lower limit of energies affected by wave-particle interactions is then

$$E \lesssim \frac{1 \text{ meV}}{\sqrt{Q}} \qquad (5\text{-}17)$$

The temperature effects could very well make a large portion of the energy spectrum inaccessible to modification. The very high energy electrons actually tend to <u>stabilize</u> the electrons with kilovolt-or-lower energies.

Some of the difficulties met in trying to remove high-energy trapped electrons from the radiation belts might be overcome by considering the non-homogeneous nature of the geomagnetic field. All that has been said above was applicable to a homogeneous magnetic field. This is valid because the strongest wave growth is usually expected at the equator, with a rapid diminishment of the effectiveness of wave-particle interactions away from the equator (Kennel and Petschek, 1966). But waves generated at the equator

can interact with electrons in other locations where the resonance conditions may be quite different. This so called parasitic diffusion has been applied with some success to the natural trapped radiation belts (Lyons, Thorne and Kennel, 1972), but its implications in regard to modification of radiation belts are completely unexplored.

It is also likely that a proper treatment of the non-linear aspects of wave growth could alter some details of the work discussed here.

Given the difficulties of removing the highest energy electrons from the trapping belts, it could still be asked whether cold plasma injection is a feasible method for inducing the generation of whistler waves. All the computations of wave amplification rates, shown in Figures 5.4 - 5.11 indicate that strongly growing waves can occur at high plasma densities. The effects of cold plasma injection at lower densities are less certain, being extremely dependent on the trapped electrons' energy spectrum. Any operational application of cold plasma injection would necessitate a thorough knowledge of radiation belt conditions immediately before the injection event, requiring far better electron spectral information than is presently available over the range from sub-kilovolt energies to millions of electron volts. In sum, modification of trapped radiation belts by cold plasma injection appears possible, but not likely feasible under expected operational conditions.

5.5 REFERENCES

Brice, N., "Fundamentals of Very Low Frequency Emission Generation Mechanisms," J. Geophys. Res., 69, 4515-4522, 1964.

Brice, N., "Artificial Enhancement of Energetic Particle Precipitation Through Cold Plasma Injection. A Technique for Seeding Substorms?," J. Geophys. Res., 75, 4890-4892, 1970.

Brice, N., "Harnessing the Energy in the Radiation Belts," J. Geophys. Res., 76, 4698-4701, 1971.

Chappell, C. R., "Recent Satellite Measurements of the Morphology and Dynamics of the Plasmasphere," Rev. Geophys. Space Phys., 10, 951-979, 1972

Cornwall, J. M., "Precipitation of Auroral and Ring-Current Particles by Artificial Plasma Injection," Rev. Geophys. Space Phys., 10, 993-1002, 1972

Cornwall, J. M., and M. Schulz, "Theoretical Aspects of Artificial Plasma Injection," Aerospace Corp. Report ATR-73(7279), Aerospace Corp., El Segundo, California, 1973

Davidson, G. T., "On the Modification of Trapped Radiation Belts by Cold Plasma Injection," Lockheed Palo Alto Research Laboratory, Dec. 1973.

Gendrin, R., "Pitch Angle Diffusion of Low Energy Protons Due to Gyro-resonant Interaction with Hydromagnetic Waves," J. Atmos. Terr. Phys., 30, 1313-1330, 1968.

Haerendel, G., "On the Balance Between Radial and Pitch Angle Diffusion," Particles and Fields in the Magnetosphere, B. McCormac, ed., D. Reidell, Dordrecht, Holland, p 416-428, 1970

Haerendel, G., "Diffusion Theory of Trapped Particles and the Observed Proton Distribution," Earth's Particles and Fields, B. McCormac, ed., Reinhold, New York, p 171-191, 1968

Hanson, W. B., "Structure of the Ionosphere," Satellite Environment Handbook, F. S. Johnson, ed., Stanford University Press, Stanford, California, p 20-49, 1965

Kennel, C. T., and H. E. Petschek, "Limit on Stably Trapped Particle Fluxes," J. Geophys. Res., 71, 1-28, 1966

Liemohn, J. B., "Stimulated Amplification of VLF and ULF Waves in the Magnetosphere by Localized Injections of Plasma Clouds and Particle Beams," ARPA report 1479/2141, Univ. of Washington, Seattle, Washington, 1972

Lyons, L. R., R. M. Thorne, and C. T. Kennell, "Pitch Angle Diffusion of Radiation Belt Electrons within the Plasmasphere," J. Geophys. Res., 77, 3455-3478, 1972

McCormac, B. M., and J. E. Evans, "Summary of the Second Magnetospheric Wave-Particle Interaction Workshop," February 1973, Lockheed Palo Alto Research Laboratory, LMSC D315118, 1973

Stix, T. H., The Theory of Plasma Waves, McGraw-Hill, New York, 1962

Chapter 6

CHARGED PARTICLE ENVIRONMENT IN THE EQUATORIAL REGION FROM 4 TO 9 R_e

J E. Evans

6.1 INTRODUCTION

Charged particle fluxes, energy spectra, angular distributions and energy integrals (and in some cases, densities) have been collected from the recent literature and presented as functions of L, local time, and K_p where that information is available. These environmental data are needed to perform calculations and predictions on possible experiments involving plasma injections and wave-particle interactions in the neighborhood of geosynchronous orbits. It will serve to standardize the environmental conditions for which calculations are done by offering to the experiment designer or theoretician in simple form recent measurements of particle fluxes and populations which are now detailed enough in many cases to sort the measurements into sets according to local times and K_p.

The environment is presented in terms of 4 groups of particles:

1) Energetic electrons
2) Energetic protons
3) Thermal plasmas (H^+ and He^+ ions)
4) Energetic alpha particles.

Data have been collected for L values from 4 to 9 and wherever possible grouped into low K_p (0 to 1^+), medium K_p (2^- to 4^-) and high K_p (≥ 4) groups. Data from the geosynchronous satellites, ATS-1 and ATS-5, are presented as L = 6.6 data. The variation of L with the longitudinal location of an equatorial geosynchronous satellite is given in Figure 6.1. This variation is based on the static geomagnetic field model, IGRF (10/68) consisting of 80 coefficients updated to epoch 1969.75 by Evans et al. (1969). Another environmental parameter needed for planning plasma injection experiments is the magnetic field strength, B, as a function of local time, φ, and radial distance from the earth, R_e. An approximate

local time dependent model by McIlwain (1972) is given by the equation:

$$B(\gamma) = 6 - 24 \cos \varphi + 18(\cos^2 \varphi)/(1 + 1728/R_e^3 \cdot \cdot 31000/R_e^3.$$

Values of B at the magnetic equator are tabulated in Table 6.1 for 8 local times and radial distances from 4 to 9 R_e.

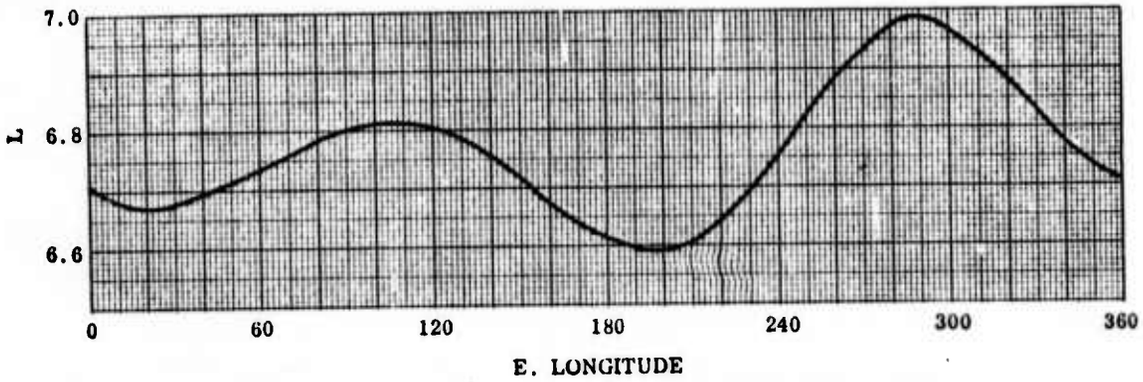

Figure 6.1 **L Value as Function of Longitude for an Equatorial Synchronous Orbit**

Table 6.1

B Field in (γ's) as Function of R_e and Local Time

hrs R_e	00 φ=0	03 φ=45	06 φ=90	09 φ=135	12 φ=180	15 φ=225	18 φ=270	21 φ=315	24 φ=360
4	467	474	490	508	515	508	490	474	467
5	323	330	346	364	371	364	346	330	323
6	128	134	150	167	176	167	150	134	128
6.6	92.4	98.1	113.8	132	140.4	132	113.8	98.1	92.4
7	75.4	80.9	96.4	114.8	123.4	114.8	96.4	80.9	75.4
8	46.7	51.6	66.5	85.6	94.7	85.6	66.5	51.6	46.7
9	29.9	34.2	48.5	68.2	77.9	68.2	48.5	34.2	29.9

6.2 ENERGETIC ELECTRON ENVIRONMENT

Energetic electron number fluxes are presented in two energy ranges; from 40 keV to 4 MeV and from 50 eV to 50 keV. For the higher energy group, the electron model AE-4 of Singley and Vette (1972) is used. Fig. 6.2 gives the equatorial omnidirectional integral electron fluxes (in $cm^{-2}sec^{-1}$) vs. electron energy thresholds and the corresponding differential number fluxes (in $cm^{-2}sec^{-1}keV^{-1}$) vs. electron energy at L = 6.6. At this radial distance and for energies > 200 keV model fluxes are identical for epoch 1964 (near solar minimum) and epoch 1967 (near solar maximum). At 10 keV epoch 1967 fluxes are about 25% higher than for epoch 1964. For the year 1964, the daily mean sunspot number was 10.2 and for 1967 it was 93.8. For 1964, 46% of the 3 hr K_p indices were $\leq 1^+$ and 8% were $\geq 4^o$ and for 1967 43% were $\leq 1^+$ and 10% were $\geq 4^o$. The integral curve is for average values of the integral number fluxes measured. The vertical bars with crosses indicate probablistic fluxes and the numbers beside the crosses on the bar at 2 MeV apply to all the bars and are the probabilities that the flux will be exceeded. The probability of 0.50 designates the median value.

Figs. 6.3 and 6.4 present the radial profiles from L=4 to L=9 of equatorial omnidirectional integral electron fluxes (in $cm^{-2}sec^{-1}$) for different energy thresholds from 10 keV to 4.5 MeV according to electron model AE-4, epochs 1964 and 1967. Figs. 6.5 and 6.6 give contours of these integral fluxes (in $cm^{-2}sec^{-1}$) on L value vs. local time plots. At the bottom of each figure an integral flux curve vs. local time is given for L=6.6.

Figure 6.7 shows differential radial profiles and angular distributions from West et al. (1973) for 7 electron energy channels from 79 ± 23 keV to 2830 ± 270 keV at 23:00 hrs. local time and when K_p=0. Figs. 6.8 and 6.9 give differential radial profiles and angular distributions, also from West et al. (1973) near 10:00 and 16:00 hrs. local times and for medium K_p values 3^- and 2^o.

A major part of the electron contribution to the plasma pressure at L=6.6 is due to electrons in the 50 eV to 50 keV energy interval. Measurements from ATS-5 have given much detailed data in this region. The curve in Fig. 6.10 gives fluxes from "typical" values of equatorial electron 4.1 minute integrals over E=50 eV to 50 keV for omnidirectional fluxes (actually 1 directional fluxes multiplied by 4π) as a function of local time for 29 days of January 1970. These data are for all K_p and are from DeForest and McIlwain (1971). Crosses on vertical bars denote maxima and minima values of electron integrals in the 29 days in which low K_p values occurred 56% of the time, medium K_p 40% and high K_p 4%. The 8 data points shown as circles with K_p values beside them indicate, but without strong statistical justification, that high K_p values tend to result in higher electron flux integrals and lower K_p in lower integrals. This conclusion is strengthened by the data of Shelley and Lew (1971) also from ATS-5 for 20 days from September through December 1969 for the energy interval 650 eV to 53 keV. Fig. 6.11 shows the average value of all data vs. local time with bars showing maxima and minima values. Average omnidirectional fluxes from 1 hr integrals are shown for low, medium and high K_p values, i.e. 1, 3^- and 5^+. The total range of integrals encountered as well as variation with K_p is somewhat less in the afternoon and early evening local time period than for other local time periods. Fig. 6.12 shows the omnidirectional electron energy flux integrals for 50 eV < E < 50 keV for 29 days in Jan. 1970 from the data of DeForest and McIlwain (1971) as a function of local time. Data are not available for sorting into K_p intervals.

Figs. 6.13 and 6.14 are plots of differential electron number fluxes (1 directional fluxes multiplied by 4π) vs. E for the 1 to 50 keV range and are separated into spectra for medium and high K_p times. The data of DeForest and McIlwain (1971) have been smoothed for this presentation of a few cases where published data are available. Local times and K_p values are given for each curve. At the top of each figure the shapes of exponential spectra, $dN/dE = N_o \exp(-E/E_o)$, for E_o= 50, 20, and 10 keV are given for comparison purposes. Figs. 6.15 and 6.16 extend these same spectra from 1 keV down to 50 eV. Shapes of exponential spectra with average energy values E_o from 5 keV to 0.2 keV are shown at the top of the figures.

Angular distributions of electrons in the 50 eV to 50 keV energy range are quite variable from time to time and from one location to another, but they vary within a fairly small range. DeForest and McIlwain (1971) have measured fluxes $\perp$ (perpendicular) and $\parallel$ (parallel) to the earth's magnetic field lines at L=6.6 on ATS-5 and found that the two directional fluxes of electrons and protons with instrument field of view of 0.015 sr usually differed by less than a factor of 3. To understand the environment of energetic particles and their variabilities in this energy range, it is important to understand how substorms inject groups of particles with several peak energies in the midnight sector and that these groups disperse as they move in different parts of the magnetosphere in untrapped, partially trapped or completely trapped modes. An example how these groups move and disperse after a substorm injection is shown in Fig. 6.17, a diagram taken from McIlwain (1972). This diagram is essentially a time schedule of how the energy of particle groups change as they move into the different local time sectors being observed by geosynchronous satellite borne instruments. These particle groups change energies as they proceed into different parts of the magnetosphere as they interact with the electric and magnetic fields around the earth. Fig. 6.17 is an idealized example of the energies of groups of particles from substorm injections occurring at 4 hr. intervals in UT. A vertical cut across the figure will give the energies at which peaks occur in the electron and proton differential number and energy spectra. For example, when ATS is at 15 hrs. local time peaks in electron spectra occur near 30, 10, 2.5 and 0.35 keV and in the proton spectra near 0.40, 0.80, 1, 1.3, 8, 12, 20 and about 200 keV. At 20 hrs. local time nearly all the ATS observed peaks (except electron peaks at $E < 3$keV will have shifted to lower energies. Some of the peaks may maintain their identities for 2 days such as the dispersion curve marked -48 indicating the substorm injecting this peak occurred at -48 hrs. on the UT scale at the bottom of Fig. 6.17.

6.3 ENERGETIC PROTON ENVIRONMENT

Energetic proton number fluxes are presented in two energy ranges; from 100 keV to 3 MeV and from 50 eV to 50 keV. For the higher energy group, the proton model AP5 of King(1967)and Vette(1970)is used. Fig. 6.18 gives the equatorial omnidirectional integral proton fluxes (in $cm^{-2}sec^{-1}$) for several energy thresholds from 100 keV to 5 MeV for L values from 4 to 6.6. The integral proton number spectrum with E_0=111 keV and the corresponding differential spectrum at L = 6.6 are also plotted in Fig. 6.18. Fig. 6.19 gives the proton differential number spectrum ($cm^{-2}sec^{-1}keV^{-1}$) for L = 6.6 at the geomagnetic equator taken from Frank and Owens (1970). These data were from OGO-3 at mid and low latitudes and normalized to the geomagnetic equator. The data were taken during the 44 day period, 10 June through 23 July, 1966, and the daily averages were divided into 28 days in which ΣK_p (for 8 3-hr periods) $\leq$ 12 (low K_p) and 16 days in which $12 < \Sigma K_p < 32$ (medium K_p). The two groups gave data which differed by < 2% which is so much less than the uncertainties in the measured directional intensities (assessed at $\leq$ 30%) that they were considered equal. Inspections of the contour diagrams of Frank and Owens (1970) will show that differences for different K_p's will become noticeable for L values below 6.6. The integral omnidirectional proton curve in Fig. 6.19 was calculated from the differential curves of Figs. 6.18 and 6.19 with a smooth connection from 50 to 100 keV. The angular distribution of low energy particles have an approximate functional dependence on equatorial pitch angle α_0 of

$$j(\alpha_0) = j \sin^n \alpha_0,$$

where j and n depend on L. Frank and Owens (1970) found that low energy proton intensities are not greatly anisotropic; that $0.5 \leq n \leq 2.0$ over pitch angles observed with their instruments $20^\circ \leq \alpha_0 \leq 90^\circ$.

Fig. 6.20 presents average integral omnidirectional proton fluxes (actually $\perp$ directional fluxes multiplied by 4π) for 50 eV < E < 50 keV at L = 6.6 (from ATS-5)geosynchronous satellite as a function of local

time. There is a minimum near noon and a maximum near midnight local time for averages over 29 days data. The total range of values observed for the 4.1 minute proton averages (ratio of maximum to minimum value) was ~ 5 for the local time intervals studied.

Fig. 6.21 presents proton omnidirectional integral data for $E > 5$ keV and for $L = 6.6$ (ATS-5 geosynchronous satellite) as a function of local time with indication of total ranges of intensities and the effect of K_p. Both Figs. 6.20 and 6.21 show approximately the same local time dependence and consistent integral intensities but the integral proton intensities are only about 20% of the values from the OGO-3 data of Frank and Owens (1970)(Fig. 6.19).

This difference may be due to differences in proton population at the different epoches or it may be due to some measurement problem such as the vehicle charging to high potentials and affecting the instruments different amounts or for different fractions of the observing times. Another possible problem is that of heavy particle contamination. Electrostatic analyzers, such as used by Frank and Owens (1970) and by DeForest and McIlwain (1971) can admit all positively charged particles. No data exist which can be used to evaluate this effect. The Shelley and Lew proton data were taken with a foil threshold detector which will at least reduce the contamination from He^+ to O^+ by absorbing the fraction of their spectra below the threshold. The threshold is 5 keV for protons, about 20 keV for He^+ ions, and about 80 keV for O^+ ions.

Figs. 6.22 to 6.25 give examples of differential proton number fluxes for two energy ranges $1 < E < 50$ keV and 50 eV $< E < 1$ keV and for medium K_p (2^- to 4^-) and high K_p (≥ 4). These cases are from DeForest and McIlwain (1971) and correspond to the spectra of electrons, 50 eV $< E < 50$ keV shown in Figs. 6.13 to 6.16. Data have been smoothed to eliminate some of the small scaled structure in the spectral data. The large fluctions will depend on the time and intensities of

substorms occurring within the past ~ 24 hours (or in some cases, over 48 hours). The way groups of electrons and protons injected by substorms move around and through the magnetosphere was described briefly in the previous chapter on Energetic Electron Environment in connection with Fig. 6.17. With the aid of the exponential spectral shapes at the top of the figures, a very rough characteristic energy E_0 can be obtained. The flux integrals for 50 eV < E < 50 keV and associated K_p values for each of these cases are shown in Fig. 6.20.

Average energies can be obtained for the 50 eV < E < 50 keV interval by dividing the integral energy flux by the integral number flux of DeForest and McIlwain (1971). However, not enough such values are available at present to find typical or average values for several local times and for low medium and high K_p values. Fortunately, the proton energy flux and the proton number flux do not vary much with local time in this energy interval and this is the interval which for most cases contains a large fraction of the total proton energy. Fig. 6.26 gives the omnidirectional proton energy flux as a function of local time. For an approximate K_p effect on average proton energies, values from the solid curve of Fig. 6.26 through the "typical" integral values of energy flux of DeForest and McIlwain (1971) can be divided by the low, medium, and high K_p values from the number flux curve (Fig. 6.20) of Shelley and Lew (1971).

6.4 THERMAL PLASMAS

The thermal plasmas between L=4 and 9 and in the equatorial region of the magnetosphere vary with local time, K_p, and how recently a substorm has injected plasma in the midnight sector. Many techniques with ground and satellite based instruments have been used to detect the plasmapause location. The satellite borne swept grid ion density gauge has been used extensively to measure H^+ ion densities (and in many cases He^+ and O^+) with relatively high temporal and spatial resolution ($\sim$ 3 sec and $\sim$ 30 km) (Harris et al., 1970 and Harris, 1973). However, these data have errors when the satellite accumulates sufficient electrostatic charge to influence the number of ions getting to the ion gauge. Whistler experiments and their interpretations (Carpenter and Park, 1973) require assumptions on ion distributions which make it difficult to determine the local plasma density.

Shaw and Gurnett (1972) are developing a new and highly accurate technique for determining the electron number density in the magnetosphere in the region beyond the plasmasphere boundary. The technique involves making measurements on the frequency behavior of the electric field strength of the upper hybrid resonance radio noise in the 10 to 100 kHz frequency range and calculating the local electron number density. Figs. 6.27 and 6.28 show 2 cases of outbound passes by Imp-6 with plasmapause crossings near 6:00 hrs LT. For Fig. 6.27, $K_p=1^-$ and the magnetic latitude at the plasmapause was 27°. For Fig. 6.28, $K_p=2^-$ and the magnetic latitude at the plasmapause was -35°. The time resolution of the measurements is about 5 sec. It is not known whether the method will work in disturbed times or when there are regions of detached plasma (or where the plasma density is not spherically stratified and decreasing monotonically with radius).

Examples of measurements of radial profiles of H^+ or electron densities in the magnetosphere for 4 hr local time intervals and for low (0 to 1^+), medium (2^- to 4^-), and high (≥ 4) K_p values are given in Figs. 6.29 to 6.31. Some of the curves are graphical averages of up to 5 curves for a given local time interval and range of K_p, others are single

examples of measurements, and a few profiles presented as dotted lines are interpolations between curves for adjoining time intervals. These profiles are from 2 electron density profile measurements from Imp-6 by Shaw and Gurnett (1972) and 37 ion density measurements from an ion gauge on OGO-6 by Harris et al. (1970) and Harris (1973). These profiles should be revised when more data become available from the new technique of Shaw and Gurnett (1972).

Outside the plasmapause the density is generally less than 10 cm^{-3}. Out at synchronous orbit the density is generally in the 0.1 to 1 cm^{-3} but according to the measurements presented in Figs. 6.29 to 6.31, the densities are at least sometimes higher than this in the noon and afternoon sectors. When the plasmapause is beyond L=4 and the instrument sensitivity is sufficient to measure the He^+ density, the He^+ density is about 0.5 to 1 percent of the H^+ density.

6.5 ENERGETIC ALPHA PARTICLE ENVIRONMENT

Energetic alpha particles peak near L=3.5 and have sharply peaked equatorial pitch angle distributions centered at 90°. Several measurements have been reported by Krimigis (1970), Blake and Paulikas (1970), and Fritz and Williams (1972) but they have mainly been from low altitude satellites. The data of Fritz and Williams (1972) (Fig. 6.32) extends out to L=5 but these data apply to one day, 6 Jan. 1972, a very quiet day with $\Sigma K_p = 4^-$. The corresponding angular distribution is also shown.

6.6 REFERENCES

Blake, J.B. and Paulikas, G.A.; "Measurements of Trapped Alpha Particles: $2 \leq L \leq 4.5$,"Particles and Fields in the Magnetosphere, B.M. McCormac, Editor, p. 380, Reidel Publ. Co., 1970.

Carpenter, D.L. and Park, C.G.; "On What Ionospheric Workers Should Know About the Plasmapause-Plasmasphere," Rev. of Geophys. and Space Physics, 11, 133 (1973).

DeForest, S.E. and McIlwain, C.E.; "Plasma Clouds in the Magnetosphere," J. Geophys. Res., 76, 3587, 1971.

Evans, J.E., Newkirk, L.L. and McCormac, B.M.; "North Polar, South Polar, World Maps and Tables of Invariant Magnetic Coordinates," Lockheed Palo Alto Research Laboratory Report (DASA 2347), Oct. 1969.

Frank, L.A. and Owens, H.D.; "Omnidirectional Intensity Contours of Low Energy Protons ($0.5 \leq E \leq 50$ keV) in the Earth's Outer Radiation Zone at the Magnetic Equator," J. Geophys. Res., 75, 1269, 1970.

Fritz, T.A. and Williams, D.J.; "Initial Observations of Geomagnetically Trapped Alpha Particles at the Equator," NOAA Technical Memorandum, ERL SEL-20, June 1972, also J. Geophys. Res., 78, 4719, 1973.

Harris, K.K., Sharp, G.W. and Chappell, C.R.; "Observations of the Plasmapause from OGO-5," J. Geophys. Res., 75, 219 (1970).

Harris, K.K.; "The Measurement of Cold Ion Densities in the Plasma Trough," submitted for publication, 1973.

King, J.H.; "Models of the Trapped Radiation Environment," NASA SP-3024, Vol. IV: Low Energy Protons, 1967.

Krimigis, S.M.; "Alpha Particles Trapped in the Earth's Magnetic Field," Particles and Fields in the Magnetosphere, B.M. McCormac, Editor, p.364, Reidel Publ. Co., 1970.

McIlwain, C.E.; "Plasma Convection in the Vicinity of the Geosynchronous Orbit," Earth's Magnetospheric Processes, B.M. McCormac, Editor, p.268, D. Reidel Publ. Co., 1972.

Shaw, R.R. and Gurnett, D.A.; "Magnetospheric Electron Density Measurements from Upper Hybrid Resonance Noise Observed by Imp-6," Univ. of Iowa Report 72-37, Dec. 1972.

Shelley, E.G. and Lew, S.K.; "Low Energy Radiation Environment at Synchronous Altitude," Proceedings of the National Symposium on Natural and Manmade Radiation in Space, held in Las Vegas, Nevada, 2-5 March 1971.

Singley, G.W. and Vette, J.I.; "Model of the Outer Radiation Zone Electron Environment," NSSDC 72-06, NASA Goddard, Dec. 1972.

Singley, G.W. and Vette, J.I.; "A Model Environment for Outer Zone Electrons," NSSDC 72-13, NASA Goddard, Dec. 1972.

Vette, J.I.; "Summary of Particle Populations in the Magnetosphere," Particles and Fields in the Magnetosphere, Ed. by B.M. McCormac, p. 305, D. Reidel Publ. Co., 1970.

West, H.I., Buck, R.M., and Walton, J.R.; "Electron Pitch Angle Distributions Throughout the Magnetosphere as Observed on OGO-5," J. Geophys. Res., 78, 1064, 1973.

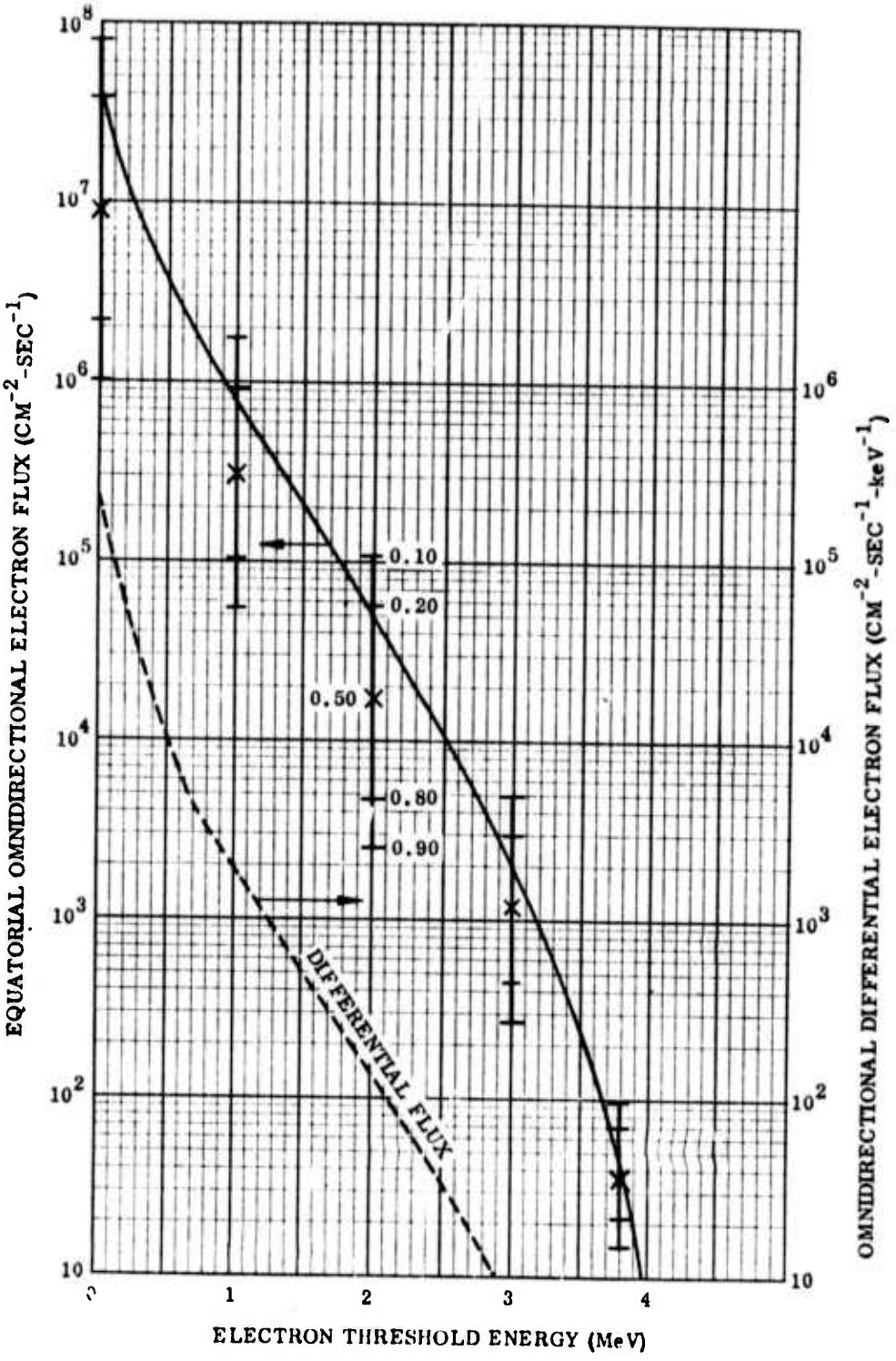

Fig. 6.2 Integral and differential equatorial omnidirectional electron fluxes for L = 6.6. The integral curve gives averaged values of observed fluxes. The vertical bars with crosses indicate probabilistic fluxes and the numbers by the bar at 2 MeV give the probability of a higher flux occurring. Average values are above the median values (marked by an X). These data are given by the AE-4 model electron spectrum and are the same for 1964 and 1967 epochs. (Singley and Vette, 1972, NSSDC 72-06 and NSSDC 72-13.)

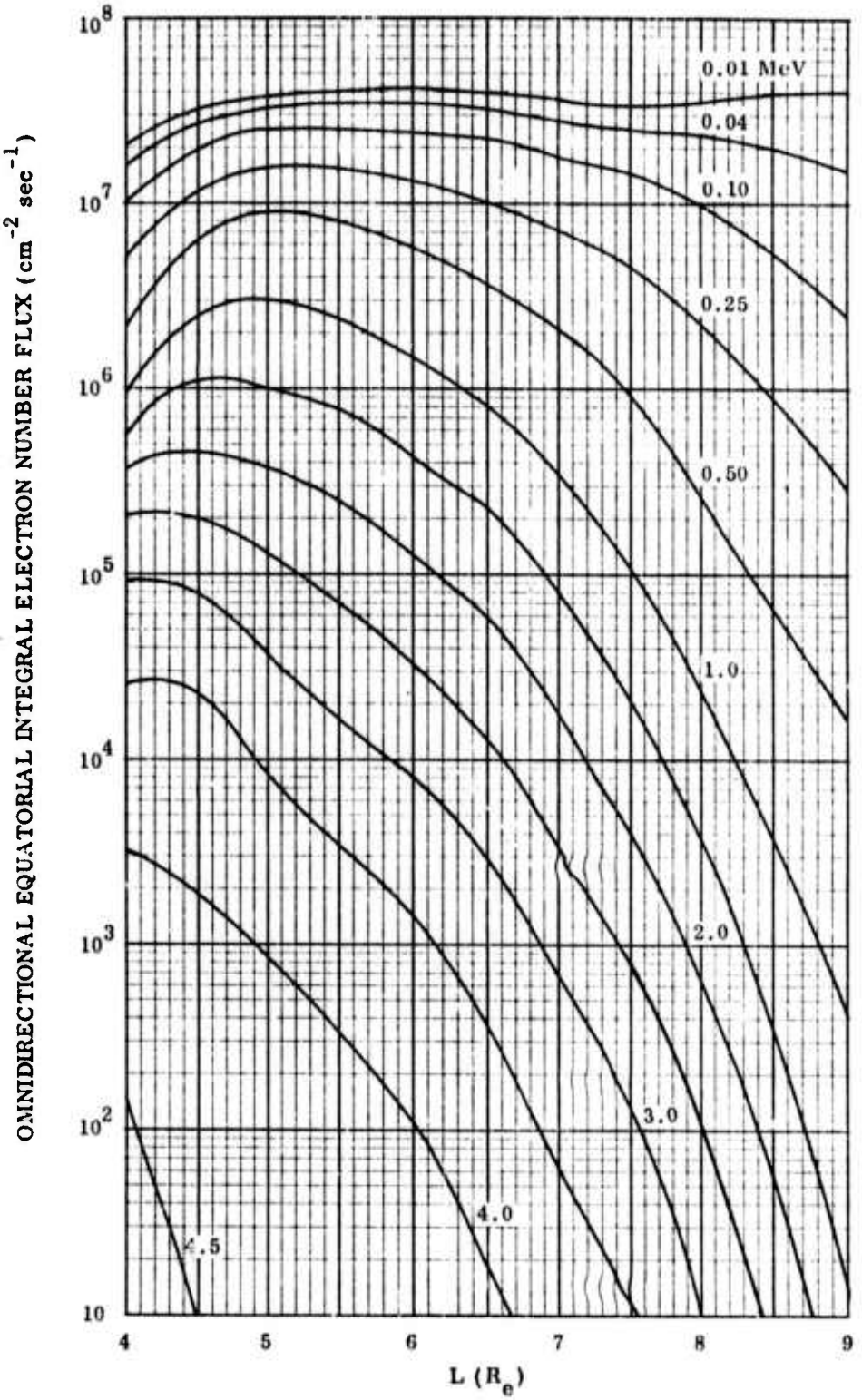

Fig. 6.3 Radial profiles of equatorial omnidirectional electron flux for different energy thresholds from 10 keV to 4.5 MeV. Model AE-4, average values for epoch 1964 Singley and Vette (1972), NSSDC 72-06. For 1964, the daily mean sunspot number was 10.2 and 46% of the 3 hr K_p indices were $\leq 1^+$ and 8% were $\geq 4^o$.

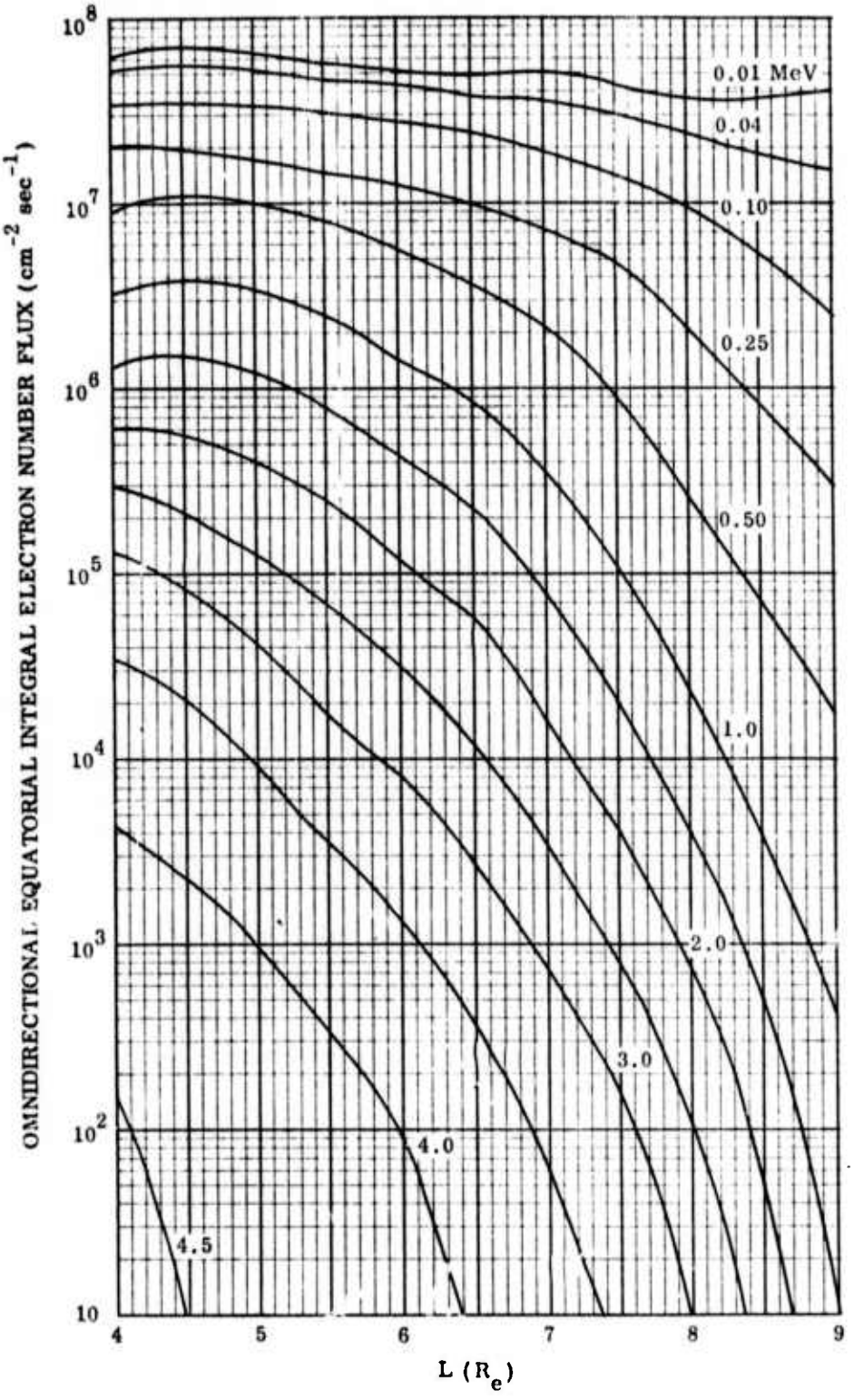

Fig. 6.4 Radial profiles of equatorial omnidirectional electron flux for different energy thresholds from 10 keV to 4.5 MeV. Model AE-4, average values for epoch 1967, Singley and Vette (1972), NSSDC 72-06. For 1967, the daily mean sunspot number was 93.8 and 43% of the 3 hr K_p indices were $\leq 1^+$ and 10% were $> 4^0$.

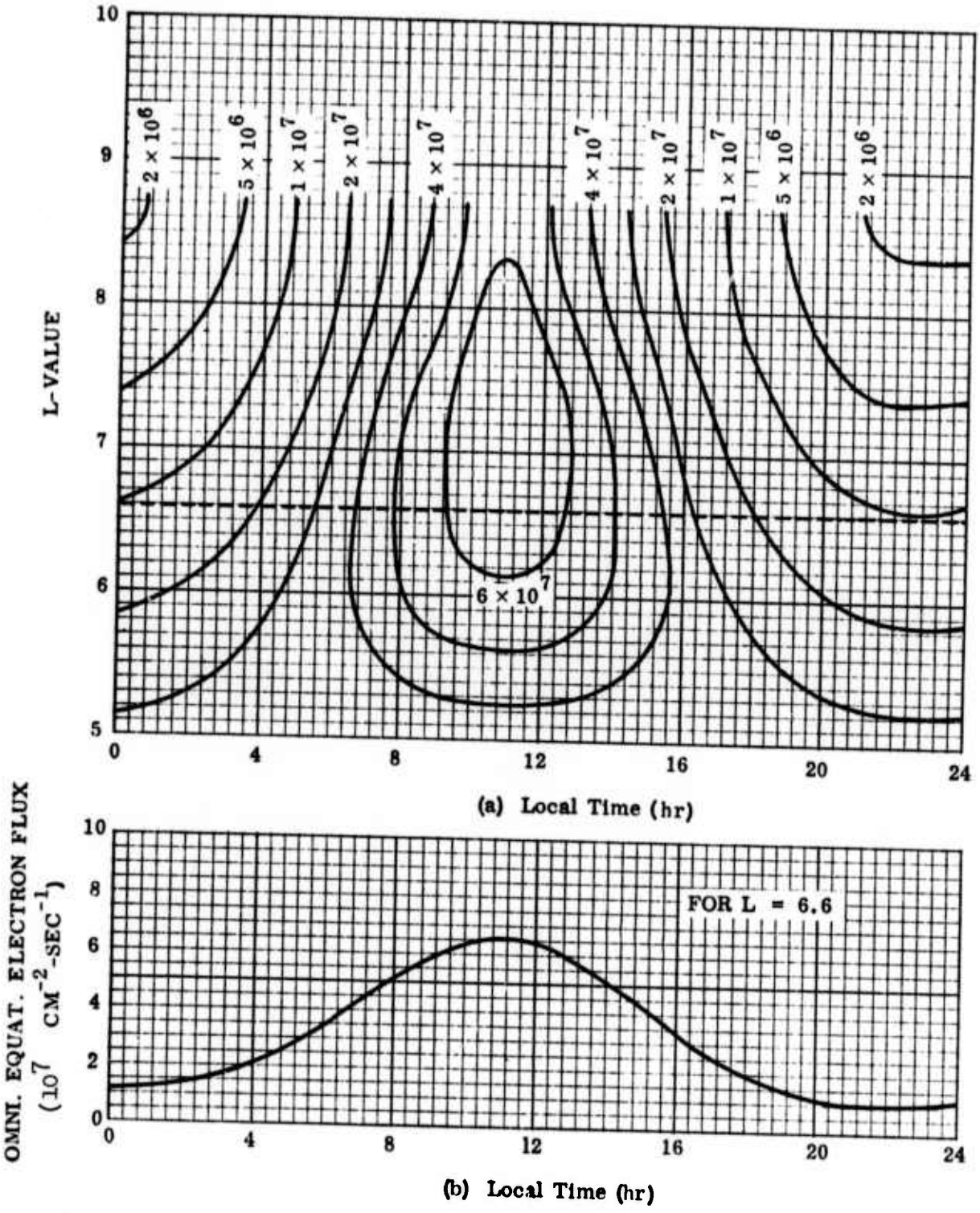

Fig. 6.5 (a) Equatorial omnidirectional integral electron flux (in $cm^{-2}sec^{-1}$) contours on an L value local time plot and (b) electron flux dependence on local time for L = 6.6, E > 40 keV (Model AE-4, average values for epoch 1964, Singley and Vette, 1972, NSSDC 72-06).

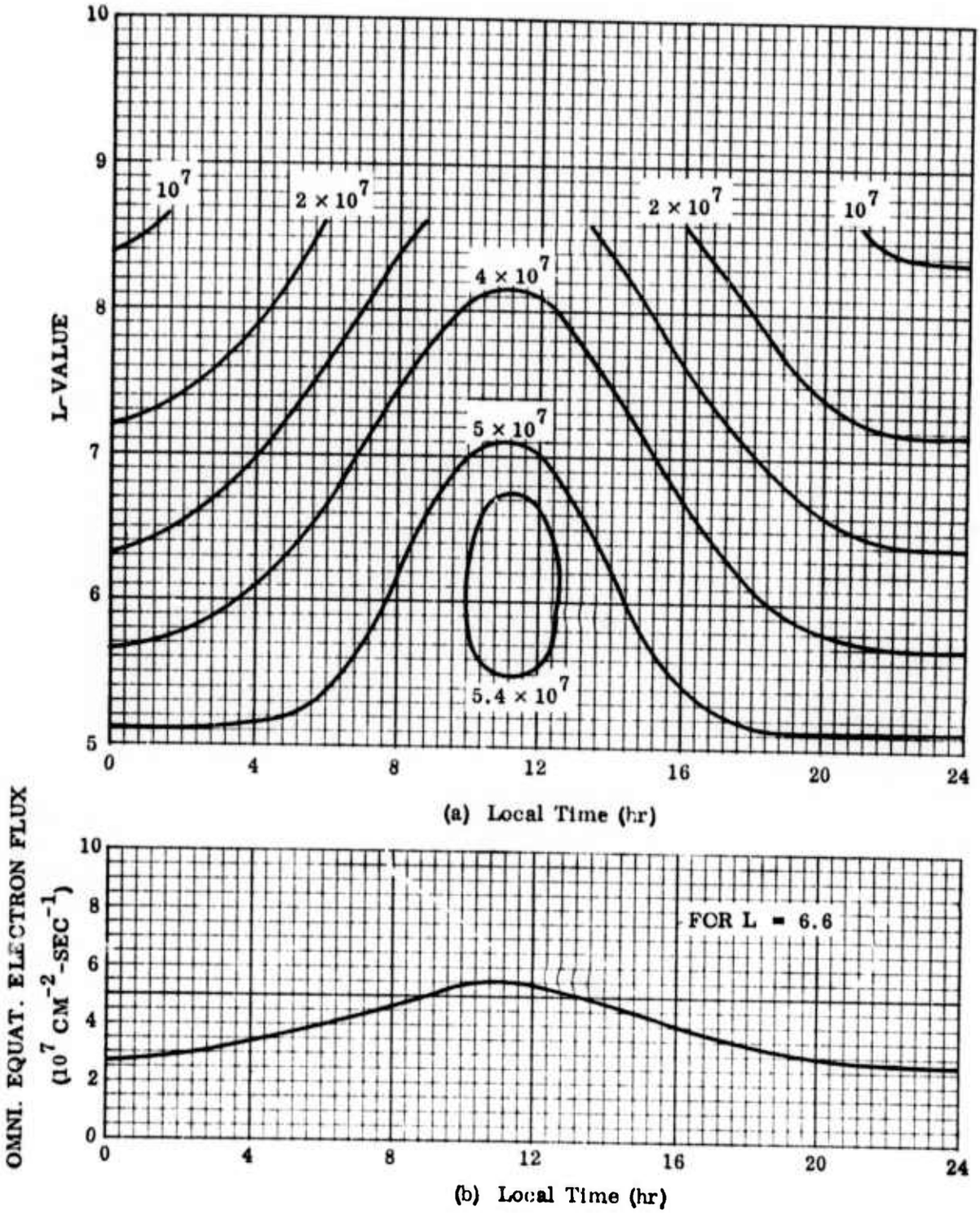

Fig. 6.6 (a) Equatorial omnidirectional integral electron flux (electrons with E > 40 keV in $cm^{-2}sec^{-1}$) contours on an L value local time plot, and (b) electron flux dependence on local time for L = 6.6 and E > 40 keV. (Singley and Vette, 1972, Model AE-4, average values epoch 1967, NSSDC 72-06.)

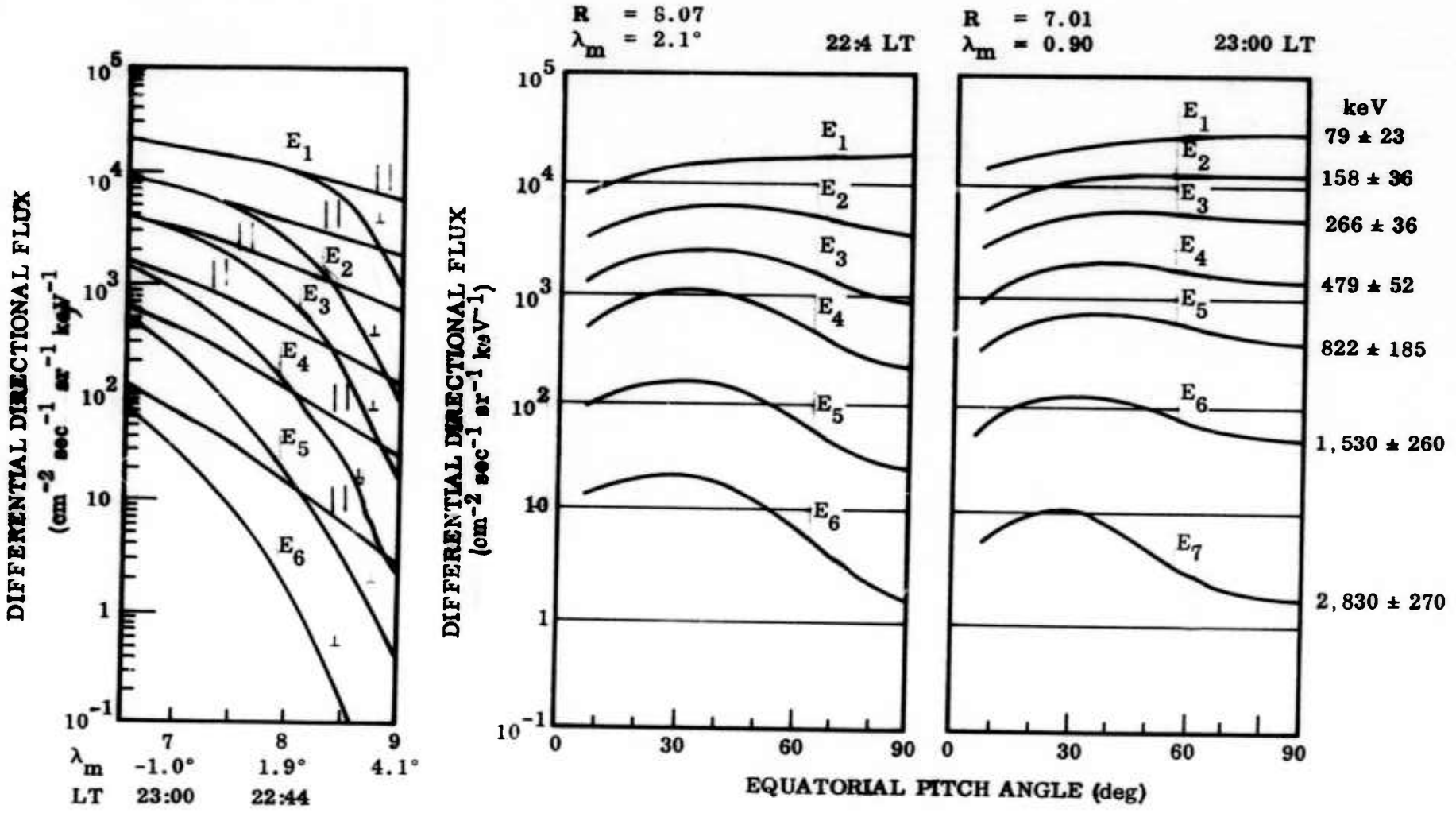

Fig. 6.7 Radial electron flux profiles for September 18, 1968 for 6 energy channels and pitch angle distributions just before midnight local time which are typical for the entire nighttime sector during a magnetically quiet time ($K_p = 0^+$). The fluxes labelled ⊥ are those perpendicular to the geomagnetic field lines while those labelled || are in reality the peak fluxes in the butterfly distribution at pitch angles 20° to 40° (West et al., 1973).

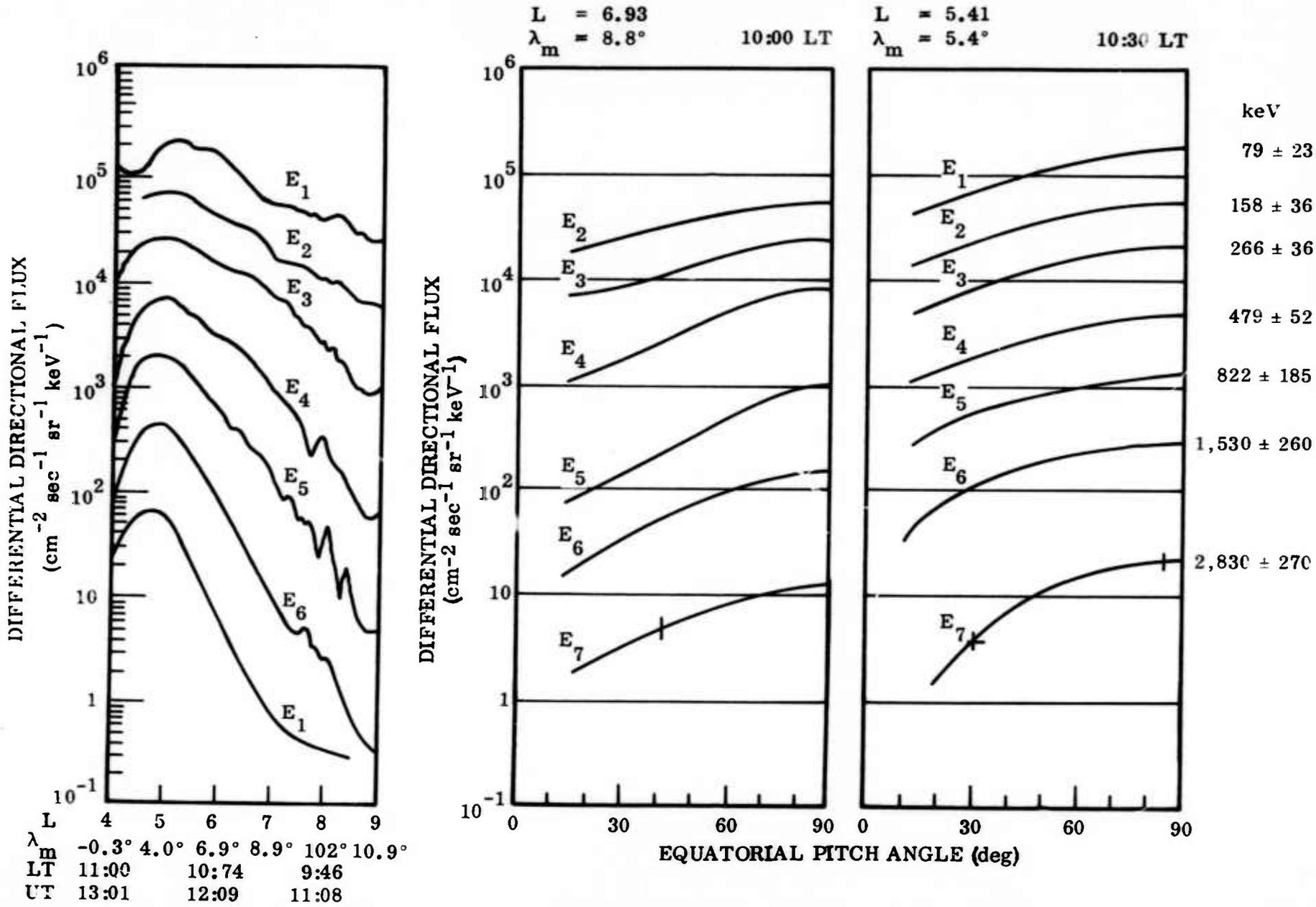

Fig. 6.8 Radial electron flux profiles for March 30, 1968 for 7 energy channels and typical pitch angle distributions on the morning side of the earth during a period of medium K_p ($K_p = 3^-$) (West et al., 1973).

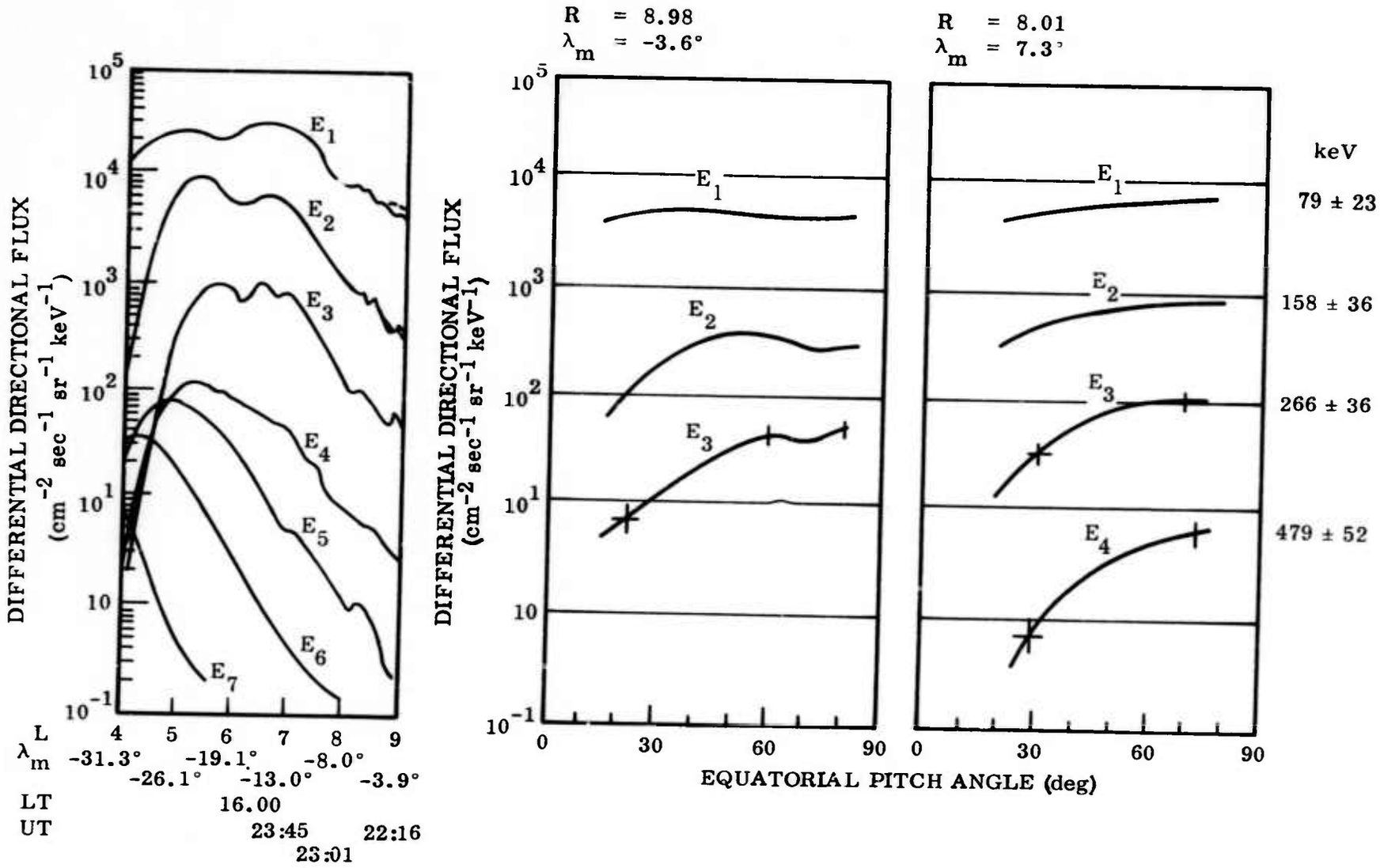

Fig. 6.9 Radial electron flux profiles for January 7, 1969 for 7 energy channels and pitch angle distributions for the early afternoon sector during a period of medium K_p (K_p = 2). Pitch angle distributions have been transformed to the magnetic equator (West et al., 1973).

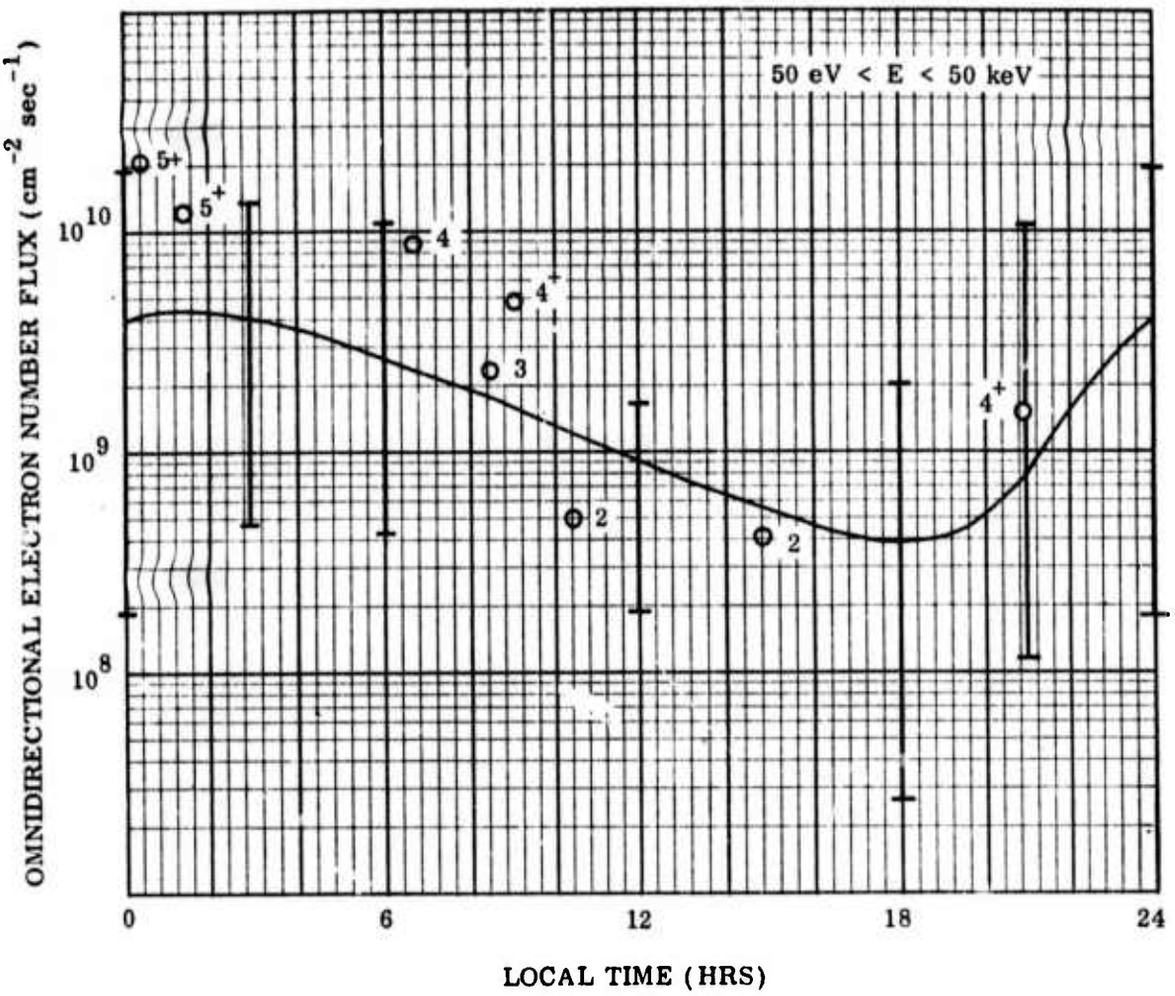

Fig. 6.10 Electron integral (50 eV < E < 50 keV) directional fluxes (⊥ to earth's spin axis) multiplied by 4π as a function of local time at synchronous altitude (L= 6.6, ATS-5). The solid line gives data from "typical" 4.1 minute integrals for 29 days of January 1970, a period in which 4.4% of the 3 hr K_p values were ≥ 4, 39.6% were 2^- through 4^- and 56.0% were $\leq 1^+$. The crosses on the bars denote maxima and minima values of the electron integrals. The 8 data points shown as circles with the K_p values beside them are specific cases published. (DeForest and McIlwain, 1971.)

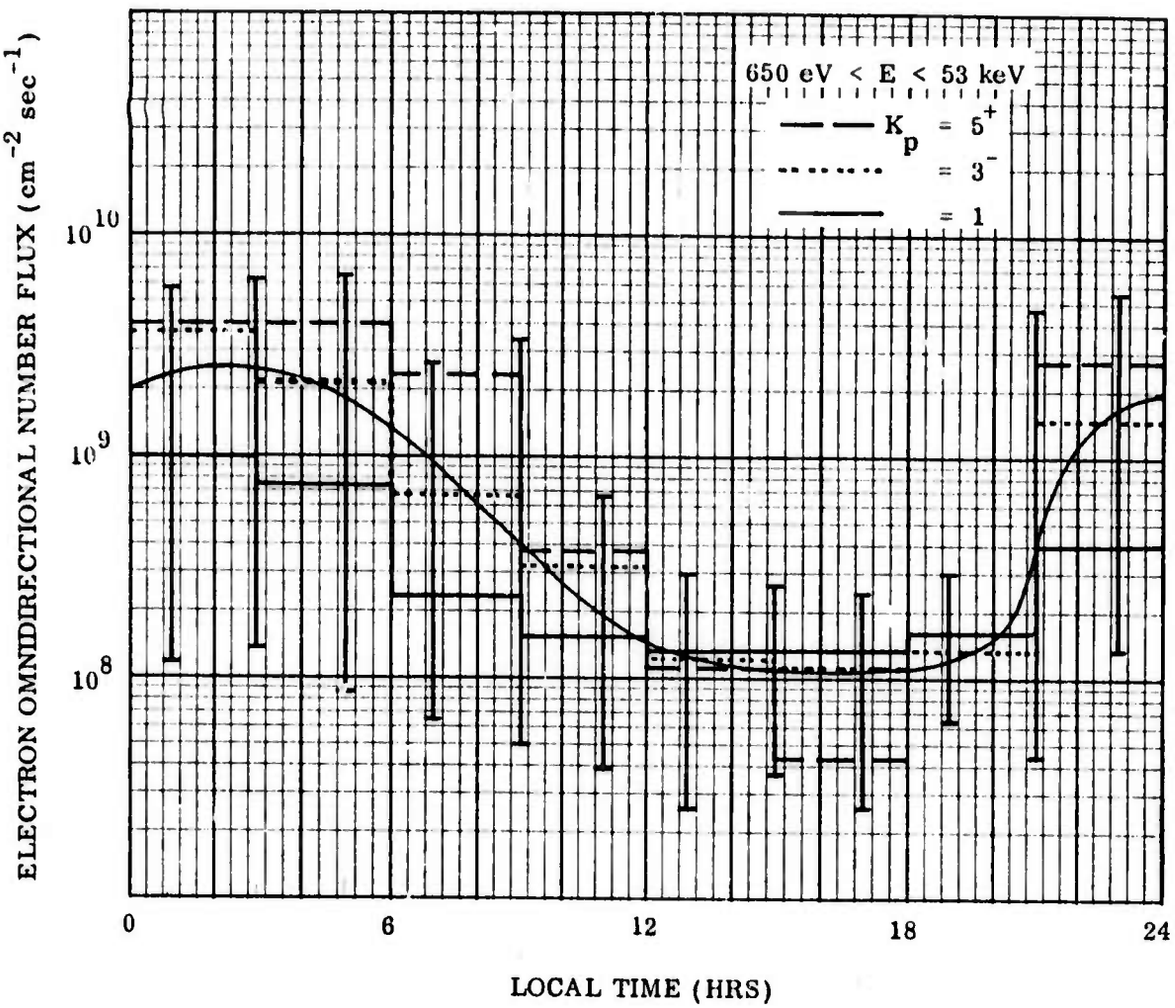

Fig. 6.11 Electron integral (650 eV < E_o < 53 keV) directional fluxes (central angle of detector 11° from earth's spin axis) multiplied by 4π as a function of local time at geosynchronous altitude (L = 6.6, ATS-5). The solid curve gives fluxes from the average 1 hr integrals over 20 days from September through December 1969 in which 16% of the 3 hr K_p values were ≥ 4, 48% were 2^- through 4^-, and 36% ≤ 1^+. 443 one hour integrals were sorted according to K_p and the bar graphs give the average integrals for 3 hr local time periods of 3 K_p values; 1, 3^- and 5^+. The crosses on the vertical bars give maxima and minima values of the electron integrals in the 2 hr local time intervals (Shelley and Lew, 1971).

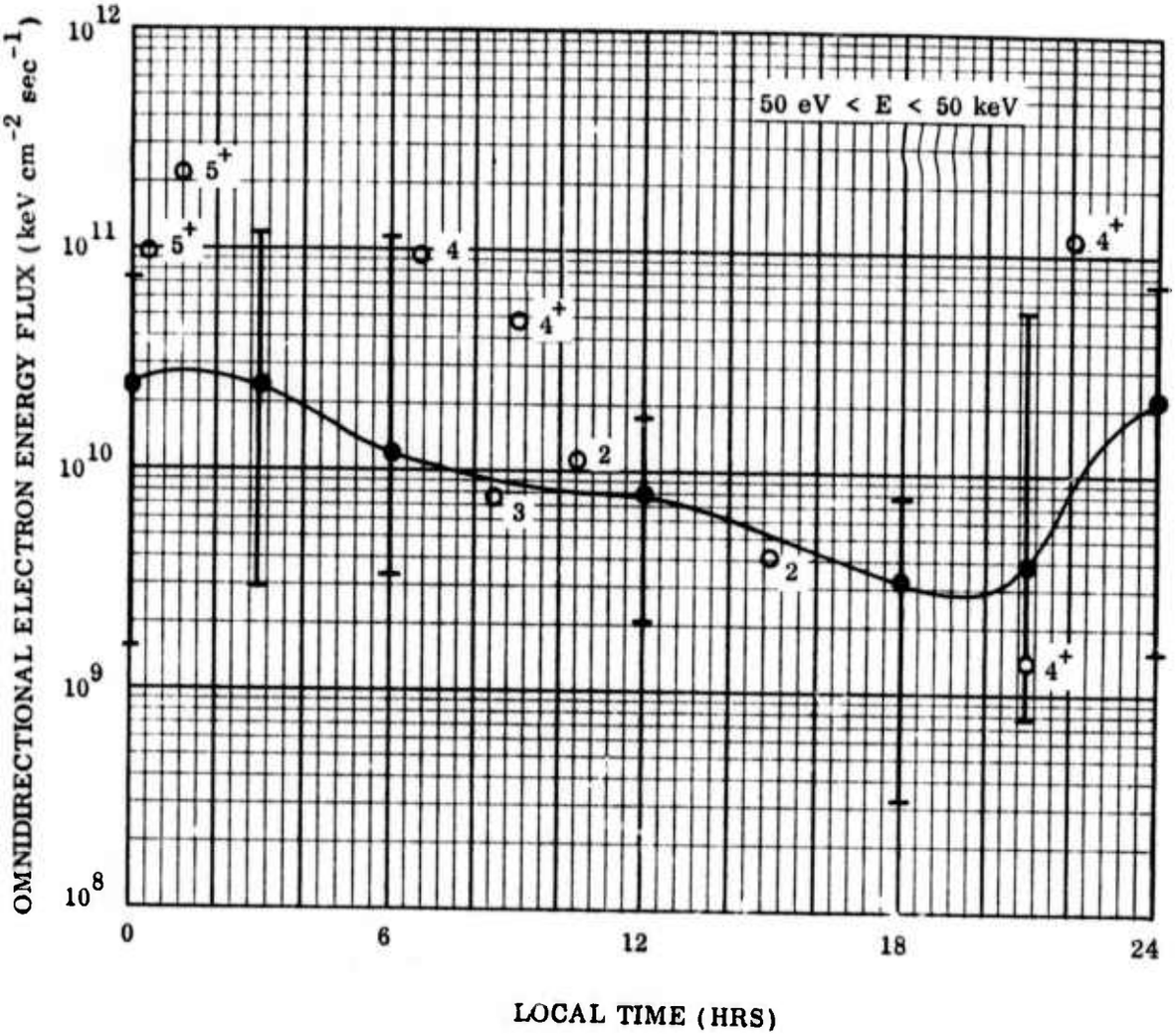

Fig. 6.12 Omnidirectional electron energy flux integrals (1 directional flux x 4π) as a function of local time for 50 eV < E < 50 keV for 29 days in January 1970. The solid curve goes through the "typical" values and the bars with crosses denote maxima and minima values of the energy flux. The 8 data points shown as circles with K_p values beside them are specific cases published (DeForest and McIlwain, 1971).

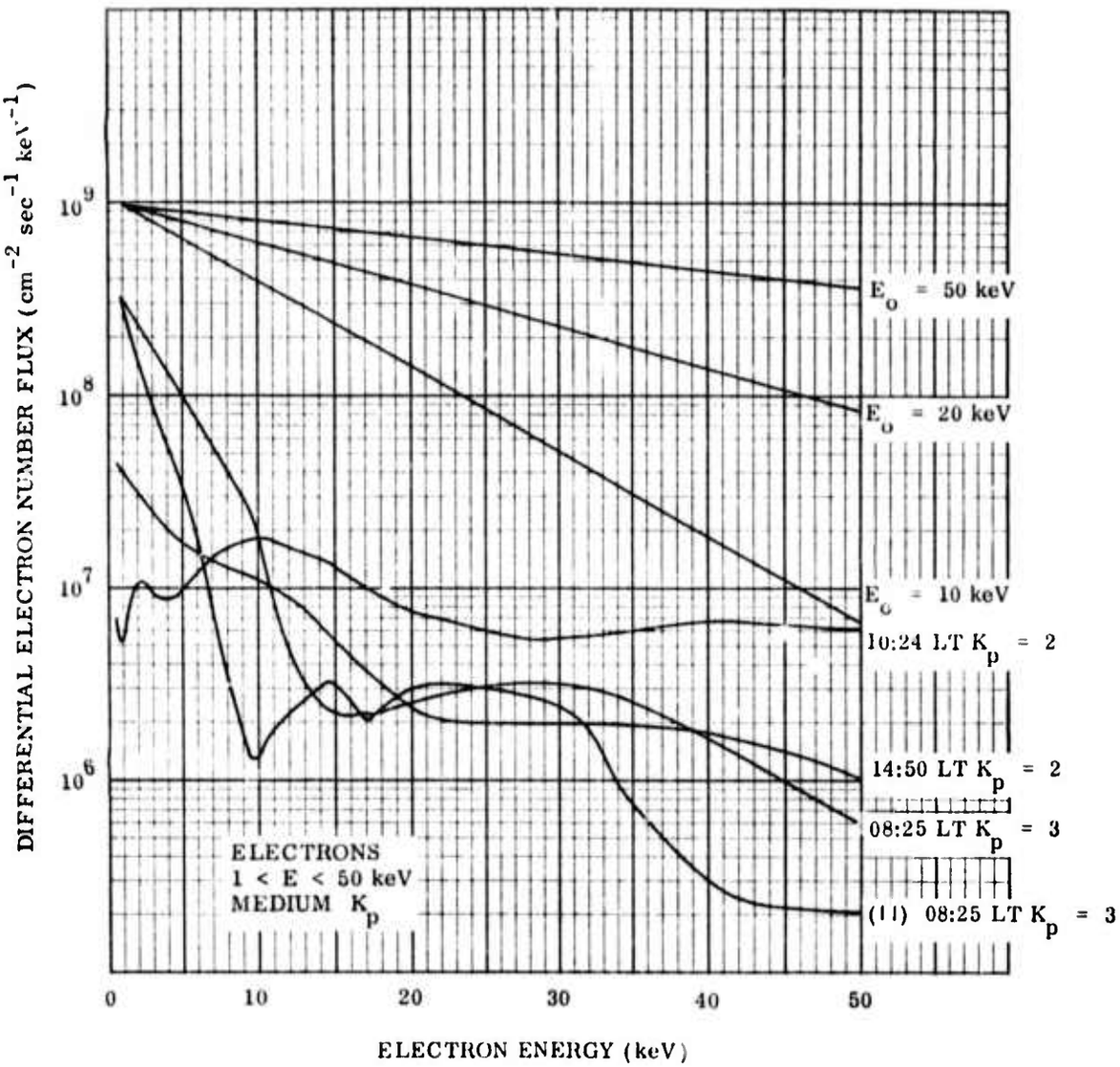

Fig. 6.13 Examples of electron energy spectra ($\perp$ directional number flux x 4π, and one case of parallel ($\parallel$) directional flux x 4π) from 1 keV to 50 keV (DeForest and McIlwain, 1971). Local times and K_p indices (2 to 3 for cases given here) are listed. The shapes of exponential spectra $dN/dE = N_o \exp(-E/E_o)$ are given above for E_o = 50, 20 and 10 keV.

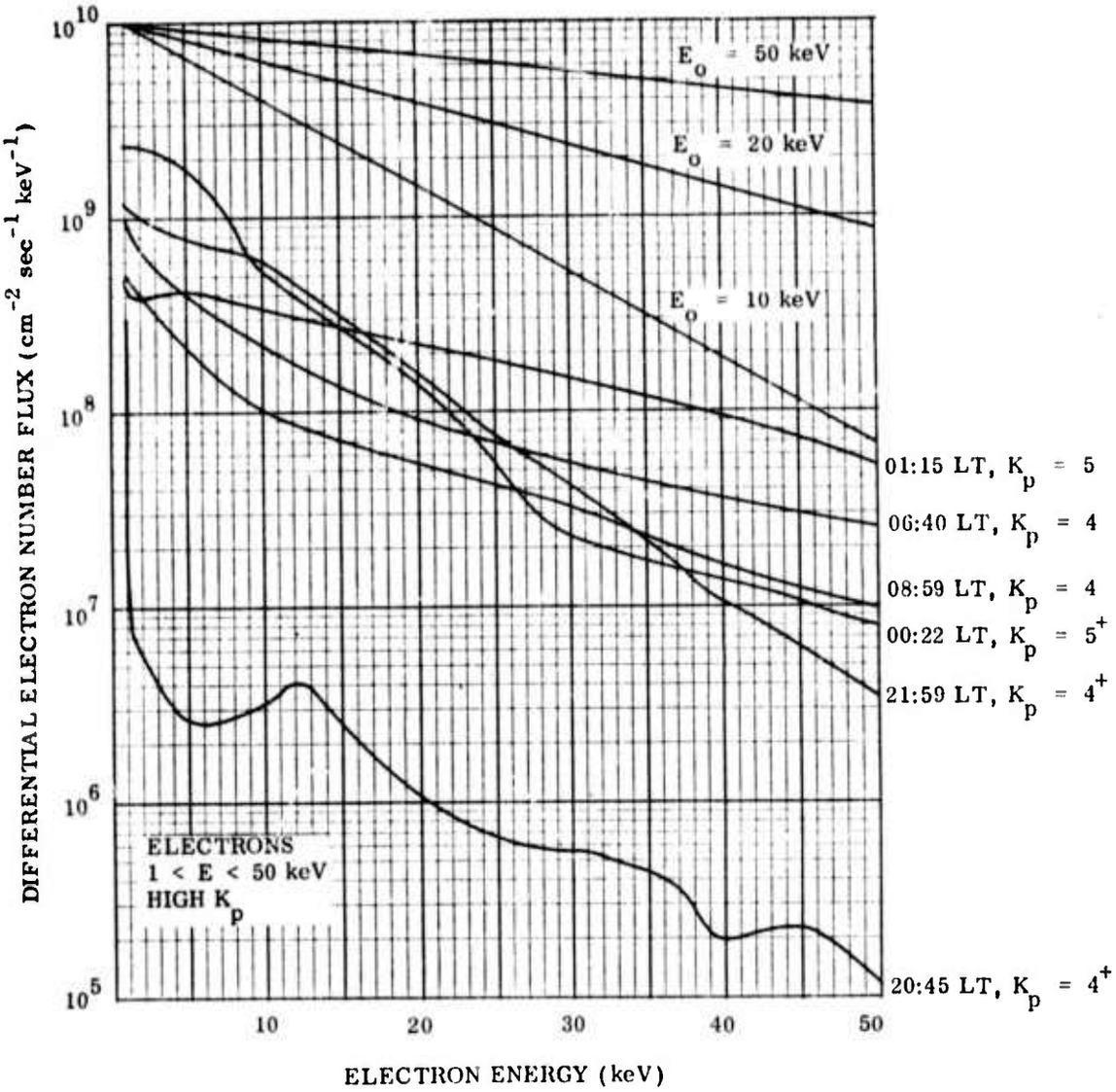

Fig. 6.14 Examples of differential electron number fluxes ($\perp$ directional number flux x 4π) from 1 keV to 50 keV. Local times and 3 hr K_p indices (4 to 5^+ for cases given in this figure) are listed. The shapes of exponential spectra $dN/dE = N_o \exp(-E/E_o)$ are given for E_o = 50, 20 and 10 keV at the top (De Forest and McIlwain, 1971).

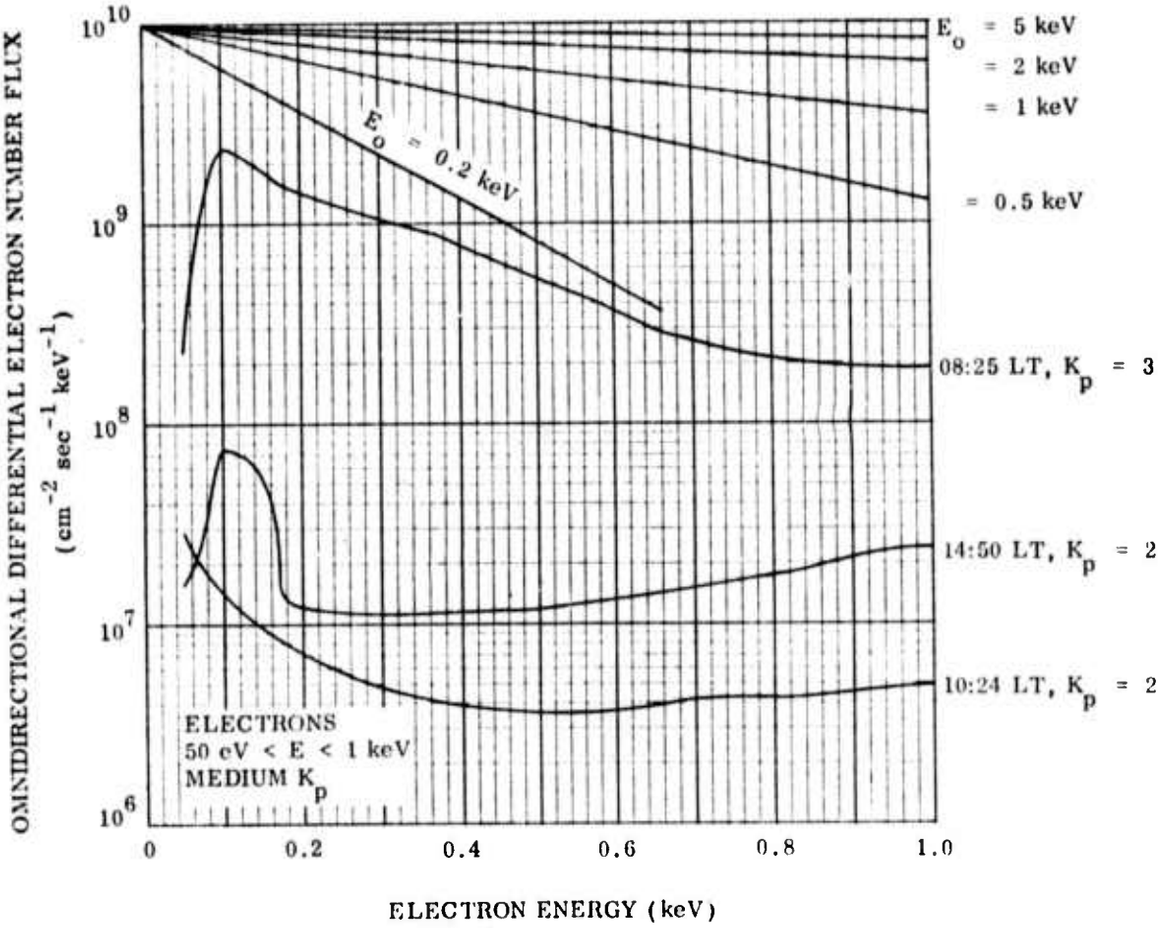

Fig. 6.15 Examples of differential electron number fluxes ($\perp$ directional number flux x 4π) for 50 eV < E < 1 keV for medium K_p (DeForest and McIlwain, 1971). Local times and 3 ^{p}hr K_p indices are listed. The shapes of exponential spectra $dN/dE = N_o \exp(-E/E_o)$ are given for E_o from 5 to 0.2 keV at the top.

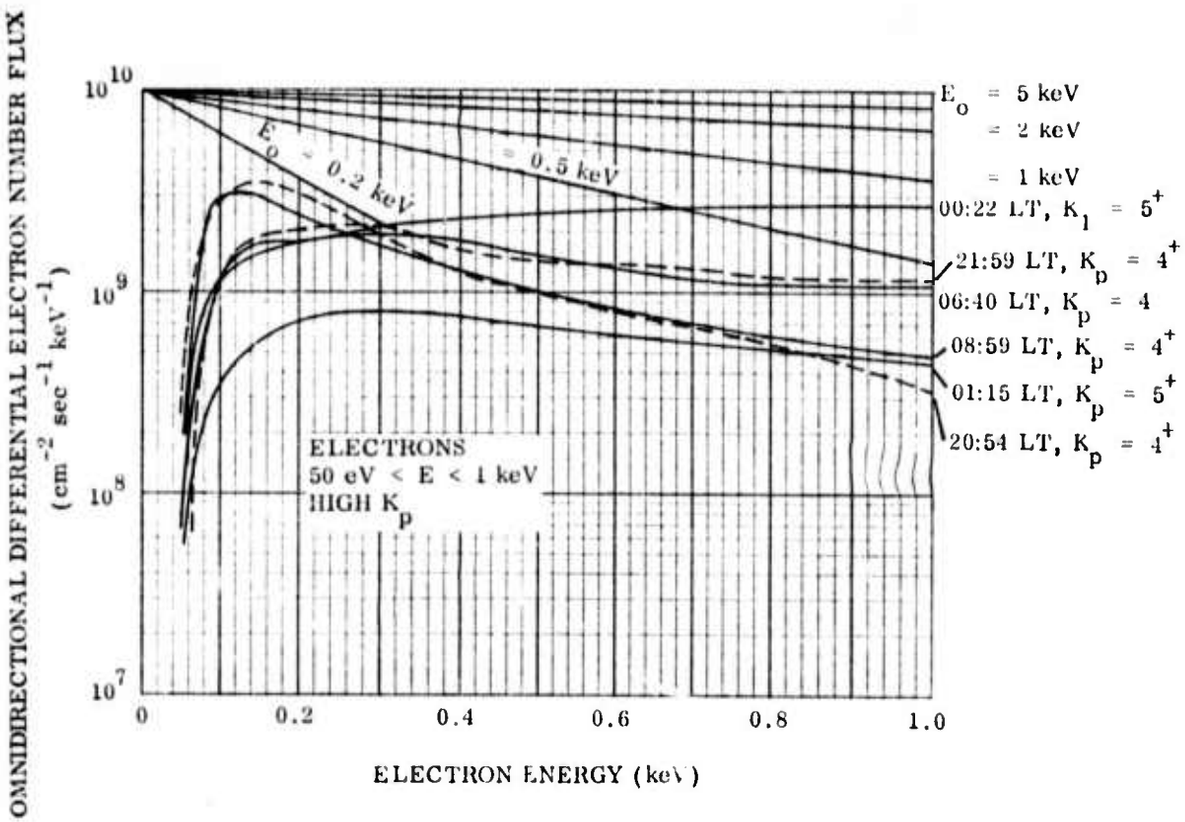

Fig. 6.16 Examples of differential electron number fluxes (1 directional number flux x 4π) for 50 eV < E < 1 keV for high K_p (DeForest and McIlwain, 1971). Local times and 3 hr K_p indices are listed. The shapes of exponential spectra $dN/dE = N_o \exp(-E/E_o)$ are given for E_o from 5 to 0.2 keV at the top.

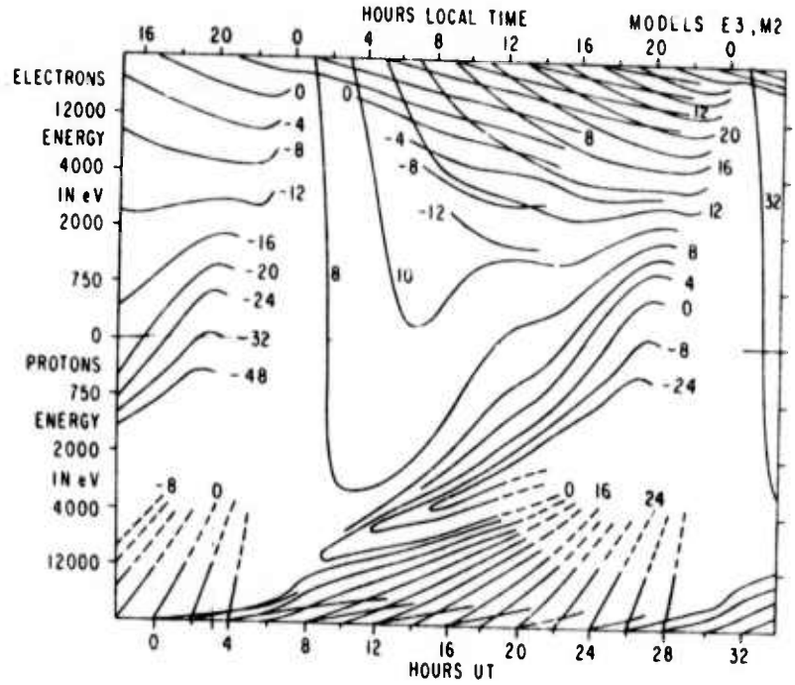

Fig. 6.17 A plot of the times (local and UT) and energy changes of groups of particles moving through and around the magnetosphere according to the electric and magnetic field models of McIlwain (1972). This is an observational pattern expected at a geosynchronous satellite of groups of protons and electrons injected at the 2300 LT meridian at the UT's indicated (mostly at 4 hr time intervals on the UT scale at the bottom of the diagram) as the satellite observes them at different local times. Two energy groups of both electrons and protons are shown injected by several substorms; the higher energy group become trapped and move around the earth for more than one 24-hour period, lower energy groups of electrons are decelerated in the midnight sector and low energy protons are accelerated. In the morning hours single low energy proton groups can be split into 2 energy groups.

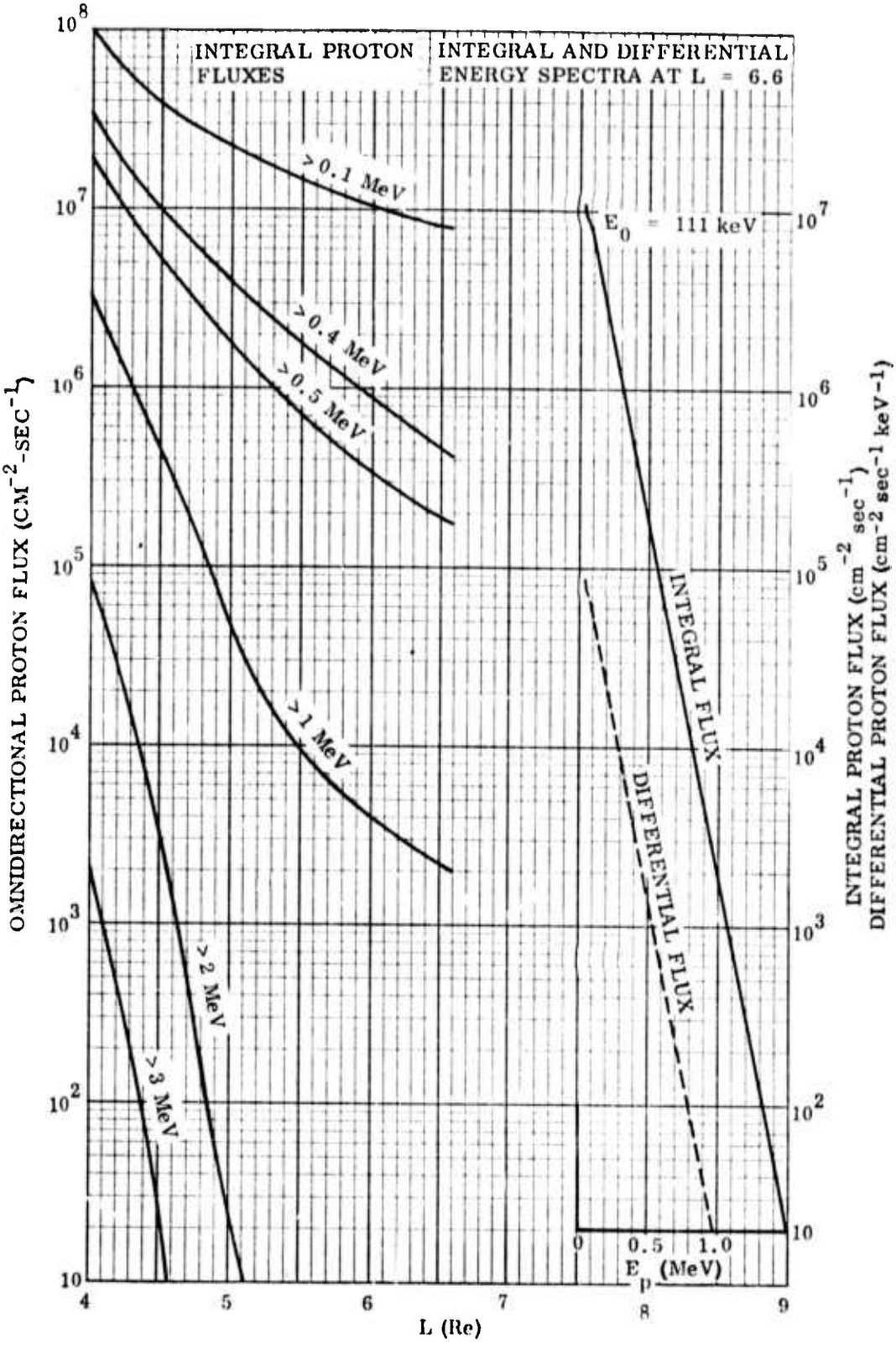

Fig. 6.18 Radial profiles of equatorial omnidirectional proton flux for different energy thresholds from 100 keV to 5 MeV and the proton integral and differential energy spectra at L = 6.6 (Model AP-5 from King, 1967).

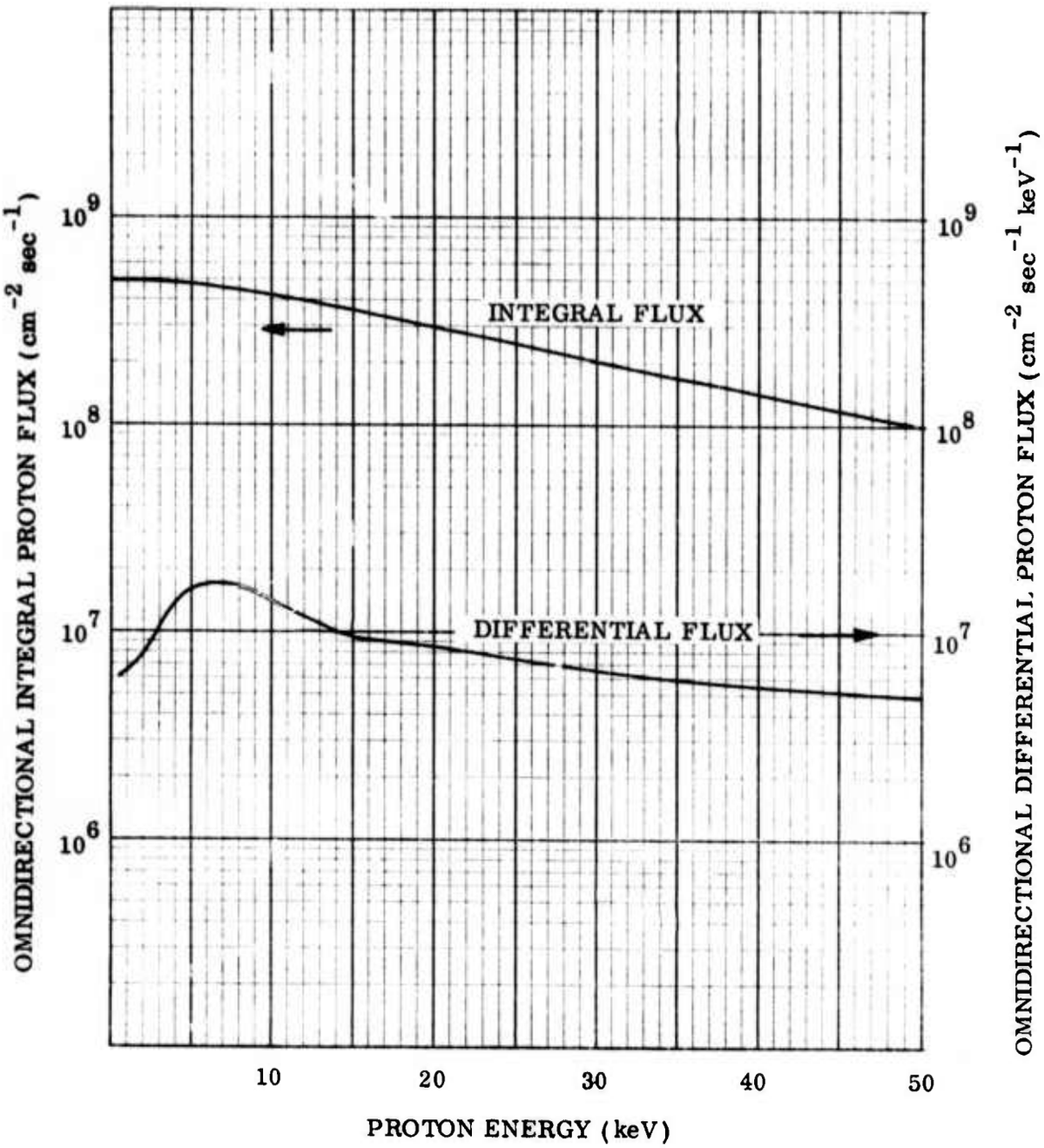

Fig. 6.19 Equatorial omnidirectional integral and differential proton fluxes $0.5 \leq E \leq 50$ keV for L= 6.6 (Frank and Owens, 1970). These data were taken over a 44-day period from 10 June to 23 July 1966 in which the largest ΣK_p was 32. Average values for the differential fluxes did not differ noticeably for the 28 days for which $\Sigma K_p \leq 12$ and for the 16 days for which $12 < K_p \leq 32$. The integral flux curve was calculated from the differential curve smoothly connected to the Model AP5 (King, 1967) differential flux curve above 100 keV.

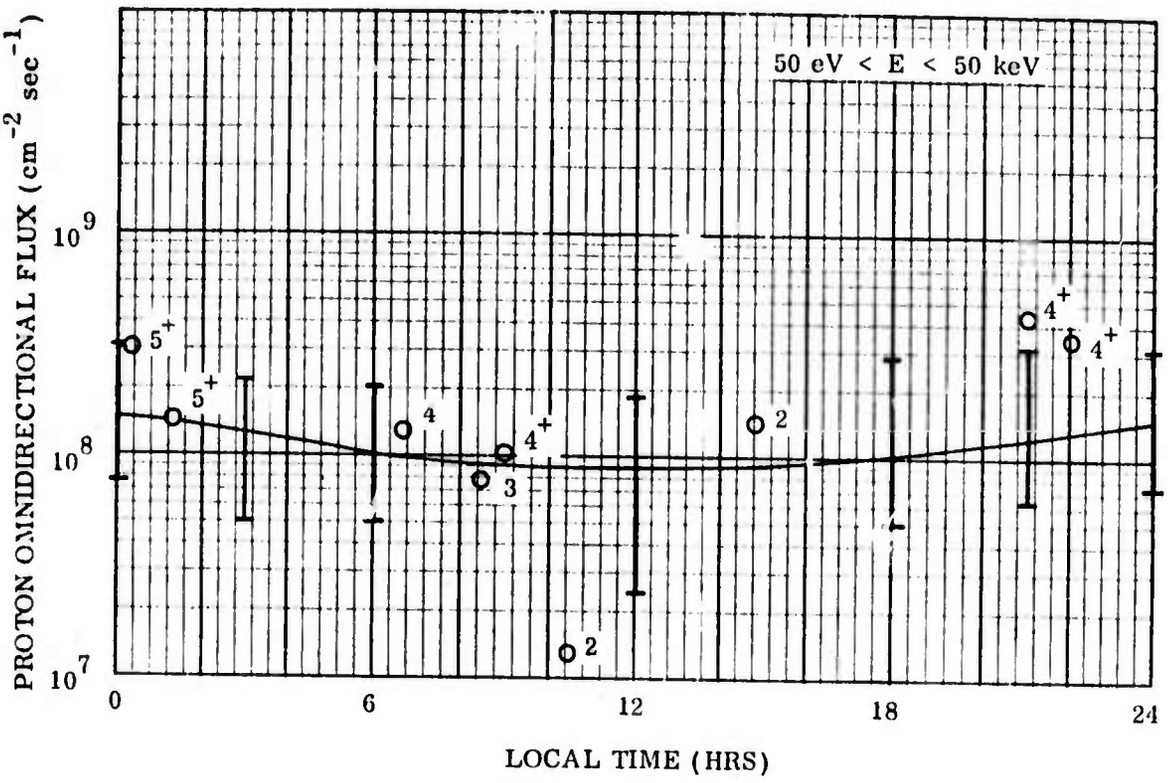

Fig. 6.20 Proton integral (50 eV < E < 50 keV) directional flux (⊥ to earth's spin axis) multiplied by 4π as a function of local time at geosynchronous altitude (L=6.6, ATS-5). The solid line gives "typical" integrals for 29 days of January 1970, a period in which 4.4% of the 3-hr K_p values were ≥ 4, 39.6% were 2^- through 4^- and 56% were $\leq 1^+$.[p] The crosses on the bars denote maxima and minima values of the proton integrals. The 8 data points shown as circles with the K_p values beside them are specific cases published by DeForest [p] and McIlwain (1971).

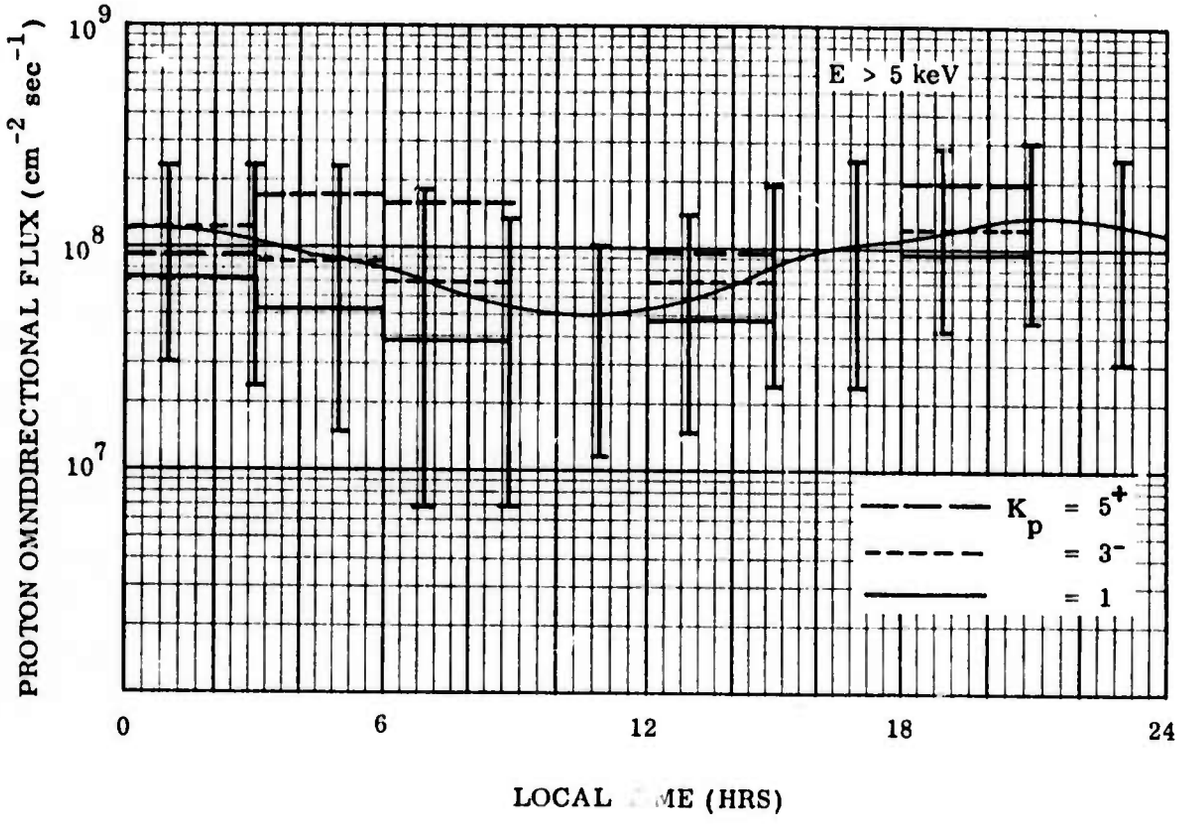

Fig. 6.21 Proton integral (> 5 keV) directional flux (central angle of detector 11° from earth's spin axis) multiplied by 4π as a function of local time at geosynchronous altitude (L = 6.6, ATS-5). The solid curve gives the average integrals over 20 days from September through December 1969 in which 16% of the 3 hr K_p values were ≥ 4, 48% were 2^- through 4^-, and 36% $\leq 1^+$. 443 one hour integrals were sorted according to K_p and the bar graphs give the average integrals for 3 hr local time periods of 3 K_p values 1, 3^- and 5^+. The crosses on the vertical bars give maxima and minima values of the proton integrals in the 2-hr local time intervals (Shelley and Lew, 1971).

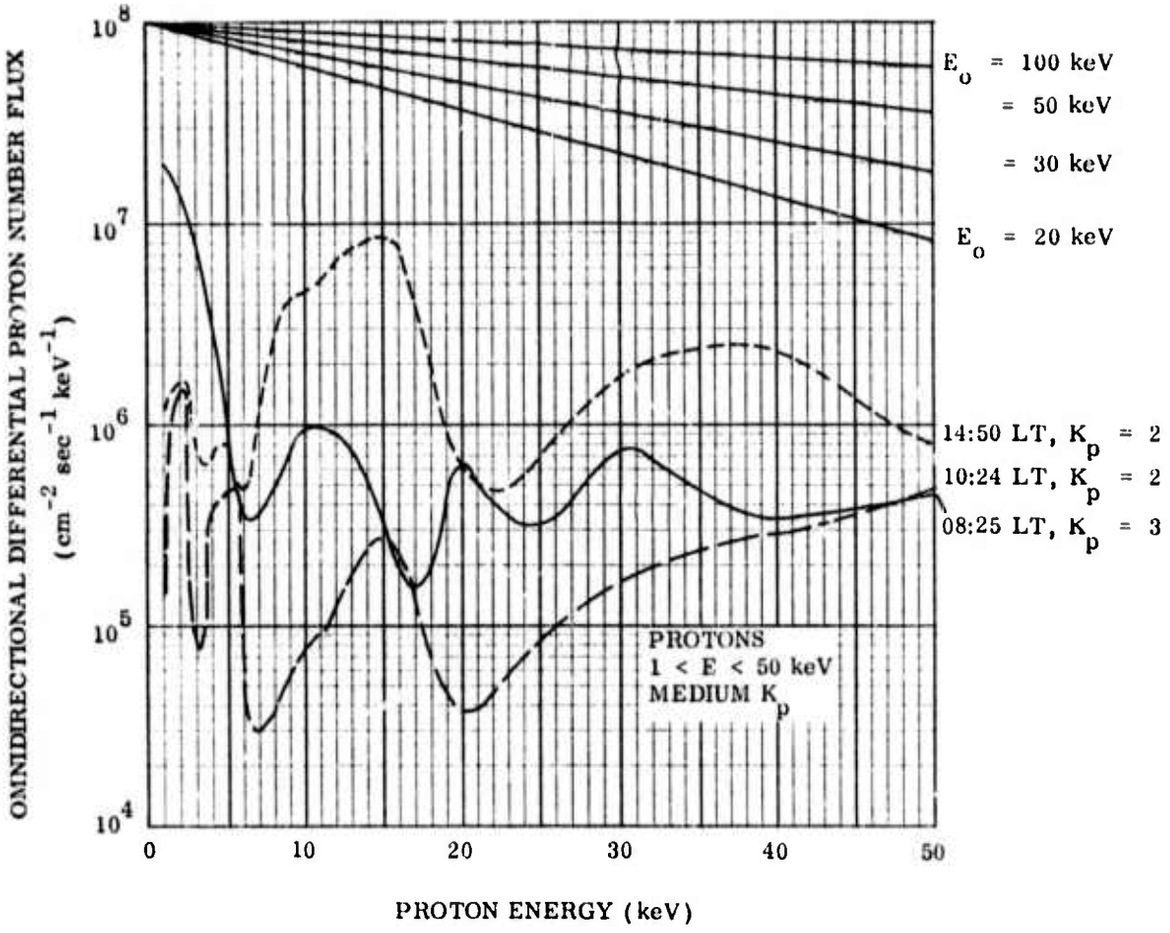

Fig. 6.22 Examples of differential proton number fluxes (1 directional flux x 4π) for $1 < E < 50$ keV for medium K_p at $L = 6.6$ (DeForest and McIlwain, 1971). Local times and 3 hr K_p indices are listed. The shapes of exponential spectra, $dN/dE = N_o \exp(-E/E_o)$, are given for E_o from 100 keV to 20 keV at the top.

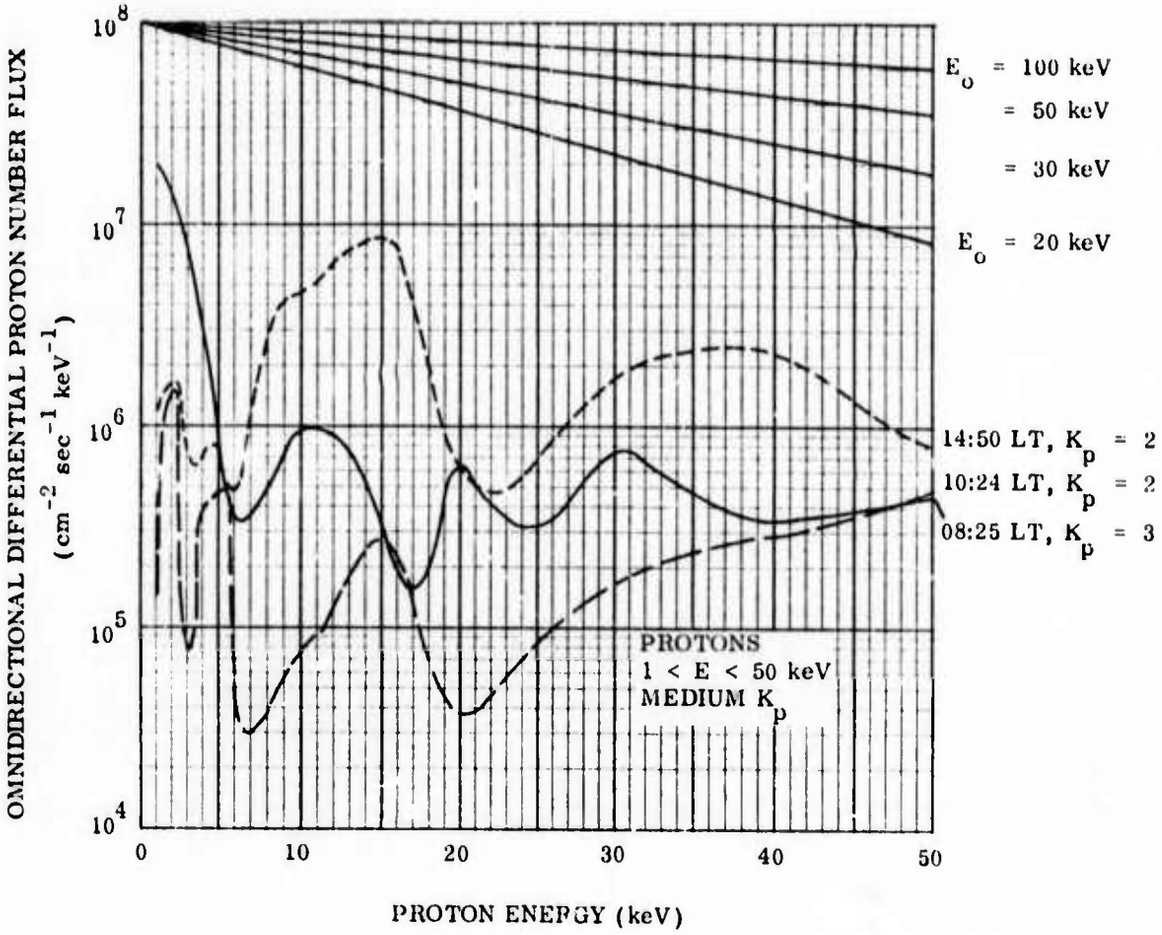

Fig. 6.22 Examples of differential proton number fluxes (1 directional flux x 4π) for $1 < E < 50$ keV for medium K_p at $L = 6.6$ (DeForest and McIlwain, 1971). Local times and 3 hr K_p indices are listed. The shapes of exponential spectra, $dN/dE = N_o \exp(-E/E_o)$, are given for E_o from 100 keV to 20 keV at the top.

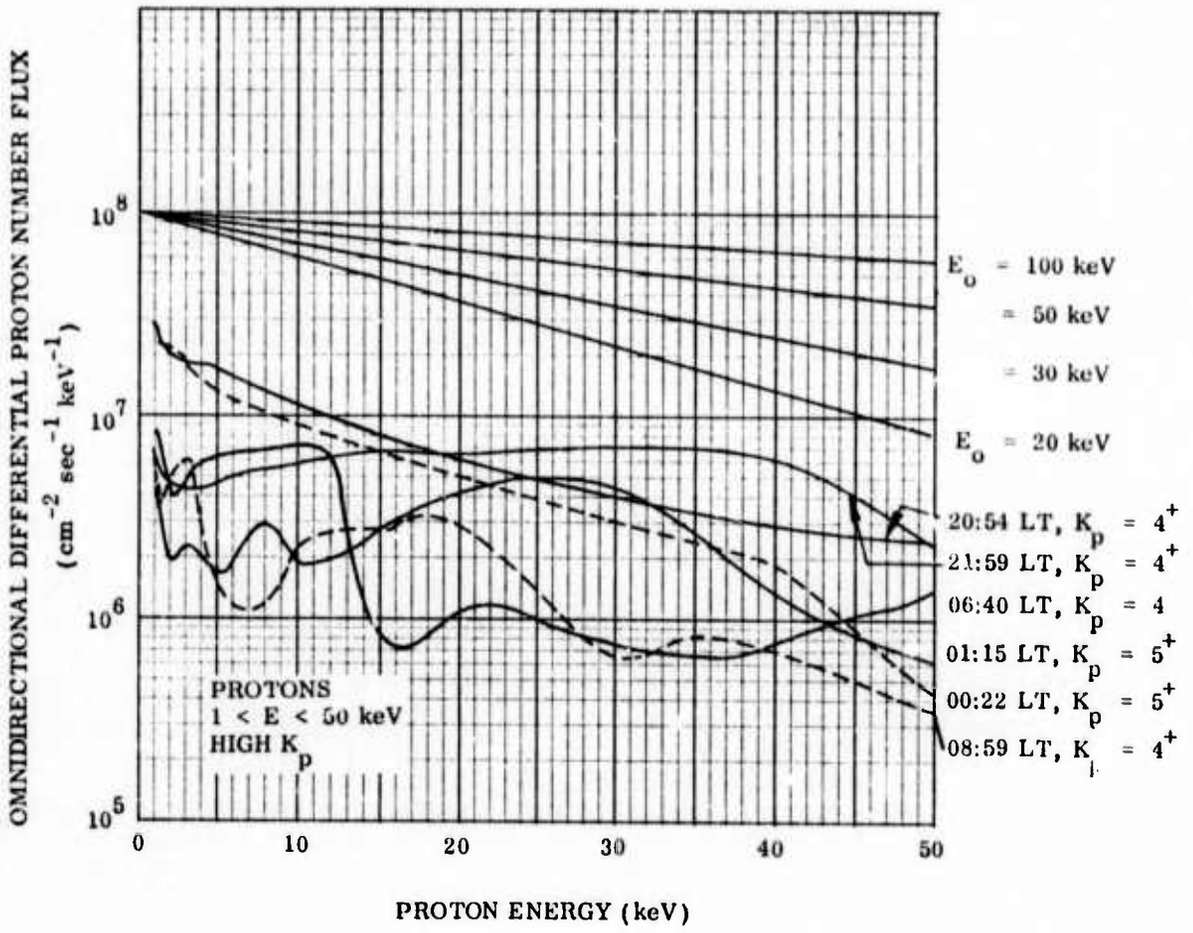

Fig. 6.23 Examples of differential proton number fluxes (⊥ directional flux x 4π) for $1 < E < 50$ keV for high K_p at L = 6.6 (DeForest and McIlwain, 1971). Local times and 3 hr K_p indices are listed. The shapes of exponential spectra, $dN/dE = N_o \exp(-E/E_o)$, are given for E_o from 100 keV to 20 keV at the top.

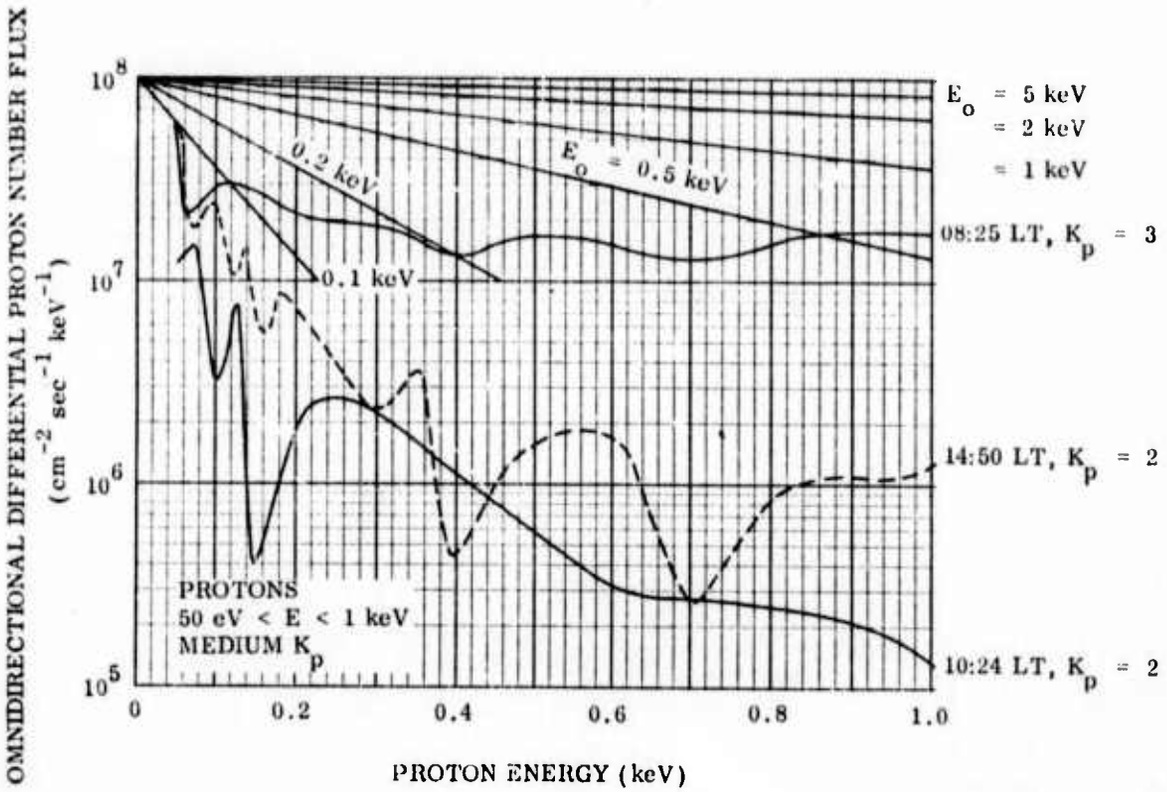

Fig. 6.24 Examples of differential proton number fluxes ($_\perp$ directional flux x 4π) for 50 eV < E < 1 keV for medium K_p at L = 6.6 (DeForest and McIlwain, 1971). Local times and K_p indices are listed. The shapes of exponential spectra, $dN/dE = N_o \exp(-E/E_o)$, are given for E_o from 5 to 0.2 keV at the top.

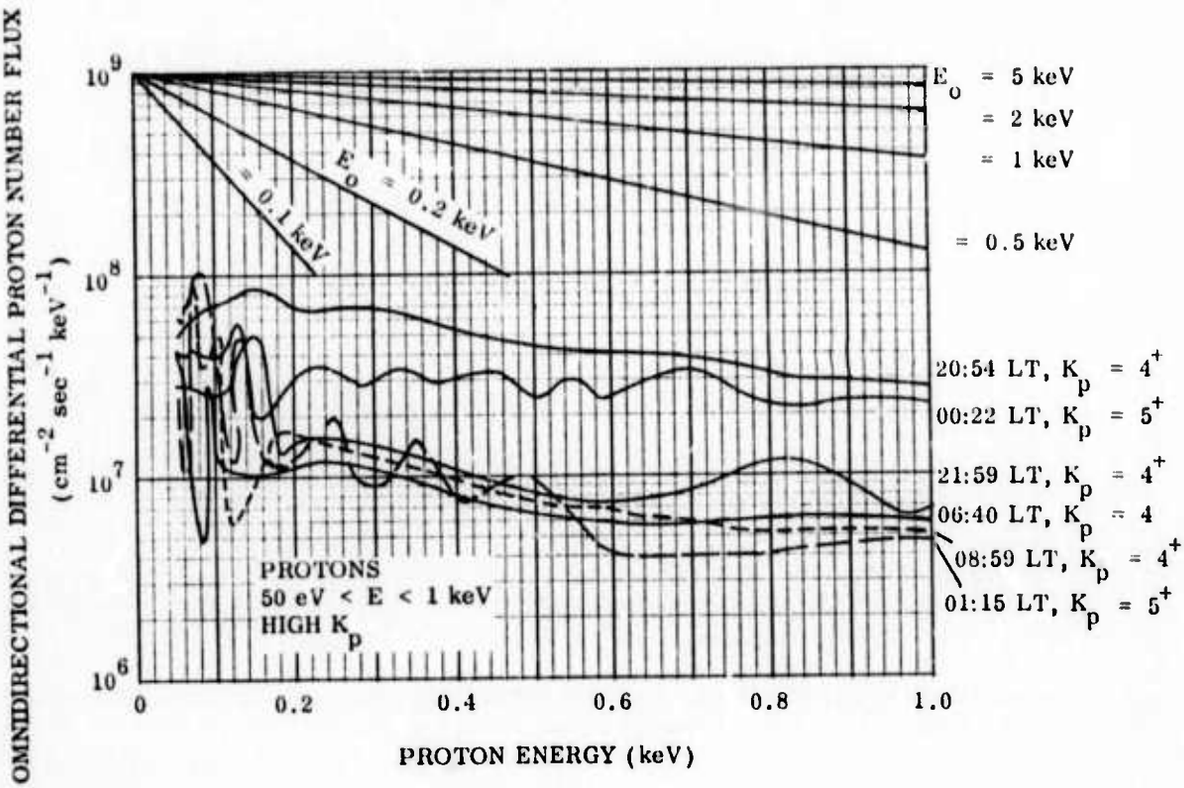

Fig. 6.25 Examples of differential proton number flux (⊥ directional flux x 4π) for 50 eV < E < 1 keV for high K_p at L = 6.6 (DeForest and McIlwain, 1971). Local times and K_p indices are listed. The shapes of exponential spectra, dN/dE = $N_o \exp(-E/E_o)$ are given for E_o from 5 to 0.1 keV at the top.

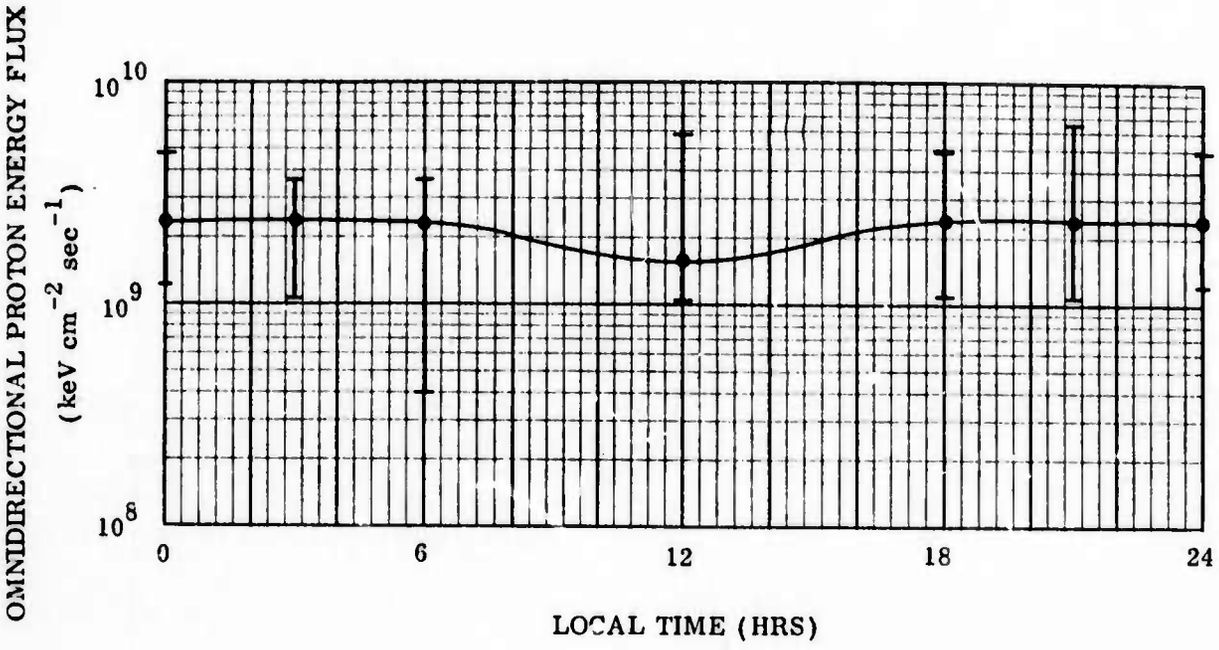

Fig. 6.26 Omnidirectional proton energy flux integrals (ı directional energy flux x 4π) as a function of local time for 50 eV < E < 50 keV. The solid curve goes through the "typical" values of DeForest and McIlwain (1971) and the bars with crosses denote maxima and minima values of the energy flux. The data are for 29 days of January 1970.

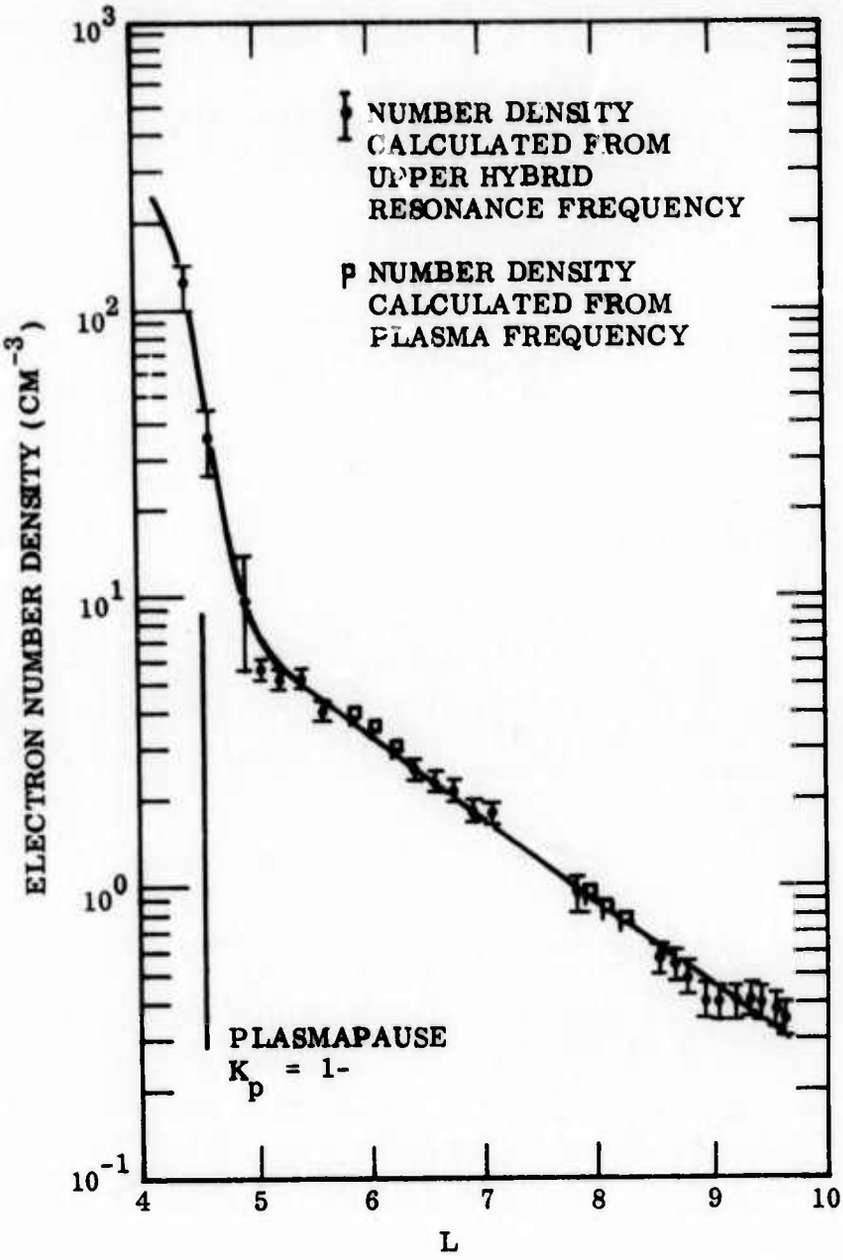

RADIAL DISTANCE	3.0 R_E	4.0 R_E	5.0 R_E	6.0 R_E	7.0 R_E
MAG. LATITUDE	25°	30°	32°	33°	
LOCAL TIME	6.0 HRS		7.0 HRS	7.5 HRS	

Fig. 6.27 Radial profile of electron number density vs. L at a magnetic latitude near 30°, local time near 6:00 hrs on an Imp-6 outbound pass on April 7, 1971 (from Shaw and Gurnett, 1972).

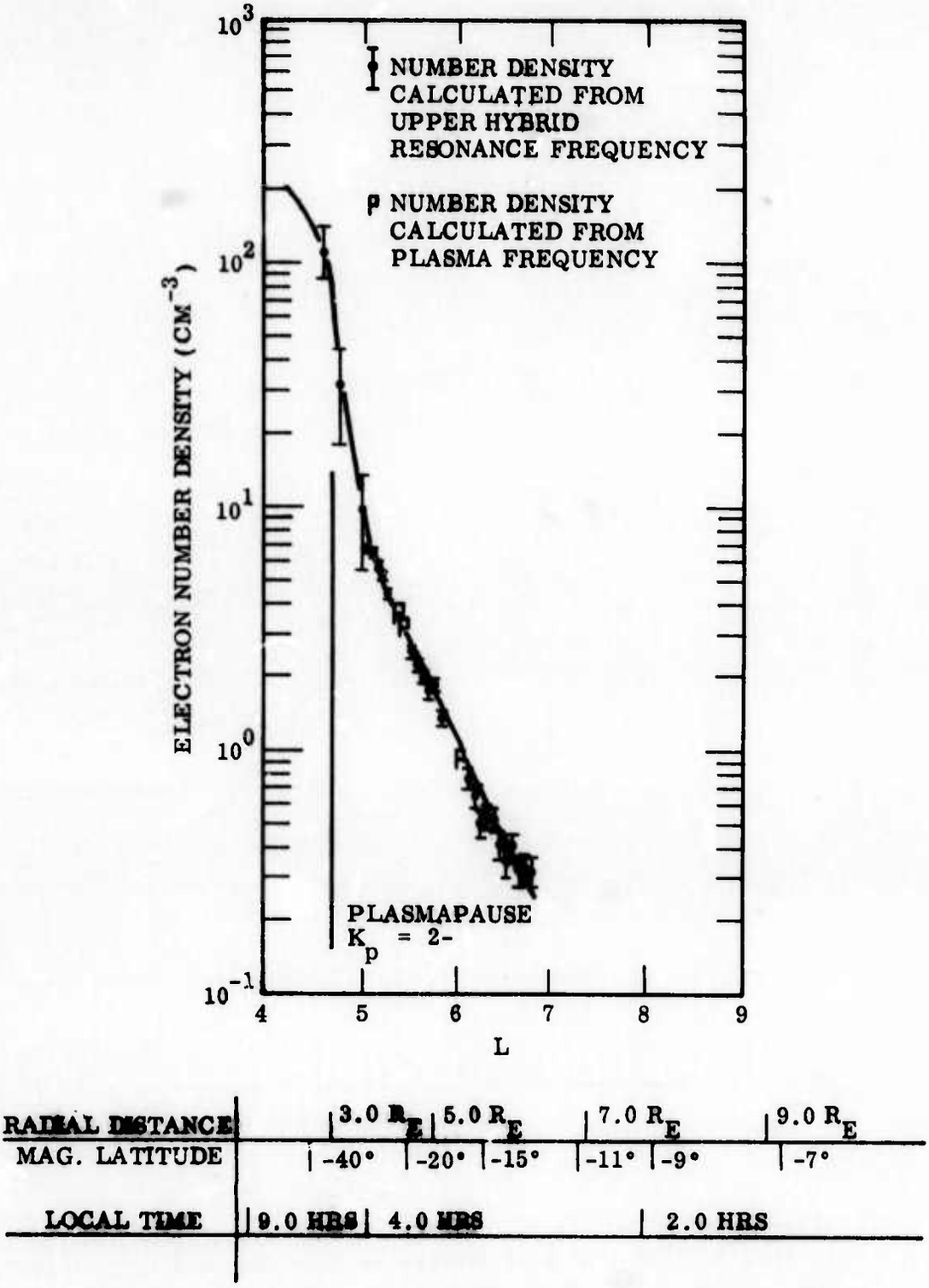

Fig. 6.28 Radial profile of electron number density vs. L at a magnetic latitude near -30°, local time near 6:00 hrs, on an Imp-6 inbound pass on Oct. 11, 1971 (from Shaw and Gurnett).

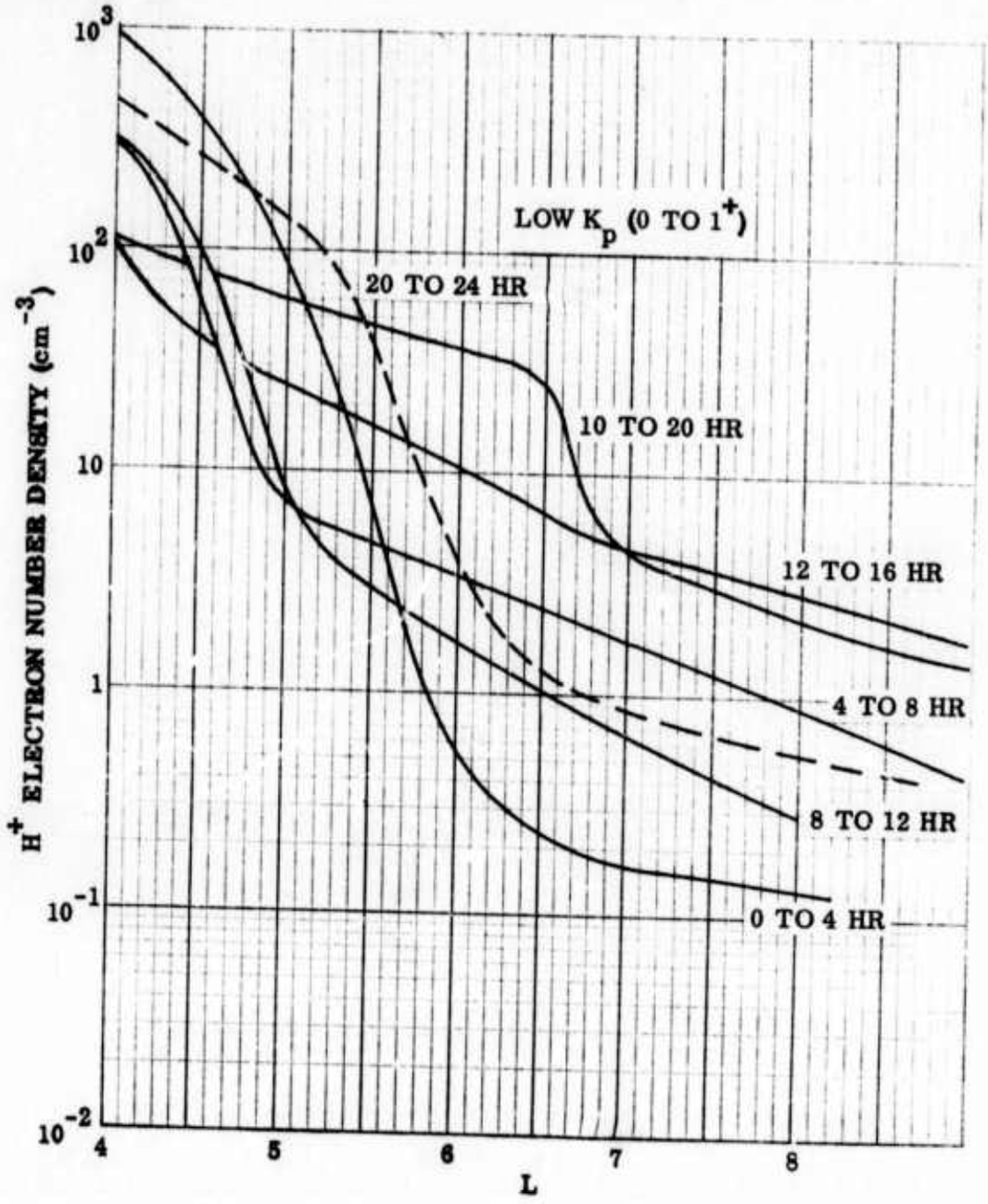

Fig. 6.29 Examples of H^+ or electron number density radial profiles for low K_p (0 to 1^+). The 4 to 8 hr profile is from Shaw and Gurnett (1972), the 4 other solid curves represent either single measurements or are the mean of up to 5 measurements from Harris et al. (1971), and the dotted curve is an interpolation between the curves for the preceeding and following time periods.

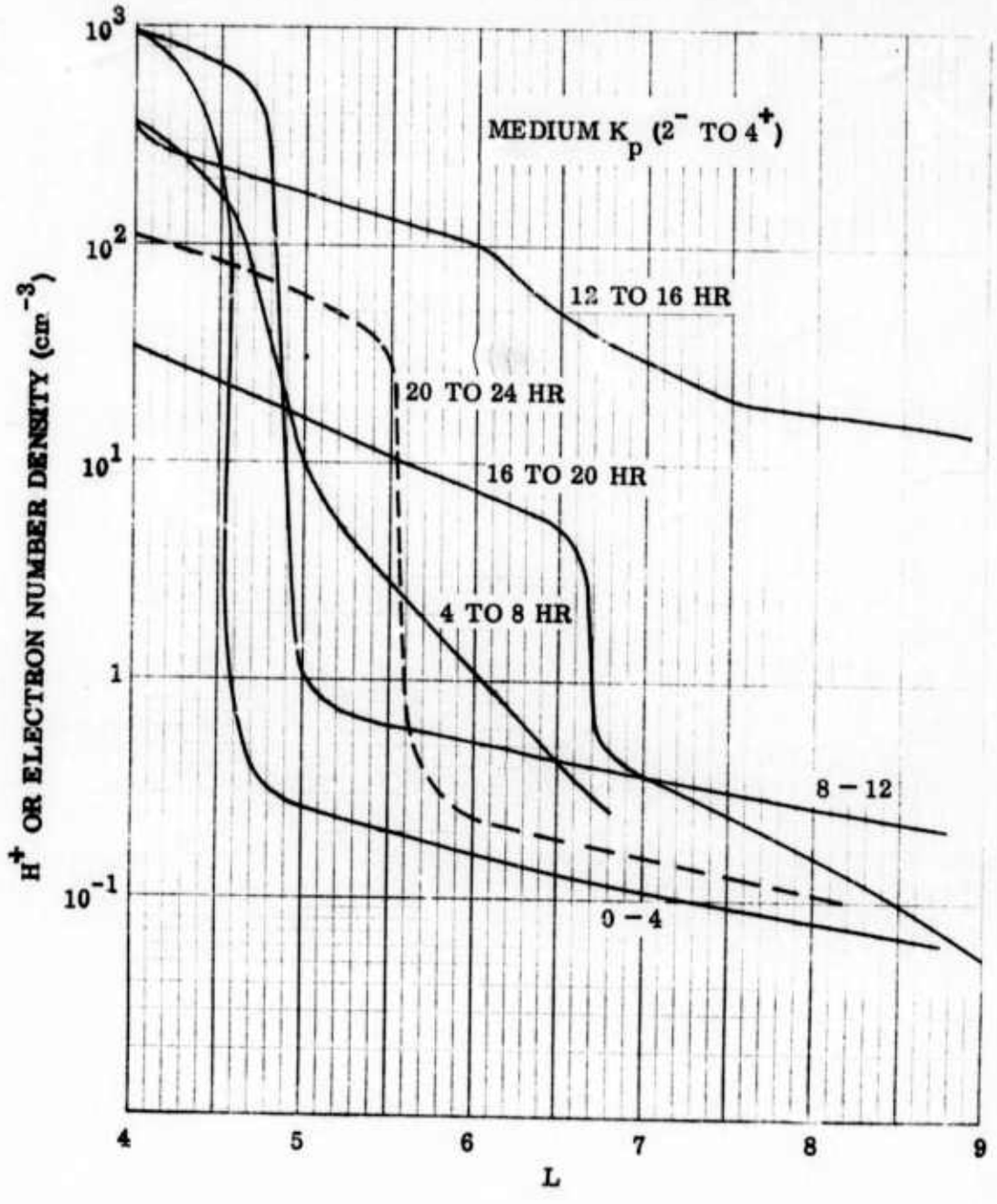

Fig. 6.30 Examples of H^+ or electron number density radial profiles for medium K_p (2^- to 4^-). The 4 to 8 hr profile is from Shaw and Burnett, 1972, the 4 other solid curves represent either single measurements or are the mean of up to 4 measurements from Harris et al., 1971, and the dotted curve is an interpolation between the curves for the preceeding and following time periods.

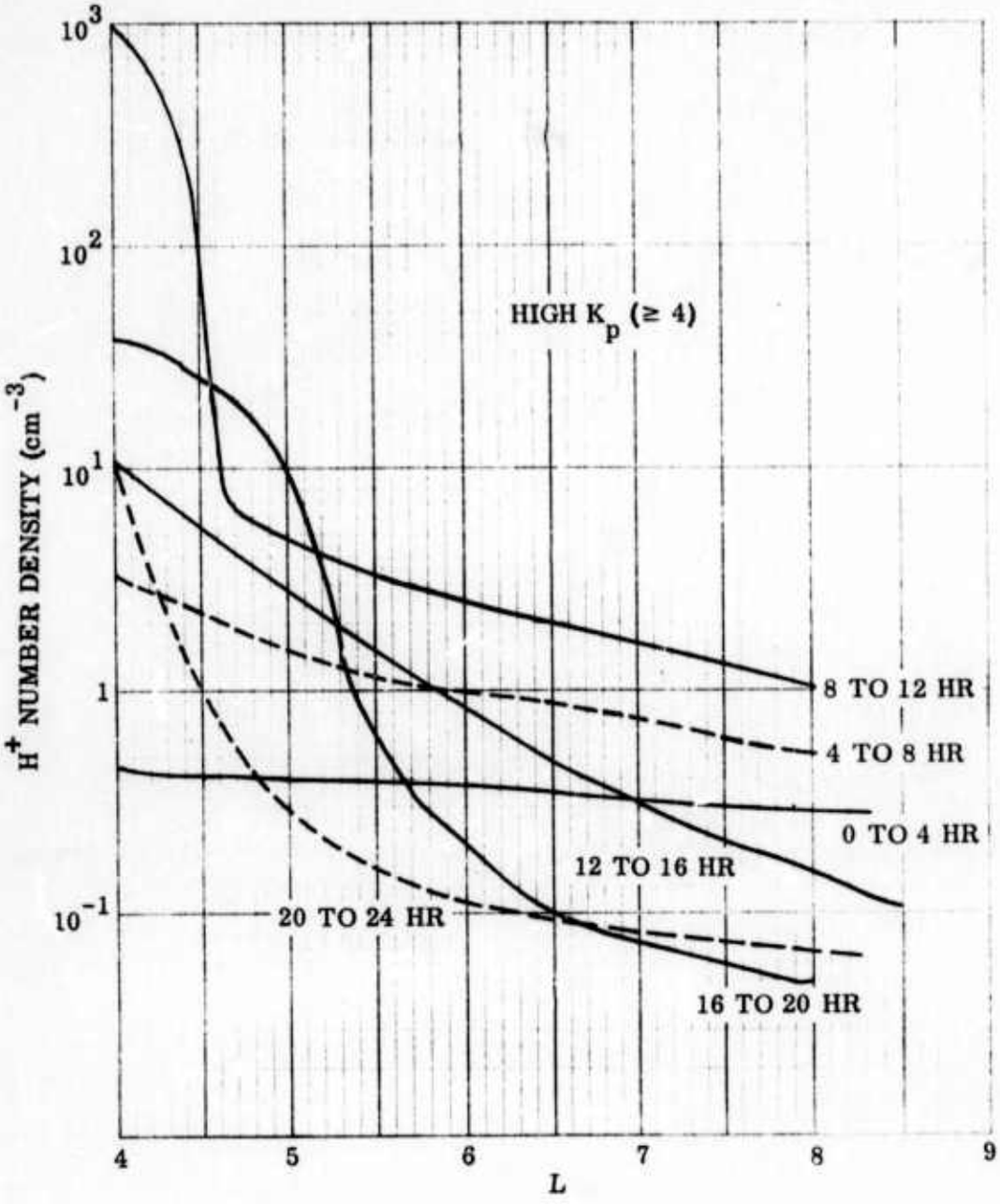

Fig. 6.31 Examples of H^+ number density radial profiles for high K_p (≥ 4). The 4 solid curves are means of from 2 to 4 measurements from Harris et al., 1971, and the dotted curves are interpolations between the curves for the previous and following time periods.

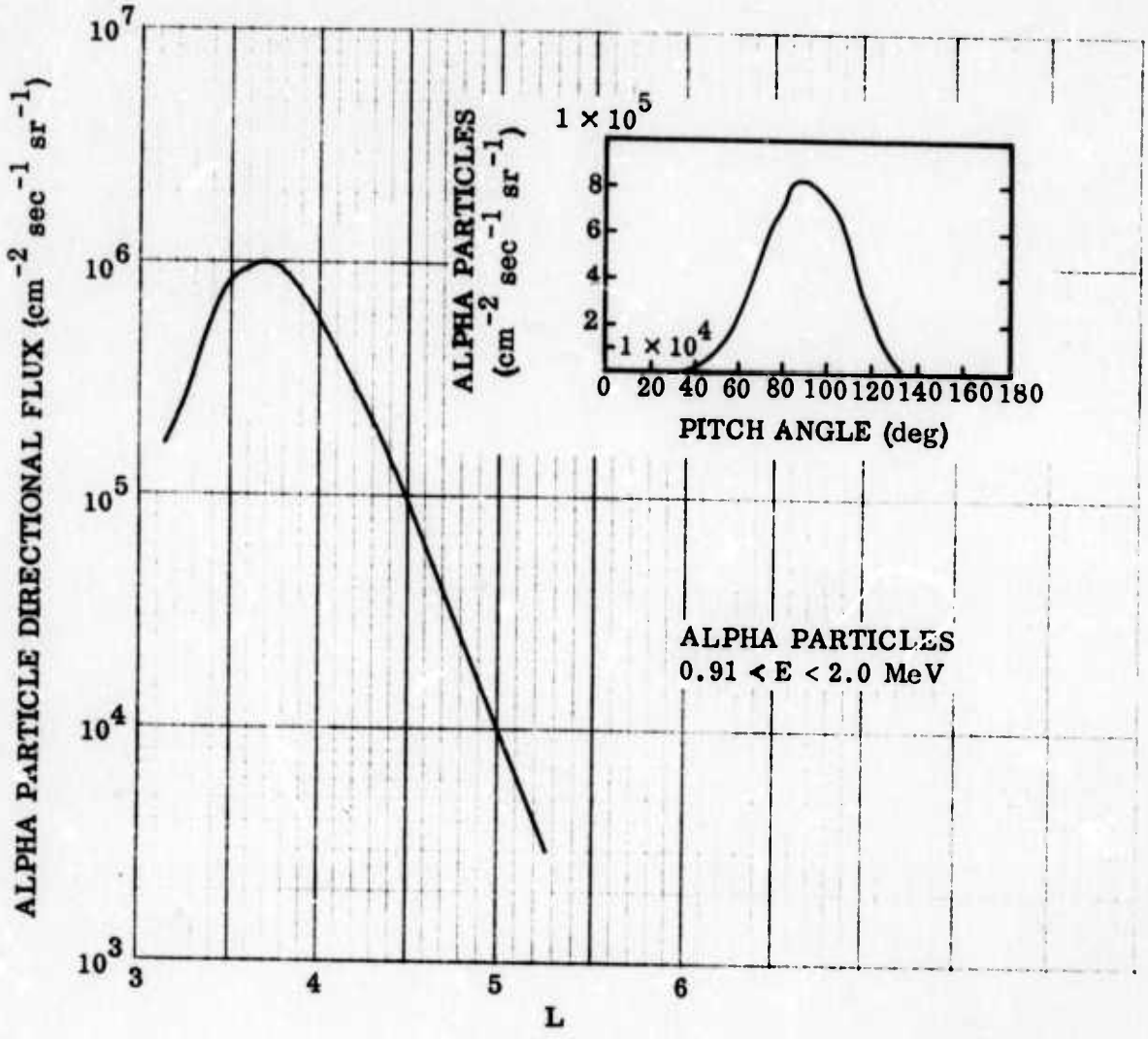

Fig. 6.3 An example of alpha particle directional flux (1 to) measured near the equator by S^3-A satellite on 6 January 1972 with $0.91 < E < 2.0$ MeV. This was a very quiet day with $\Sigma K_p = 4^-$. The equatorial pitch angle distribution which is best fit by the expression $j(\alpha_o) = j_{max} \sin^8 \alpha_o$ is shown in the insert. (Fritz and Williams, 1972).